Optimizing photon utilization in LED-based photocatalytic reactors

Khodadadian, Maryam

DOI
10.4233/uuid:68bc7aa0-914c-4d2d-8e32-9d0ef996fdcc

Publication date
2019

Document Version
Final published version

Citation (APA)
Khodadadian, M. (2019). *Optimizing photon utilization in LED-based photocatalytic reactors*. [Dissertation (TU Delft), Delft University of Technology]. https://doi.org/10.4233/uuid:68bc7aa0-914c-4d2d-8e32-9d0ef996fdcc

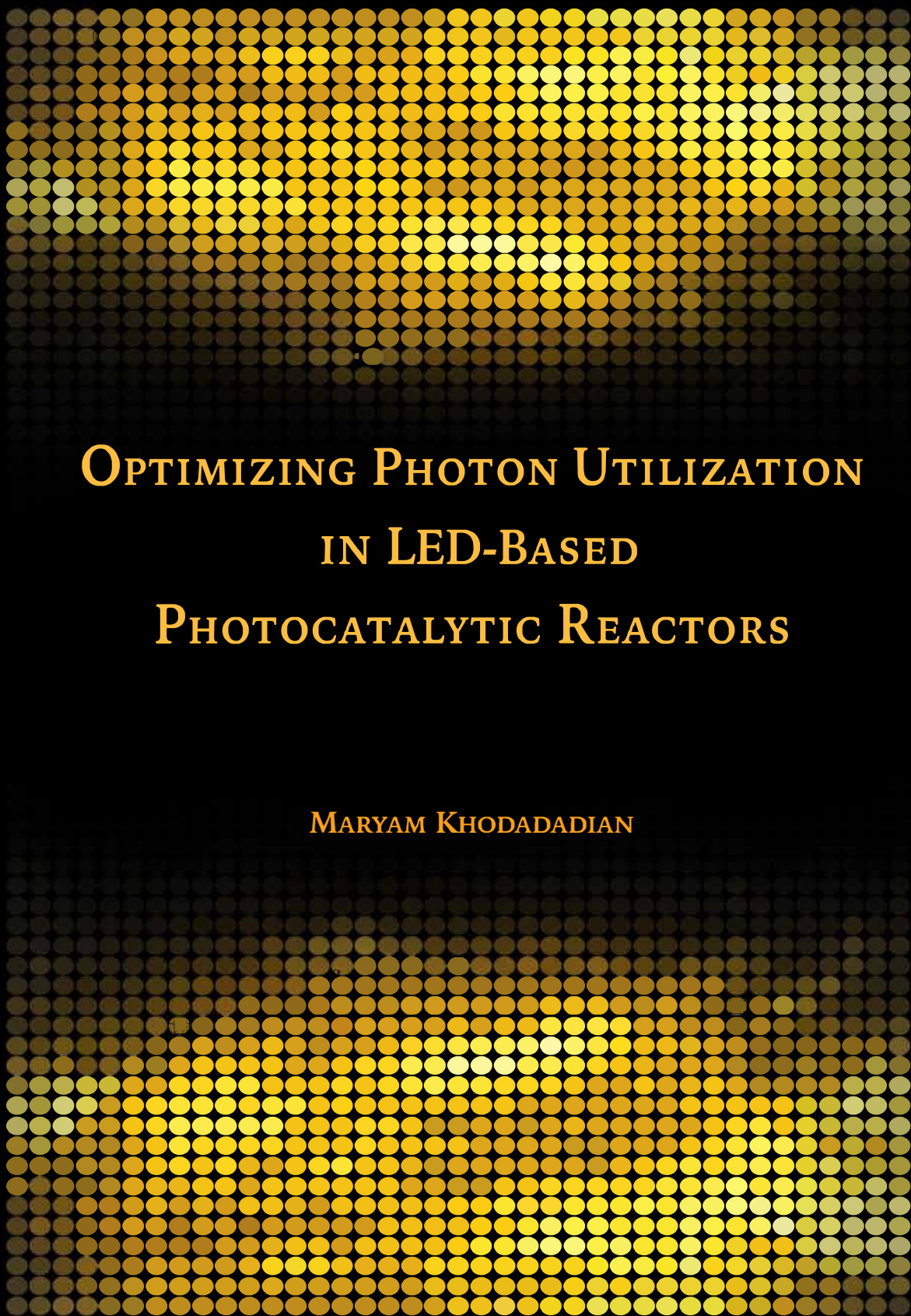

Optimizing Photon Utilization in LED-Based Photocatalytic Reactors

Maryam Khodadadian

OPTIMIZING PHOTON UTILIZATION
IN
LED-BASED PHOTOCATALYTIC REACTORS

FATEMEH (MARYAM) KHODADADIAN

OPTIMIZING PHOTON UTILIZATION IN LED-BASED PHOTOCATALYTIC REACTORS

Proefschrift

ter verkrijging van de graad van doctor

aan de Technische Universiteit Delft,

op gezag van de Rector Magnificus, Prof.dr.ir. T.H.J.J. van der Hagen,

voorzitter van het College voor Promoties,

in het openbaar te verdedigen op woensdag 12 juni 2019 om 15.00 uur

door

FATEMEH KHODADADIAN

Scheikundig ingenieur, Tarbiat Modares University, Iran

geboren te Teheran, Iran

Dit proefschrift is goedgekeurd door de promotoren:
Prof. dr. ir. A. I. Stankiewicz
Prof. dr. ir. R. Lakerveld
Prof. dr. ir. J. R. van Ommen

Samenstelling promotiecommissie:

Rector Magnificus	voorzitter
Prof. dr. ir. A. I. Stankiewicz	Technische Universiteit Delft
Prof. dr. ir. R. Lakerveld	The Hong Kong University of Science and Technology
Prof. dr. ir. J. R. van Ommen	Technische Universiteit Delft

Onafhankelijke leden:

Prof. dr. A. Urakawa	Technische Universiteit Delft
Prof. dr. J. Marugán	Rey Juan Carlos University
Prof. dr. G. Mul	Universiteit Twente
Dr. T. Noël	Technische Universiteit Eindhoven
Prof. dr. ir. J.T. Padding	Technische Universiteit Delft (reservelid)

This research is funded from the European Research Council in the framework of the Seventh Framework Programme (FP7) under grant agreement no ERC-2010-AdG-267348.

ISBN 978-94-6375-436-1

Cover design by Reza Asadi & Mostafa Zahmatkesh
Printed in the Netherlands by Ridderprint B.V.
an electronic version of this thesis is available at TUDelft repository

تا در طلب گوهر کانی، کانی

تا در هوس لقمه نانی، نانی

این نکته رمز اگر بدانی، دانی

هر چیز که در جستن آنی، آنی

مولانا (۵۸۶-۶۵۲ هجری شمسی)

You are a treasure, if the gems are your aim
No more than a grain, if a loaf is your claim
Recall this secret when you play this game
Whatever you pursued is what you became

Rumi (1207-1273 AC)
Translation by M. Dilmaghani

Contents

Summary

Photocatalysis involves the absorption of photons by a semiconductor to enhance chemical reactions. Examples of important applications include the degradation of hazardous chemicals, reduction of carbon dioxide to valuable chemicals and (partial) oxidation of hydrocarbons. Despite many successful demonstrations of this technology at lab-scale, its industrial application has been hindered by the low overall efficiency of the process due to several challenges that need to be resolved. One of the main challenges is efficient utilization of light within a photocatalytic reactor, which affects the economic feasibility of the process especially when using artificial light sources.

In the last few years, the feasibility of using UV-LEDs as an alternative light source for conventional UV-lamps, such as mercury and xenon lamps, has been shown for applications in the gas and liquid phase. Yet, strategies that would allow for optimal light utilization within LED-based reactors during design and operation are lacking. Therefore, the focus of this thesis is on the efficient use of photons by development and validation of novel approaches for the design, optimization, and control of LED-based photocatalytic reactors. The photocatalytic degradation of toluene in the gas phase is adopted as the model reaction, since toluene is one of the most common indoor pollutants threatening human health.

In the design phase of a LED-based reactor, the flexible positioning of LEDs enabled by their small size, in combination with the reactor design parameters, provides a large degree of freedom. When using all of those degrees of freedom simultaneously, mathematical optimization techniques are a necessity. Hence, a model-based approach for optimization of the design of LED-based photocatalytic reactors is developed. A photocatalytic reaction rate is not only a function of the chemical species adsorbed on the catalytic surface, but also on the rate of photons absorbed by the catalyst. Therefore, an efficient photocatalytic reactor design optimizes both the mass transfer as well as the photon transfer. First, an integrated model is developed that describes the distribution of reactants and photons within an annular LED-based photocatalytic reactor. Second, an objective function, representing a trade-off between capital and operating costs is defined and several design variables related to the reactor dimensions and light sources are optimized simultaneously. Furthermore, the capability of the LED-based photocatalytic reactor in controlling the local reaction rate is shown by changing the objective function of the optimization problem. The results demonstrate the importance of model-based optimization to systematically incorporate the inherent trade-offs that exist in the design and operation of LED-based photocatalytic reactors.

A validated process model is essential for optimization. Furthermore, characterization of process trends is needed when developing operational strategies such as automated control. For this purpose, a mini-pilot plant including an annular LED-based photocatalytic reactor has been developed to validate the integrated process model including a radiation field, reaction kinetics, and material balances experimentally for the photocatalytic degradation of toluene. Because water is inevitably present in many photocatalytic applications, a special focus is on the effect of water on reaction kinetics, toluene conversion, mineralization, and catalyst deactivation for

characterization of the process trend. The results from parameter estimation studies demonstrate that a competitive reaction rate model can best describe the experimental data with varying water concentration. Furthermore, experimental results demonstrate that toluene conversion is highest at a low water concentration; however, mineralization and catalyst lifetime are enhanced by the presence of water. The validation of the integrated process model and understanding of the role of water allow for improved design and operation of future LED-based photocatalytic reactors.

Following the conclusion from the process characterization study that electron-hole recombination is dominant in the system, the impact of periodical illumination of LEDs on the photonic efficiency of toluene degradation is investigated. It has been suggested that intermittent introduction of photons on the catalytic surface can possibly reduce the electron-hole recombination and, consequently, can improve the photon utilization of the photocatalytic process during operation. Therefore, the impact of light/dark periods and duty cycles is studied. However, no transition or change in the photonic efficiency when moving from a short to a long light/dark time at a fixed duty cycle is observed experimentally for the system studied in this thesis. Furthermore, the results of the experiments at two different periods show an increase in photonic efficiency with a decrease in the duty cycle. However, the photonic efficiency under controlled periodic illumination, regardless of the duty cycle or period, is found to be similar to that under continuous illumination at an equivalent average irradiance, suggesting no mass-transfer limitations in the system. Therefore, it is concluded that periodical illumination does not improve photon utilization in a system where electron-hole recombination is dominant but there is no mass transfer limitation.

During operation, the performance of an optimally designed reactor may deviate from optimal conditions because of design uncertainties and disturbances acting on the system. Therefore, the application of automated feedback and feedforward controllers to maintain the reactor conversion close to a desired value by adjusting the photon irradiance within a LED-based photocatalytic reactor is studied. The excellent capability of the feedback controller in tracking different conversion set points is shown in the presence of unmeasured and measured disturbances, which allows for a desired conversion of toluene to be maintained. Furthermore, a feedforward controller has been designed based on an empirical steady-state model to mitigate the effect of changing toluene inlet concentration and relative humidity, which are typical measured input disturbances. The results demonstrate that the feedback and feedforward controllers are complementary and can mitigate the effects of disturbances effectively such that the photocatalytic reactor operates close to the desired output at all times. This study delivers the first example of how online analytical technologies can be combined with “smart” light sources such as LEDs to implement automated process control loops that optimize photon utilization. Future work may expand on this concept by developing more advanced control strategies and exploring applications in different areas.

This thesis focuses on the development and validation of methods that provide optimal photon utilization within an annular LED-based photocatalytic reactor for design and operation. However, the proposed approaches and findings of this work can in principle be applied to different configurations of LED-based photocatalytic reactors as well. In addition, the

suggested mathematical model in this thesis can be applied as a useful tool for the prediction of mass and photon transfer rate during scale-up studies of LED-based photocatalytic reactors. Furthermore, the developed control structures can be transferred to a larger scale since control structures are generally known to scale-up well. Providing approaches for optimum photon utilization, the outcome of this thesis could facilitate the realization of more economically viable photocatalytic processes when transferring the technology from lab-scale to the industrial applications.

Samenvatting

Fotokatalyse omvat de absorptie van fotonen door een halfgeleider om chemische reacties te versnellen. Voorbeelden van belangrijke toepassingen zijn de afbraak van gevaarlijke chemicaliën, reductie van koolstofdioxide tot waardevolle chemicaliën en (gedeeltelijke) oxidatie van koolwaterstoffen. Ondanks vele succesvolle demonstraties van deze technologie op laboratoriumschaal, is de industriële toepassing ervan gehinderd door de lage efficiëntie van het gehele proces als gevolg van verschillende uitdagingen die nog moeten worden opgelost. Een van de belangrijkste uitdagingen is het efficiënte gebruik van licht in een fotokatalytische reactor. Vooral bij het gebruik van kunstmatige lichtbronnen beïnvloedt dit de economische haalbaarheid van het proces.

De mogelijkheid om UV-LEDs te gebruiken als een alternatieve lichtbron in plaats van conventionele UV-lampen, zoals kwik- en xenonlampen, is in de afgelopen jaren aangetoond voor toepassingen in de gas- en vloeistoffase. Strategieën die een optimale benutting van het licht in op LED gebaseerde reactoren mogelijk zouden maken tijdens het ontwerp en de bedrijfsvoering ontbreken desalniettemin. Daarom ligt de aandacht van dit proefschrift op het efficiënte gebruik van fotonen door middel van de ontwikkeling en de validatie van een nieuwe benadering voor het ontwerp, de optimalisatie en de regelbaarheid van op LED gebaseerde fotokatalytische reactoren. De fotokatalytische afbraak van tolueen in de gasfase wordt gebruikt als de modelreactie, omdat tolueen een van de meest voorkomende verontreinigende stoffen binnenshuis is die de volksgezondheid bedreigt.

De flexibele positionering van LEDs biedt in combinatie met de ontwerpparameters van een reactor een grote mate van vrijheid in de ontwerpfase van een op LED gebaseerde reactor dankzij het kleine formaat van LEDs. Wiskundige optimalisatietechnieken zijn noodzakelijk wanneer al deze vrijheidsgraden tegelijk worden gebruikt. Daarom is een modelgebaseerde benadering voor de optimalisatie van het ontwerp van op LED gebaseerde fotokatalytische reactoren ontwikkeld. De snelheid van een fotokatalytische reactie is niet alleen afhankelijk van de hoeveelheid chemicaliën die op het katalytische oppervlak zijn geadsorbeerd, maar ook van de snelheid waarmee fotonen door de katalysator worden geabsorbeerd. Daarom optimaliseert een efficiënt ontwerp van een fotokatalytische reactor zowel de massa-overdracht als wel de fotonenoverdracht. Een geïntegreerd model wat de verdeling van reactanten en fotonen binnen een op LED gebaseerde ringvormige fotokatalytische reactor beschrijft wordt eerst ontwikkeld. Daarna wordt een doelfunctie gedefinieerd die een afweging tussen kapitaal- en bedrijfskosten beschrijft en worden verschillende ontwerpvariabelen die gerelateerd zijn aan de reactorafmetingen en lichtbronnen tegelijkertijd geoptimaliseerd. Verder wordt de mogelijkheid om een lokale reactiesnelheid te regelen in de op LED gebaseerde fotokatalytische reactor aangetoond door de doelfunctie van het optimalisatieprobleem te veranderen. De resultaten tonen het belang van modelgebaseerde optimalisatie aan om systematisch de inherente compromissen die bestaan in het ontwerp en de bedrijfsvoering van op LED gebaseerde fotokatalytische reactoren af te wegen.

Een gevalideerd procesmodel is essentieel voor optimalisatie. Verder is karakterisering van procestrends noodzakelijk voor het ontwikkelen van operationele strategieën zoals geautomatiseerde besturing. Daarom is een opstelling op laboratoriumschaal ontwikkeld met een ringvormige op LED gebaseerde fotokatalytische reactor om het geïntegreerde procesmodel inclusief een stralingsveld, reactiekinetiek en materiaalbalansen experimenteel te valideren voor de fotokatalytische ontleding van tolueen. Omdat water onvermijdelijk aanwezig is in vele fotokatalytische toepassingen, is een speciale aandacht gericht op het effect van water op de reactiekinetiek, tolueenomzetting, mineralisatie en het deactiveren van de katalysator voor het karakteriseren van de procestrends. De resultaten van de studies om parameters te schatten tonen aan dat een model met een concurrerende reactiesnelheid de experimentele waarnemingen het beste kan beschrijven als de waterconcentratie varieert. Bovendien tonen de experimentele resultaten aan dat de omzetting van tolueen het hoogst is bij een lage waterconcentratie. Mineralisatie en de levensduur van de katalysator worden echter verbeterd door de aanwezigheid van water. De validatie van het geïntegreerde procesmodel en het inzicht in de rol van water zorgen voor een verbeterd ontwerp en gebruik van toekomstige op LED gebaseerde fotokatalytische reactoren.

Na de conclusie uit de studie over de karakterisering van het proces dat de recombinatie van elektronen en gaten dominant is in het systeem, wordt de invloed van periodieke verlichting van LEDs op de fotonische efficiëntie van tolueenafbraak onderzocht. Er is gesuggereerd dat intermitterende belichting van het katalytische oppervlak met fotonen mogelijk de recombinatie van elektronen en gaten kan verminderen en dientengevolge het gebruik van fotonen tijdens de bedrijfsvoering van een fotokatalytische proces kan verbeteren. Daarom wordt de invloed van afwisselende perioden van licht en donker en verschillende cycli bestudeerd. Er is echter geen overgang of verandering in de efficiëntie van de fotonen bij het veranderen van een korte naar een lange licht/donker tijd bij een vaste cyclus experimenteel waargenomen voor het systeem dat in dit proefschrift is bestudeerd. Verder tonen de resultaten van experimenten met twee verschillende perioden een toename in de fotonische efficiëntie als de werkcyclus afneemt. De fotonische efficiëntie onder gecontroleerde periodieke verlichting, ongeacht de cyclus of periode, blijkt echter vergelijkbaar te zijn met die onder continue verlichting bij een gelijkwaardige gemiddelde bestralingssterkte, wat suggereert dat er geen beperkingen in massa-overdacht in het systeem zijn. Daarom wordt geconcludeerd dat periodieke verlichting het gebruik van fotonen niet verbetert in een systeem waarbij de recombinatie van elektronen en gaten dominant is, maar er verder geen beperking van de massa-overdracht is.

Tijdens bedrijfsvoering kan de prestatie van een optimaal ontworpen reactor afwijken van optimale omstandigheden vanwege ontwerponzekerheden en storingen die op het systeem inwerken. Daarom wordt de toepassing van geautomatiseerde feedback en feedforward regelsystemen bestudeerd om de conversie van tolueen in de reactor dicht bij een gewenste waarde te houden door middel van het aanpassen van de fotonbestraling in een op LED gebaseerde fotokatalytische reactor. Het uitstekende vermogen van het feedback regelsysteem om verschillende gewenste conversies te volgen wordt getoond in de aanwezigheid van ongemeten en gemeten verstoringen. Dit maakt het mogelijk om een gewenste conversie van tolueen te behouden. Verder is een feedforward regelsysteem ontworpen op basis van een

empirisch steady-state model om het effect van veranderende inlaatconcentraties van tolueen en relatieve vochtigheid, wat typisch gemeten verstoringen zijn, te verminderen. De resultaten tonen aan dat de feedback en feedforward regelsystemen complementair zijn en dat de effecten van verstoringen effectief kunnen worden verminderd, zodanig dat de fotokatalytische reactor te allen tijde dicht bij het gewenste gedrag werkt. Deze studie levert het eerste voorbeeld van hoe online analytische technologieën kunnen worden gecombineerd met "slimme" lichtbronnen zoals LEDs om geautomatiseerde regelsystemen te bewerkstelligen die het gebruik van fotonen optimaliseren. Toekomstig werk kan dit concept verder uitbreiden door meer geavanceerde regelsystemen te ontwikkelen en toepassingen in andere gebieden te verkennen.

Dit proefschrift richt zich op de ontwikkeling en validatie van methoden die zorgen voor een optimaal gebruik van fotonen in een op LED gebaseerde ringvormige fotokatalytische reactor voor het ontwerp en de bedrijfsvoering. De voorgestelde aanpak en bevindingen uit dit werk kunnen echter in principe ook worden toegepast op andere configuraties van op LED gebaseerde fotokatalytische reactoren. Daarnaast kan het wiskundige model wat is voorgesteld in dit proefschrift ook worden toegepast als een nuttig hulpmiddel voor de voorspelling van de snelheid van massa- en fotonenoverdracht in opschalingsstudies van op LED gebaseerde fotokatalytische reactoren. Verder kunnen de ontwikkelde regelsystemen ook op een grotere schaal worden toegepast, omdat het algemeen bekend is dat de structuur van regelsystemen ook goed op een grotere schaal toegepast kan worden. De uitkomst van dit proefschrift kan de realisatie van economisch haalbare fotokatalytische processen bevorderen tijdens het vertalen van de technologie van een laboratoriumschaal naar industriële toepassingen dankzij de benadering die leidt tot een optimaal gebruik van fotonen.

Chapter 1. Introduction

This chapter is Partially adopted from: F. Khodadadian, M. Nasalevich, F. Kapteijn, A.I. Stankiewicz, R. Lakerveld, J. Gascon, CHAPTER 8 Photocatalysis: Past Achievements and Future Trends, Alternative Energy Sources for Green Chemistry, The Royal Society of Chemistry 2016, pp. 227-269.

1.1 Background

Heterogeneous photocatalysis is receiving much attention for its promise to enable more efficient and sustainable chemical processes. In 1972, Fujishima and Honda reported the observation that water could be split on an irradiated TiO_2 electrode in a photo-electrochemical cell [1]. Thereafter, much research has been conducted on hydrogen production via water splitting with heterogeneous photocatalysis to convert solar energy to fuel. Later studies demonstrated that organic and inorganic compounds can be oxidized with illuminated semiconductors in both liquid and gas phases [2]. More recently, photocatalysis has been successfully applied to degrade a large variety of organic contaminates including alkanes, alcohols, carboxylic acids, alkenes aromatics, phenols, dyes and pesticides [3-5]. The possibility of full mineralization of pollutants to harmless compounds has raised much interest from academia and industry. Moreover, heterogeneous photocatalysis can degrade very low concentrations of pollutants. Therefore, heterogeneous photocatalysis is expanding rapidly as one of the main so-called *advanced oxidation technologies* (AOT) for water and air purification. Also, the demand for renewable energy resources is increasing dramatically due to depleting fossil fuels reservoirs and enhanced global warming from CO_2 emissions. Since the late 70s, a renewed interest has been raised to the reduction of carbon dioxide over a photocatalyst as one of the promising solutions to convert harmful CO_2 to valuable chemicals such as methanol and acetaldehyde [6-11]. Although significant progress has been achieved, the process efficiency of CO_2 reduction remains low and detailed mechanistic insights are lacking, which hampers economic viability.

As with any heterogeneous catalytic process, the conversion of chemicals with heterogeneous photocatalysis follows several steps: 1) reactants transfer from bulk to the catalyst surface, 2) reactants adsorb on the catalyst surface, 3) conversion of reactants on the catalyst surface, 4) desorption of products from the catalyst surface, 5) products transfer from the catalyst surface to the bulk. An important difference in heterogeneous photocatalysis is the method of catalyst activation. A photocatalytic process is driven by photon absorption to provide the required energy for the reduction-oxidation reaction. In general, semiconductors can be suitable photocatalysts as they can absorb a photon with energy equal or higher than the band gap of the semiconductor, which excites an electron from the valence band to the conduction band. Simultaneously, a hole (i.e., a positive charge) is generated in the valance band of the semiconductor. Subsequently, the photo generated electron-hole pair migrates to the catalyst surface where they either recombine or initiate chemical reactions with the reactants adsorbed on the surface of the semiconductor. The most widely used semiconductor is titania, which needs light in the ultraviolet or near ultraviolet range to excite electrons.

Features of heterogeneous photocatalysis that can make it a suitable alternative for implementation of redox reactions are a) availability of cheap semiconductors such as TiO_2 as catalyst; b) mild reaction conditions c) ability to use solar energy directly, d) possibilities for applications in both liquid and gas phases. However, industrial applications of photocatalysis require scalable photocatalytic reactors with high efficiency, which remains notoriously challenging. Improving the efficiency of a photocatalytic process requires both the development of more efficient photocatalysts and reactor equipment.

Several design challenges exist for photocatalytic reactors. First, an efficient photocatalytic reactor needs to optimize the mass transfer of reactants and products. Second, a major challenge in design of a photocatalytic reactor is efficient catalyst illumination [12]. The former challenge is not unique for photocatalytic reactors, but applies equally well to any other catalytic reactor. However, the latter challenge complicates the design of photocatalytic reactors compared to conventional catalytic reactors. The source of photons for a sustainable photocatalytic process can either be directly from the sun or, indirectly, via conversion to electricity and subsequent use of artificial lights. In any case, effective photon utilization within the reactor is important for economic feasibility. Scale up of a photocatalytic reactor is a complex process, which has to take into account many factors including providing high catalyst surface area that is illuminated with an optimal profile as well as dose and allows for high mass transfer of reactants and products. Despite important research efforts and significant progress, the development of photocatalytic processes for commercial purposes has been hindered by the scale-up complexities [13]. Fundamental research to develop improved photocatalysts and novel design methods for improved reactor equipment that would provide a higher effective utilization of photons is needed to enable future sustainable chemical processes that are driven by photocatalysis.

In the next section, current state-of-art and challenges in the design of photocatalytic reactors are discussed including alternative options for light source to enhance efficiency.

1.2 Challenges in design, modelling and optimization of photocatalytic reactors

A photocatalytic reactor has to bring the reactants in an effective contact with the catalysts and facilitate effective photon absorption of the catalyst. The details of reactor geometry and integration of a light source within the reactor design are, therefore, highly important. When using artificial light sources, the main expenses of the process are related to the light source (electricity, maintenance) [14]. The key challenge for design is to integrate the photocatalyst and light source in such a way that each part of the catalyst receives the optimal number of photons with the right amount of energy, which complicates scale up and optimization.

Considerable numbers of different designs have been proposed by different research groups [15] of which some of the proposed designs are empirically developed [16]. The design of photocatalytic reactors using rigorous mathematical models has been done mainly during the last two decades [17-25]. Mathematical models are efficient tools to analyse and optimize chemical reactors at different scales. Studies on the mathematical modelling of photocatalytic reactors with integrated modelling of a radiation field have demonstrated high potential [17, 26, 27]. The complexity of such integrated models poses significant challenges for analysis and rigorous optimization for design. Furthermore, many degrees of freedom are available due to the large variety of designs, method for catalyst preparation, catalyst material, operation conditions, radiation intensity, and light sources, which makes it difficult to optimize the performance of different photocatalytic reactors. In general, photocatalytic reactors can be categorised in two main configurations based on the manner in which the photocatalyst has been deployed: 1) a reactor with suspended photocatalytic particles and, 2), a reactor with an

immobilized catalyst on an inert substrate. Within those categories numerous variations exist of which a number of common configurations are described below.

1.3 Suspended system

In a suspended system, the catalyst is immobilized on an inert support that can be fluidized such as, for example, glass beads or sand grains. Suspended systems normally operate at higher catalysts loading compared to most other photocatalytic reactors, where the catalyst is coated on the reactor wall, since they utilize the whole volume rather than just a surface [28]. Subsequently, the number of available catalyst active sites per unit of reactor volume is higher resulting in an efficient contact between reactant and catalyst with excellent mass transfer characteristics. Although there is typically no external mass transfer resistance in suspended system, there are other limitations such as internal mass transfer, mainly due to particle agglomeration [29]. In addition, achieving a uniform light distribution within this system is difficult, because the particles that are close to the light source shield the particles that are further away. Therefore, when catalyst particles are suspended in the solution, the depth of light penetration is limited [13, 28, 30, 31]. The aforementioned limitations make it difficult to design a suspended reactor for large-scale applications. Slurry and fluidized bed reactors are two examples of suspended systems that are used for photocatalytic applications.

Slurry photocatalytic reactors have shown great potential to degrade contaminants in aqueous solution [32, 33] and to oxidize liquid hydrocarbons [34-36]. However, the separation and recycling of very fine catalyst particles from the treated stream remains a major disadvantage of this reactor type [32]. Post separation of catalyst particles from the reactor effluent is necessary to prevent attrition of catalyst and, consequently, the introduction of new pollutants, which may make the operation of slurry reactors expensive and troublesome [13,38].

In a fluidized bed reactor, a fluid (gas or liquid) flows upward in the reactor resulting in suspension of catalyst particles. The fluid velocity should be chosen such that the particles are suspended but are not carried out of the vessel. A fluidized bed reactor has the ability to process large volumes of fluid with a low-pressure drop. However, the success of this reactor type depends on the adequate attachment of the photocatalyst to the supporting particles, because of attrition of the photocatalyst particles by the flowing stream [39]. Figure 1.1 shows a schematic diagram of a bench-scale fluidized-bed that was used to degrade trichloroethylene in a polluted air stream by Dibble and Raupp [40]. TiO_2 as the photocatalyst was supported on silica gel, which formed a TiO_2-silicagel. In order to reduce the momentum of the catalyst particles and to prevent them from leaving the reactor with the fluid stream, the top of reactor was designed in such a way that the cross-sectional area was 125% larger compared to the cross-sectional area in the lower part of the reactor.

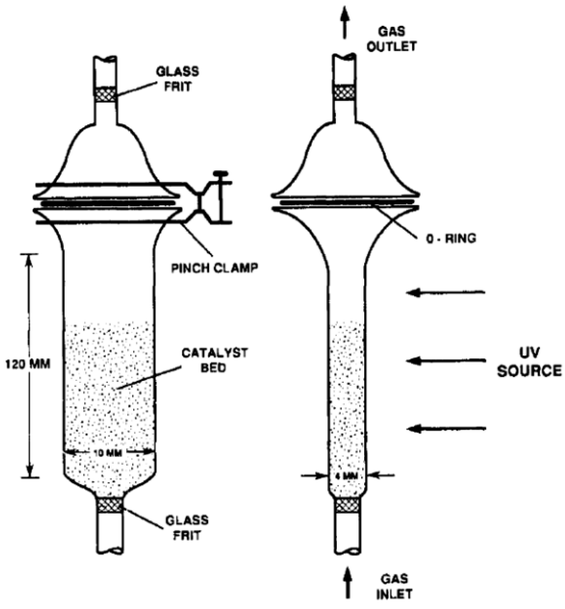

Figure 1.1. Schematic diagram of the fluidized-bed reactor used by Dibble and Raupp [40]

1.4 Immobilised systems

1.4.1 Flat plate

Flat plate reactors have been widely used for heterogeneous photocatalysis studies due to the simplicity of design and ease of operation [41, 43]. Flat plate reactors contain typically two flat plates, which are placed at a certain distance from each other forming a channel through which the fluid passes. The catalyst is coated either only on the interior surface of one the plates or on both of them depending on the position of the external or internal light source for illumination of the catalyst surface. Flat plate reactors usually provide a relatively low catalyst surface area and poor photon utilization [14, 44]. An example of a flat plate photocatalytic reactor used by Estivill et al. [45] is illustrated in Figure 1.2.

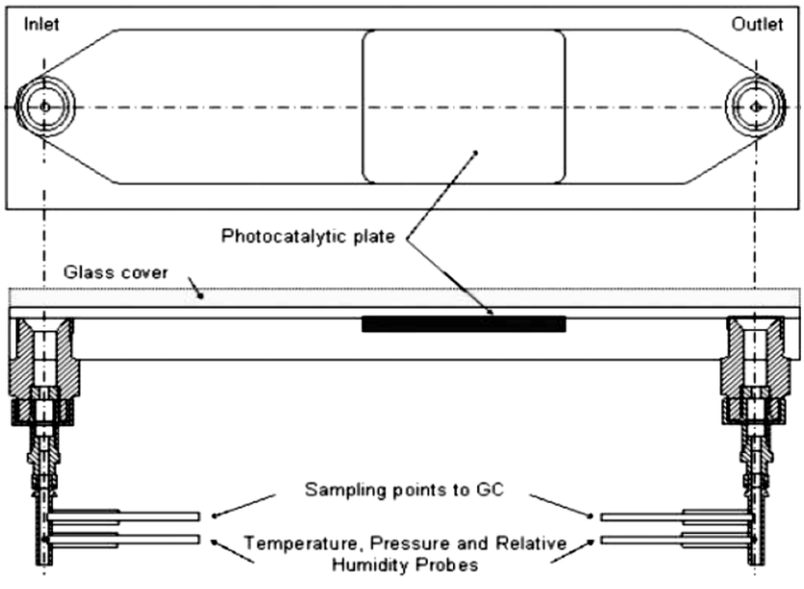

Figure 1.2. Schematic diagram of flat plate photocatalytic reactor used by Estivill et al. [45]

1.4.2 Honeycomb monolith photocatalytic reactor

Honeycomb monolith photocatalytic reactors have been widely used for the emission control of automobile exhaust and for NOx reduction in power-plant flue gases [46]. Typically, honeycomb structures consist of several channels with an internal diameter of about 1mm while the cross-sectional shape of the channels are normally square or circular. The catalyst is usually coated on the walls of the channels as a thin film. In order to achieve an energy efficient design, investigations have been conducted on the mathematical modelling of mass, momentum and radiation transfer within photocatalytic monolith reactors [26, 46, 47]. The main advantages of this design are a large ratio of the catalyst surface area over the reactor volume and a low pressure drop. Moreover, the scale-up of the monolithic reactor can be done simply by expanding the number of channels [46]. However, insufficient radiation on the catalyst surface through honeycomb channels might result in a low reaction rate and, therefore, low process efficiency [12, 49]. An example of a monolith reactor for photocatalytic oxidation of formaldehyde as used by Raupp et al. [26, 46] is shown in Figure1.3.

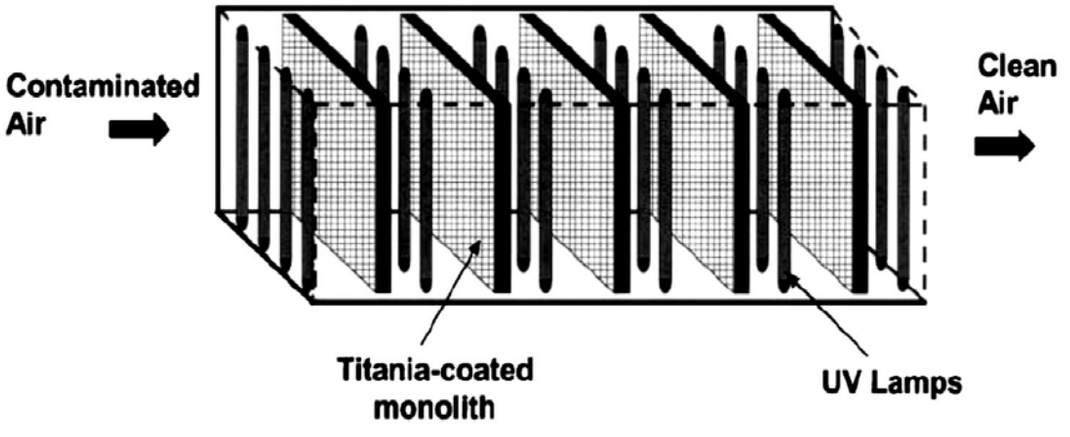

Figure 1.3. Schematic diagram of the monolith reactor used by Raupp et al. [46]

1.4.3 Optical fiber photocatalytic reactors

Marinangeli and Olis proposed the concept of applying optical fibers as both a support for catalyst immobilization and as a light-distributing guide for photocatalysis [50, 51]. Light travels through the optical fiber by reflection on the fiber wall. In a photocatalytic reactor constructed from such optical fibers, the light beam striking the inner wall of fiber splits into two parts: one part is absorbed by the catalyst layer coated on the fiber and the remaining light is reflected internally and transmitted along the fiber (see Figure 1.4(a)). This phenomenon repeats itself along the fibers resulting in the gradual distribution of photons along the reactor length [48].

The advantages of such a reactor are the more even distribution of light that can be achieved, a large allowable distance between light source and catalyst, and a versatile design in the number of fibers and the distance between them. Furthermore, the back illumination of catalyst allows no loss of photons due to the scattering or absorption by the reacting medium [52]. However, the back illumination of photocatalyst might result in the generation of electron-holes far from

the interface of the catalyst and reacting medium, which increases the possibility for recombination of generated electrons and holes before a reaction can occur [53]. Moreover, the optical fibers usually occupy around 20-30% of the reactor space while supplying relatively low surface area of the catalyst surface [54]. Consequently, the flow rate decreases due to an increase in pressure drop [12]. Oxidation of acetone in an optical fiber photocatalytic reactor employing bare quartz fibers as TiO_2 support was investigated by Choi et al [53]. Their results showed a 90% reduction of the intensity of light within 30 cm of a fiber coated with TiO_2, which reveals an exponential decay in the light intensity. Figure 1.4 (b) shows an example of an optical fiber photocatalytic reactor for CO_2 reduction to methanol, which was investigated by Nguyen et al. [55].

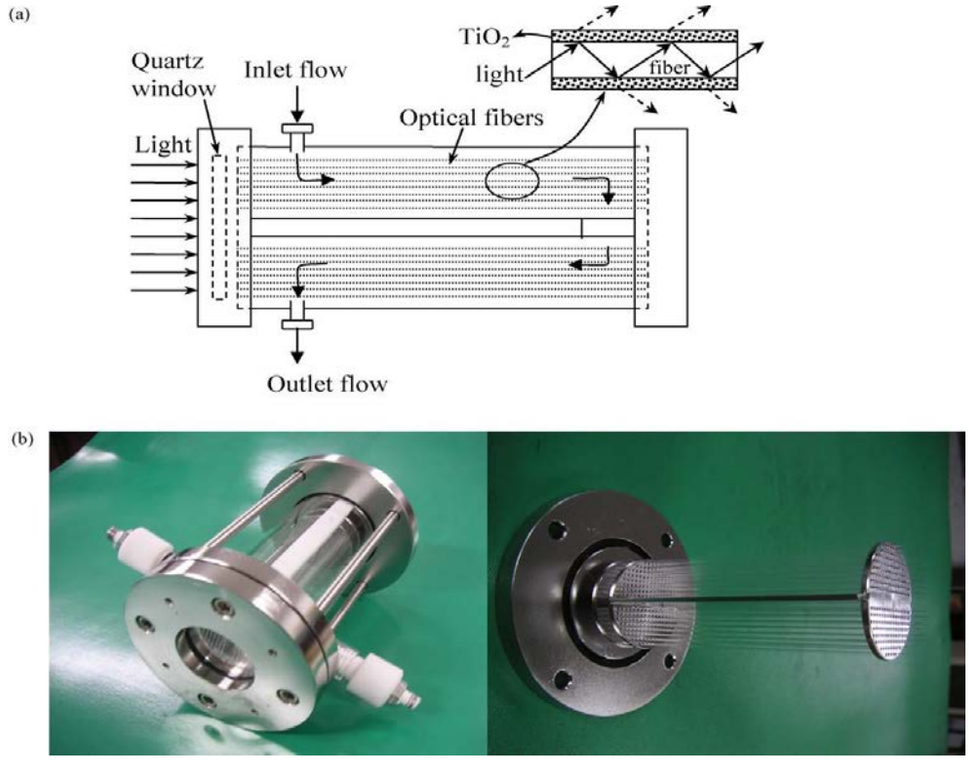

Figure 1.4 (a) Schematic diagram (b) and images of photoreactor with catalyst coated optical fibers. By Nguyen et al. [55]

Lin et al. [48] proposed an optical fiber monolith reactor for waste water treatment. They used a ceramic multichannel monolith as a support for the photocatalyst. They inserted the bare quartz fiber optics as both a light guide and catalyst support into the monolith channels. The reactor performance was tested for degradation of *o*-dichlorobenzene in water. They found an optimum photocatalyst film thickness of 0.4 µm coated on the fibers. This configuration provides a higher photocatalyst surface area compared to an optical fiber reactor. However, the short length of light propagation still remains as a disadvantage due to the exponential decay of light along the fiber optics. Du et al. [54] modified the proposed design by Lin et al. by using "side light" optical fibers instead of normal optical fibers to improve the photon utilization inside the monolith channels (Figure 1.5). Another difference is that they did not coat the fiber wall with photocatalyst to prevent the light attenuation at the interface of catalyst-reactant. TiO_2 was coated on the inner walls of the monolith channels by a wash coating method. The internally

illuminated photocatalytic monolith reactor was tested for photocatalytic oxidation of cyclohexane.

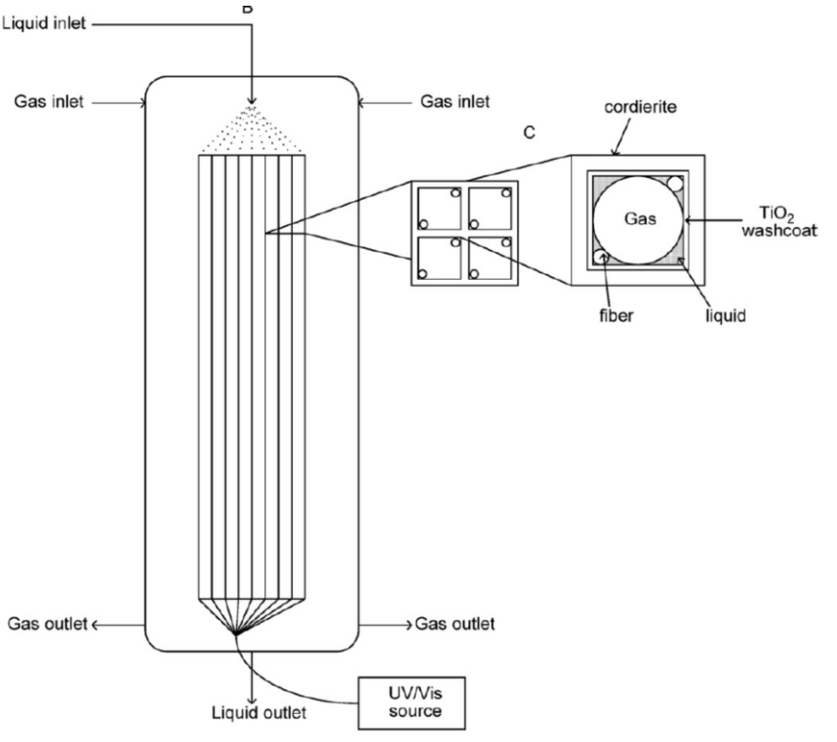

Figure 1.5 Schematic diagram of internally illuminated monolith photocatalytic reactor [54]

1.4.4 Annular reactors

In an annular reactor, the fluid flows through an annulus region that is bounded by two concentric pipes that have different diameters. The light source may be positioned either at the centre of the reactor or on the outside of the reactor. The walls of the tubes are coated with a layer of photocatalyst. The layer thickness should be thin enough to allow for the photons to illuminate the entire catalyst surface. Similar to the flat plate type of reactor, annular photocatalytic reactors offer a relative low reaction surface [31]. However, an annular geometry offers the advantage of a homogenous light distribution over the catalyst surface and, consequently, optimum photon utilization. In addition, it is possible to approach plug flow in the annular geometry, which make this reactor type ideal for studies of the kinetics of photocatalytic reactions [57]. Due to the simple design and operation, annular reactors are the most widely applied photocatalytic reactors for photocatalytic studies [58]. Figure 1.6 shows an annular flow reactor used by Imoberdorf et al. [59-61]. They proposed a scaled up multi-annular photocatalytic reactor for the degradation of pollutants in air stream. Their design is composed of four, 177 cm long, concentric pipes of borosilicate glass while the UV-lamp is located at the center. The interior walls of each annulus unit are coated by TiO_2, which provides an active surface area of 5209 cm^2. Such surface area shows a significant increase compared to the laboratory reactor of 81cm^2 active catalyst surface area tested by the same research group. The multi-annular photocatalytic reactor was modelled based on mass, momentum and radiation balances. The results predicted by the model were in good agreement with experimental results.

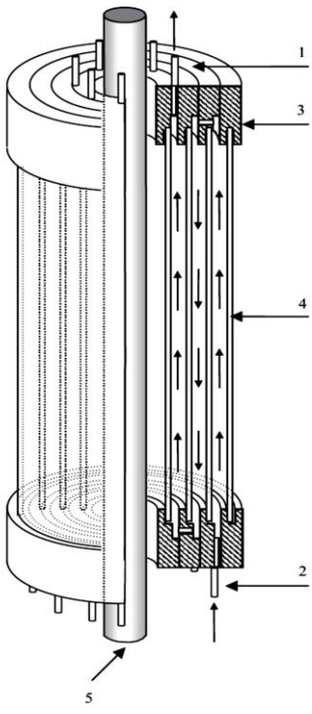

Figure 1.6. Schematic diagram of the annular reactor used by Imoberdorf et al. [61]

1.4.5 Packed bed photocatalytic reactors

A packed bed photocatalytic reactor is composed of a vessel that contains immobilized catalytic particles. The light sources can be located inside or outside of the reactor. The fluid, including reactants, contacts the illuminated catalyst particles. Quartz and borosilicate glass, which are transparent to UV light, are often used as the packing material. The catalyst is coated as a layer on the catalyst particles, which should be thin enough to allow transmission of a fraction of the UV radiation to the particles that are located further away from the UV source. Consequently, the bed volume can be activated up to a certain depth by the light source. Therefore, the light absorption factor of the catalyst layer is one of the key factors for the design of packed bed photocatalytic reactors. Guidelines to design pack-bed photocatalytic reactors have been proposed including cost analysis [62]. Raupp et al. developed a mathematical model to predict the behaviour of a continuous packed-bed photocatalytic reactor. Their reactor featured a lamp inside the tube as light source for the oxidation of a pollutant in a gas stream. The model includes a radiation field model within the reactor[19]. The constraints that this design may have are a low surface area to reactor volume ratio and a non-efficient photon utilization when taking into account both photon absorption and scattering [63, 64]. Figure 1.7 shows a schematic diagram of a (a) single lamp and a (b) multi-lamp packed bed photocatalytic reactor, which was modelled by Alexiadis et al. [62].

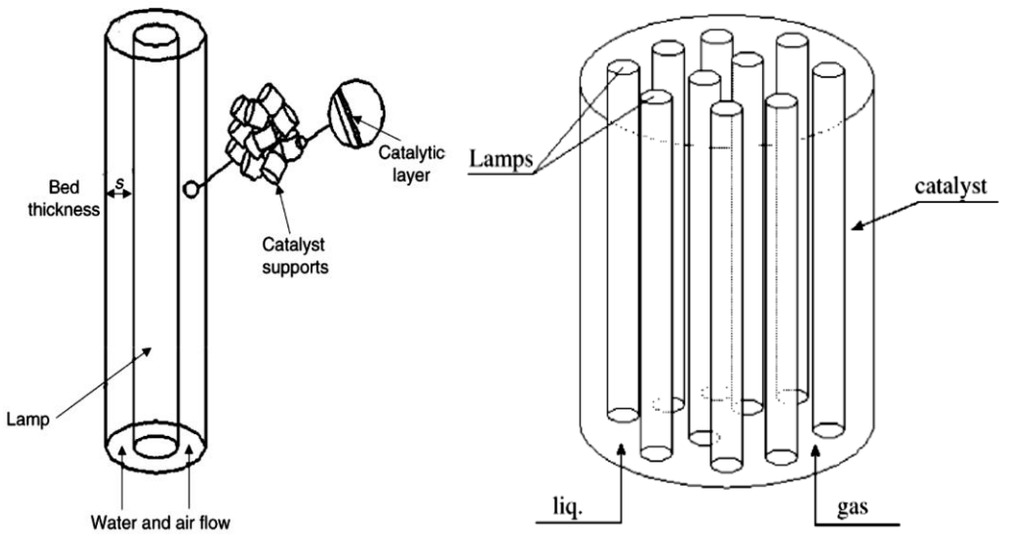

Figure 1.7. Schematic diagram of a (a) single lamp and (b) multi lamp packed bed photocatalytic reactor used by Alexiadis et al. [62]

1.4.6 Microreactors

Microreaction systems have attracted much attention for chemical applications and demonstrated significant promise in a wide range of chemical transformations [65]. Microreactors offer a small molecular path for mass transport, fast mixing times, laminar flow conditions, and a large specific surface area, which favours fast heat transfer. Microreactors also have a great potential for catalytic applications because of their large surface to volume ratio. The ratio of the irradiated surface area of catalyst to reactor volume is one of the crucial factors in the design of a photocatalytic reactor. A microreactor can provide a specific surface area of about 1.4×10^4 m^2 m^{-3} [66], which is much larger than the typical irradiated specific surface area of conventional photocatalytic reactors [67]. Another advantage of micro-photocatalytic reactors is that a small light source, and therefore lower radiation cost, is required for a miniaturized reactor. Several studies have investigated the feasibility of using microreactors for photocatalytic applications [66, 68-74]. Straathof et al. [75] reported construction and operating of a simple microphotocatalytic reactor illuminated with LEDs in the visible light range for gas-liquid applications. The experimental results from the reactor showed a lower reaction time compared to similar reactions conducted in batch reactors, which was most probably due to the improved irradiation efficiency and gas-liquid mass transfer in the segmented gas-liquid flow regime. Figure 1.8 shows a microreactor that was used by Gorges et al. [68] to decompose 4-chlorphenol in water. Their microreactor consisted of 19 channels with a cross-section of 200µm x 300µm. Compared to conventional photocatalytic reactors, the irradiated specific catalyst surface of this microreactor is about 4–400 times larger. Recent studies have shown that numbering-up the photocatalytic microreactors can be also a feasible strategy to increase the system throughput and consequently scaling-up the photocatalytic processes [76, 77].

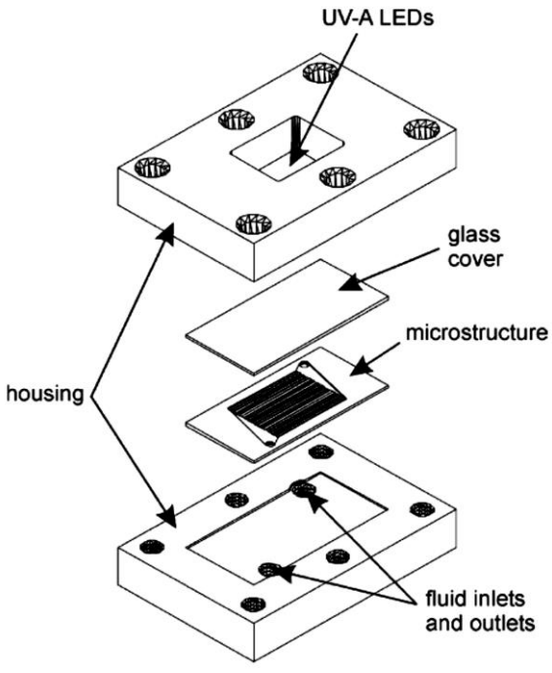

Figure 1.8. Schematic diagram a micro-photocatalytic reactor used by Gorges et al. [68]

1.5 Light sources

The design of the light source for photocatalysis has a key impact on the efficiency of photocatalytic applications. The rate of photocatalytic reactions depends in general on both the concentrations of the reactants and on the rate of photon absorption by the catalyst. The catalyst has to receive photons with a suitable amount of energy over a large area for optimal performance. At low photon intensities, the reaction rate typically increases linearly with increasing the light intensity due to the increased generation of electron-hole pairs [3]. However, upon further increasing the light intensity, the rate of electrons-holes recombination increases faster than the rate of consumption of electron-hole pairs by the chemical reaction [3]. Therefore, careful design of the radiation field within a photocatalytic reactor is important to maximize performance. Such radiation fields within photocatalytic reactors have been analysed by solving the radiative transfer equations (RTE) for different light sources by applying different numerical methods [17, 78-80] including Monte Carlo methods [20, 81-83]. In general, the light sources that have been used to activate a photocatalyst can be categorized in two groups: artificial radiation and solar radiation as described in more detail below.

1.5.1 Solar-based photocatalytic reactors

Since only 4-5% of the solar light that reaches the earth is UV-light, a great deal of research has been conducted on the development of photocatalysts that can be activated with visible light [84]. In addition to the required bandgap, using sunlight as the radiation source imposes geometrical constraints to the design of photocatalytic reactors. Solar-based photocatalytic reactors normally have a flattened geometry and thus need a large footprint [85]. Nevertheless, it is expected that current interests and developments in the application of solar energy for photocatalysis will even further increase due to the abundance and sustainability of solar

energy. The design of solar-based photocatalytic reactors may be based on either an immobilized or suspended catalyst with the option to concentrate solar light before usage. Such concentrated systems use a reflector to direct solar radiation with a solar tracking mechanism. Compared to non-concentrating systems, concentrated systems need a smaller reactor volume for the same light harvesting surface area. Therefore, in construction of the reactor, more expensive materials can be used. However, concentrated solar-based photocatalytic reactors are not able to harvest diffuse UV radiation, which is of importance especially on cloudy days. Even on a clear day, approximately 50% of the UV light that reaches the earth includes diffuse UV light [86], which limits the effectiveness of concentrating solar energy.

Non-concentrating solar photocatalytic reactors - whether using a reflector or not - are static systems. They are less expensive to construct and easier to operate compared to concentrating solar photocatalytic reactors [87]. Moreover, they can collect both direct and diffuse UV radiation. Although the collection of solar energy is less efficient due to the absence of concentration, the overall efficiency is normally higher compared to concentrating reactors due to the lower rate of electron-holes recombination at lower radiation intensities [3]. Furthermore, the optical loss is lower compared to the concentrating reactors, especially if no reflective surface is used [88]. However, a much larger photocatalytic surface area is needed compared to concentrating systems and, consequently, the material to build such a reactor should be relatively inexpensive [88]. However, inexpensive materials such as certain types of plastics typically cannot be used at high pressures. Non-concentrating solar reactors operate usually at laminar flow, while turbulent flow is more favourable in the term of mass transfer efficiency [89]. Some important additional design features of solar photocatalytic reactors are described below.

Parabolic through reactors (PTRs) are an example of a concentrating solar photocatalytic reactor, which consist of parabolic reflectors that concentrate the solar light on a tube located in the centre of a parabola (Figure 1.9). The stream including reactants flows through a tube, which allows for plug-flow behaviour. The reactor size is small and the radiation intensity per reactor volume is high [90]. However, compared to non-concentrating reactors, PTRs are relatively expensive while the optical and quantum efficiency is lower [90]. PTRs have been used to degrade different pollutants in water successfully [91-94]. Compound parabolic concentrator reactors (CPCR) are trough reactors, but with low solar light concentration properties [95]. This type of reactor has static reflectors, which differs from a PTR reflector. The reflector of a CPCR usually consists of two parabolas, which are positioned side by side. The focal line is above the connection line of two parabolas. This geometry allows for the collection of light beams from almost every direction to be concentrated on the focal line. CPCRs combine the characteristics of both concentrating and non-concentrating reflectors: they concentrate the solar light while they are static and collect the direct UV radiation as well as diffuse UV radiation. Figure 1.9 (a) and (b) show the reflector profile and schematic diagram of PTRs and CPCRs. The performance of PTRs and CPCRs were investigated in degradation of different compounds in water [92, 96-98]. Results showed that CPRC performance is more efficient for photocatalysis application compared to PTRs.

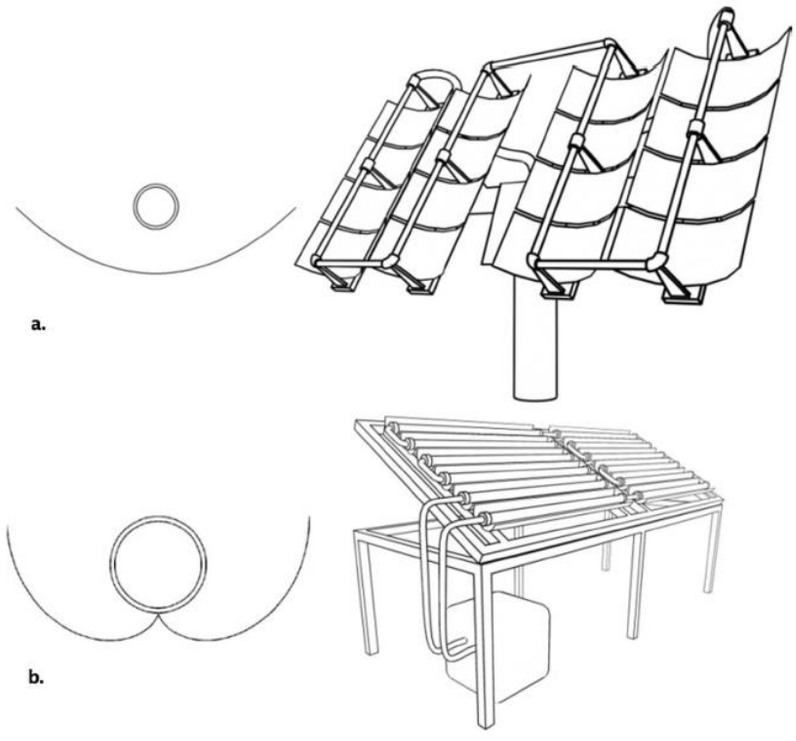

Figure 1.9 Reflector profile and schematic diagram of a (a) parabolic trough reactor (PTR) and (b) compound trough reactor (CPCR) [98].

Thin-film fixed-bed reactors (TFFBR) are one of the first non-concentrating solar photocatalytic reactors. They generally consist of inclined plates that are coated with a thin film of photocatalyst. The feed stream flows over the catalyst plate as a thin layer [88]. Figure 1.10 (a) shows a schematic drawing of a TFFBR. The efficiency of a TFFBR and a PTR has been compared in some studies [88, 89]. Results showed that TFFBRs are more efficient compared to PTRs for the same operating conditions. Moreover, the cost of construction and operation of a TFFBR is considered to be lower than that of a PTR [88].

A new type of non-concentrating solar photocatalytic reactor is the so-called double sheet skin photocatalytic reactors (DSSR) [99, 100]. This reactor is made of a transparent box of Plexiglass® including several channels (Figure 1.10 (b)). Some types of Plexiglass® are able to transmit the direct and diffuse UV light with wavelengths shorter than 400 nm. The flow including suspended catalyst and reactants is pumped into the channels. Dillert et al. [101] studied a DSSR for the degradation of a biological pollutant in water. They found that to degrade 1 m^3 of contaminated water per day, 50 m^2 of the radiated reactor surface is needed to reach the 90% conversion when applying suspended TiO_2 (P25) as a catalyst.

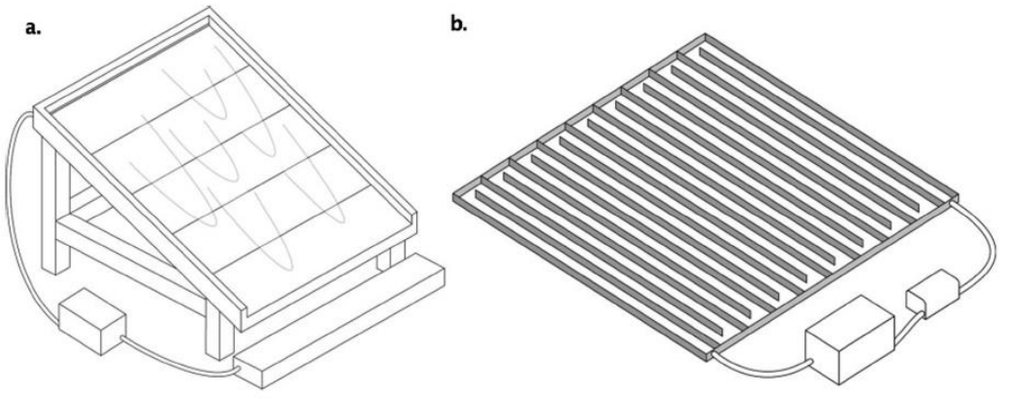

Figure 1.10 Schematic diagram of a (a) thin film fixed bed photocatalytic reactor (TFFBR) and (b) double skin sheet reactor (DSSR)[88].

1.5.2 Artificial light sources

Although many efforts have been made to develop photocatalysts that can harness visible light, TiO_2 is still the most frequently used photocatalyst, which requires ultraviolet (UV) light to be activated. Artificial UV-light sources offer independence of location, weather, and the daytime. However, additional costs in the form of investments, maintenance, and electricity are required when using artificial light sources. In addition, the design of a reactor irradiated by an artificial light source is restricted by the geometry and the size of the light source. Nevertheless, the design of a photocatalytic reactor with an artificial light source can be based on a smaller footprint compared to using solar light. Furthermore, artificial lights can provide a narrower spectrum of light that better matches the requirements of the photocatalyst compared to solar light.

Classical UV lamps have been used for laboratory and commercial photocatalytic applications. There are several studies dedicated to the analysis and modeling of the radiation field within a reactor based on conventional lamps as the light source [17]. Such lamps have usually a cylindrical shape and are based on mercury discharge or fluorescence. Artificial light sources can be classified into two groups: high and low power UV-light sources. High power UV sources, such as medium and high-pressure mercury lamps, generate high intensities of UV light, which can intensify the reaction. However, the quantum yield of TiO_2 is known to decrease at high radiation intensities [85]. Therefore, the high power UV sources are usually not favoured in photocatalytic applications [3]. Using low-power UV light sources, such as fluorescent or low-pressure mercury lamps, will enhance the quantum yields of photocatalysts. For example, Puma et al. [102] compared the performance of low pressure mercury and fluorescent lamp in a falling film photocatalytic reactor for a wastewater treatment process. Their results showed that a mercury lamp was more efficient than a fluorescent lamp. However, the disadvantages of a mercury lamp include its fragility, toxicity, short life span (<12000h) and issues relating to the complete life cycle of such a lamp (e.g., concerns for disposal) [103]. Furthermore, the size and shape of these lamps constrains the design of photocatalytic reactors. These drawbacks in addition to the low energy efficiency of conventional UV-lamps have resulted in exploring for alternative UV light sources.

Alternatively, light-emitting diodes (LEDs) can be used for photocatalytic applications. LEDs are semiconductor-based light sources, which emit photons with a narrow spectrum based on electroluminescence effect. The semiconducting material of the LED defines the wavelength of the generated photons, which can be tuned for a specific photocatalyst. LEDs are non-toxic, compact and considering their sizes, can be applied flexibly within a photocatalytic reactor both in terms of space and time, compared to the conventional UV-lamps. In addition, their life span is 5 times higher than UV-mercury lamps. The radiation pattern from LEDs varies based on their design and the light intensity is linearly proportional to the applied electric current. Since their introduction to the market, their photon flux output has improved significantly while their price has dropped [103]. In comparison with conventional UV lamps, integration of a photocatalytic reactor with LEDs can tackle the low energy efficiency of the reactor and result in an economically feasible process.

In the last few years, several studies have reported the feasibility of using UV-LEDs as a light source for photocatalytic applications in both a gas and liquid phase [104-113]. These studies showed that LEDs can be promising alternative light sources for conventional UV lamps. Domiguez et al. [114] compared the energy efficiency of a LED-based photocatalytic reactor and a mercury lamp based photocatalytic reactor for the photocatalytic degradation of sodium dodecylbenzensulfonate in the liquid phase and found that the LED-based photocatalytic reactor was more energy efficient. Levine et al. [107] compared the performance of high-power UV-LEDs and a black light blue (BLB) lamp for the oxidation of ethanol. Their results showed that at an equivalent average irradiance, the LED-irradiated reactor had a lower reaction rate. They concluded that uniformity of the irradiance on the catalyst surface had a great impact on the reaction efficiency. Martin-Somer et al. [115] reached a similar conclusion by comparing the performances of a photocatalytic reactor with LED illumination and illumination with a mercury lamp, which stresses the importance of optimizing the arrangement and design of the light source together with the design of the reactor equipment itself to provide the optimum photon utilization in LED-based photocatalytic reactors. In particular, investigation of the radiation field within an LED-based photocatalytic reactor is needed due to the importance of the rate of photon absorption in the reaction kinetics. However, studies on design of LED-based photocatalytic reactors, which allows for optimum light utilization within the reactor, have been rarely done.

Mathematical models for LED-based photocatalytic reactors have been developed to support design [116-119]. Nevertheless, the spatial and temporal flexibility of LEDs offers many degrees of freedom for design and operation, which not have all been investigated for design of LED-based photocatalytic reactors. Furthermore, when using all those degrees of freedom simultaneously, mathematical optimization techniques are a necessity. Such optimization requires an integrated reactor model, linking photon transfer from LEDs and mass transfer of reactants. However, development and validation of such integrated reactor models for LED-based catalytic reactors has been rarely reported.

In principle, a photocatalytic reaction occurs upon electron-hole pair generation after photon absorption by the electron. The generated electron-hole pair can either contribute in a chemical reaction or recombine again, limiting charge transfer and consequently initiation of chemical

reactions. Hence, electron-hole recombination is believed to be the most important factor contributing in the low efficiency of a photocatalytic reaction [120]. It has been suggested that intermittent introduction of photons on the catalytic surface can reduce the electron-hole recombination and consequently, improve photon utilization of the photocatalytic process during operation [121]. During the last decade, due to their instantaneous and linear response to the power change compared to conventional UV lamps, LEDs have been used in periodic illumination studies, where a series of alternate light and dark periods are applied. However, the mechanism and the effect of controlled periodic illumination on the photonic efficiency have been a controversial subject of research. The original hypothesis for the enhancement of photonic efficiency through Controlled Periodic Illumination (CPI) has been both proved by initial studies [122, 123] and challenged by subsequent studies [124, 125]. Moreover, the effect of controlled periodic illumination has mainly been studied in liquid-phase systems, where mass transfer limitations may be present to a higher extent when compared to gas- phase reactions. In contrast, the effect of controlled periodic illumination in gas-phase systems has rarely been reported [120, 126, 127]. Furthermore, during operation, an optimally designed reactor performance may deviate from optimal condition because of design uncertainties and disturbances acting on the system. Instantaneous and linear response of LEDs to electrical change in combination with on-line analytical technologies can facilitate self-optimizing control units for LED-based photocatalytic reactors. However, no studies on self-optimizing feedback control for LED-based catalytic reactors exist in literature despite its potential to improve the economic performance of photocatalytic reactors.

1.6 Thesis objectives

Photon utilization is one of the crucial factors in determining economic feasibility of a photocatalysis process, when using artificial light sources. Hence, the efforts in developing methods for optimum photon utilization within the reactor may advance this technology one step further toward the larger scale applications. Therefore, the overall objective of this thesis is to develop and validate novel approaches for the design, optimization, and control of LED-based photocatalytic reactors that are all aimed at efficient use of photons within such reactors. To achieve this overall objective, the research questions, which this thesis aims to address, are:

1. Can a photocatalytic reactor model, coupling the radiation field model from LEDs and reaction kinetics, be used for optimization of mass and photon transfer simultaneously in the design of the reactor?

One of the main challenges in design of photocatalytic reactors is simultaneous optimization of mass and photon transfer within the reactor. This calls for a systematic design approach, which should optimize the configuration of a LED array simultaneously with the reactor design to optimize the overall reactor performance. Analysis and optimization of mathematical models for LED-based photocatalytic reactors is needed in combination with the validation of such models.

2. Can a model that integrates a radiation field from LEDs, mass transfer and reaction kinetics be validated? What are the influences of operating conditions on the photocatalytic process trends?

The reactor model validation demands for experimental data and therefore an experimental set-up including an LED-based photocatalytic reactor. The experimental set-up should allow for a broad range of operating conditions to be tested on the reactor's performance, to create rich data sets for the model validation and investigation of the effects of operating conditions on the process trend.

3. Can Controlled Periodic Illumination (CPI) of LEDs be used as a method to achieve optimized photon utilization in the reactor?

It has been suggested that charges (electron-holes) are generated upon absorption of proper photons by the catalyst. However, photons are not required when generated charges undergo chemical reactions as well as adsorption/desorption and diffusion of chemical substrates from or to catalytic surface. Therefore, periodic introduction of photons to the catalytic surface may result in a more efficient photon utilization.

4. Can the controllability of LEDs enhance optimum photon utilization within the reactor further?

The performance of a LED-based photocatalytic reactor may deviate from optimal conditions due to design uncertainty and the presence of external disturbances. Process control is a discipline that provides mechanisms and algorithms for maintaining the output of a specific process within a desired range. In the photocatalytic process the intensity of light on the catalyst surface may be controlled, using a controlled loop over the reactor, to maintain a consistent product output.

1.7 Thesis outline

This thesis contains an introduction and four chapters corresponding to the research questions and a final chapter on the conclusion and opportunities for future studies. A brief summary of the four chapters, which form the main body of this thesis, is given below.

Chapter 2 investigates a mathematical approach to optimize the design parameters of a LED-based photocatalytic reactor. An annular reactor using light source at the centre is selected as the model reactor. Toluene degradation in the gas phase is chosen as the model reaction. The reactor is modelled by momentum, mass and radiation transport balance. An objective function representing the trade-off between capital and operational cost is defined. The optimization is addressed by minimizing the cost model while the optimization is constrained by reaching to a certain conversion. Finally, the optimization results are discussed.

Chapter 3 presents experimental validation of the reactor model that describes the operational performance of a LED-based photocatalytic reactor via a mini-pilot plant including an annular LED-based photocatalytic reactor. The model allows for kinetic parameters to be estimated from experimental data. Furthermore, the experimental setup allows for different flow rates, toluene inlet concentrations, and light intensities to be applied to validate the predictive capabilities of the developed model for a broad range of operating conditions. On the long term, the validation of the proposed model advances the design, optimization and scale-up of future LED-based photocatalytic reactors for various applications.

Chapter 4 examines whether CPI can be used as a method for optimum photon utilization within a LED-based photocatalytic reactor during operation. Particularly, the reactor performance for degrading toluene in the gas phase for a range of illumination periods and duty cycles are studied. Finally, the reactor performance under CPI and continuous illumination modes at equivalent average irradiances are compared.

Chapter 5 shows the application of automated feedback and feedforward control for a LED-based Photocatalytic Reactor. The reactor conversion and the light intensity of LEDs are set as the controlled and manipulated variable, respectively. The automated feedback controller performance is tested for tracking different conversion set points as well as mitigating the effect of catalyst deactivation on the reactor performance. In addition, a feedforward controller is designed to reject the effect of the reactant inlet concentrations as the measured disturbances on the reactor conversion.

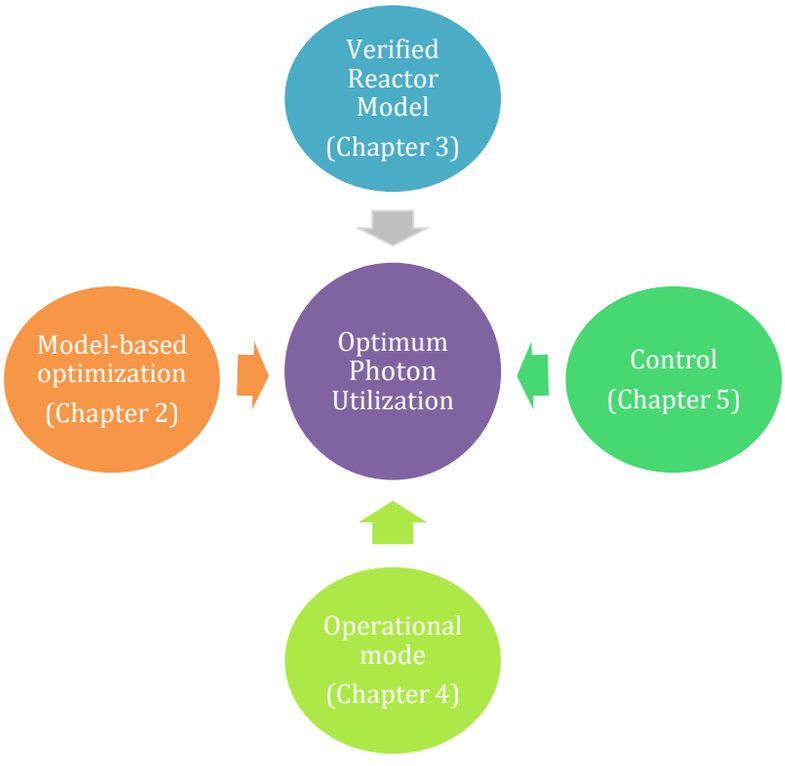

Figure 1.11 Strategies for achieving optimum photon utilization in LED-based photocatalytic reactors

References:

[1] A. Fujishima, K. Honda, Electrochemical Photolysis of Water at a Semiconductor Electrode, Nature 238 (1972) 37-38.
[2] M.A. Fox, M.T. Dulay, Heterogeneous photocatalysis, Chem. Rev. 93 (1993) 341-357.
[3] M.R. Hoffmann, S.T. Martin, W. Choi, D.W. Bahnemann, Environmental Applications of Semiconductor Photocatalysis, Chem. Rev. 95 (1995) 69-96.
[4] J.-M. Herrmann, Heterogeneous photocatalysis: fundamentals and applications to the removal of various types of aqueous pollutants, Catalysis Today 53 (1999) 115-129.

[5] C. Byrne, G. Subramanian, S.C. Pillai, Recent advances in photocatalysis for environmental applications, J. Environ. Chem. Eng. 6 (2018) 3531-3555.
[6] A.F. Tooru Inoue, Satoshi Konishi, Kenichi Honda, photoelectrocatalytic reduction of carbon dioxide in aqueus suspension of semiconductor powders, Nature 277 (1979) 2.
[7] J.C.S. Wu, H.M. Lin, C.L. Lai, Photo reduction of CO_2 to methanol using optical-fiber photoreactor, Appl. Catal. A 296 (2005) 194-200.
[8] M.M.O. Deniz Uner, On the mechanism of photocatalytic CO_2 reduction with water in the gas phase, Catal. Today 181 (2012) 82-88.
[9] J. Ran, M. Jaroniec, S.Z. Qiao, Cocatalysts in Semiconductor-based Photocatalytic CO_2 Reduction: Achievements, Challenges, and Opportunities, Adv. Mater. 30 (2018).
[10] F. Xu, K. Meng, B. Cheng, J. Yu, W. Ho, Enhanced Photocatalytic Activity and Selectivity for CO2 Reduction over a TiO_2 Nanofibre Mat Using Ag and MgO as Bi-Cocatalyst, Chem. Cat. Chem 11 (2018) 465-472.
[11] J. Low, B. Cheng, J. Yu, Surface modification and enhanced photocatalytic CO2 reduction performance of TiO_2: a review, Appl. Surf. Sci. 392 (2017) 658-686.
[12] T. Van Gerven, G. Mul, J. Moulijn, A. Stankiewicz, A review of intensification of photocatalytic processes, Chemical Engineering and Processing: Process Intensification 46 (2007) 781-789.
[13] P.S. Mukherjee, A.K. Ray, Major Challenges in the Design of a Large-Scale Photocatalytic Reactor for Water Treatment, Chem. Eng. Technol. 22 (1999) 253-260.
[14] M. Birnie, S. Riffat, M. Gillott, Photocatalytic reactors: design for effective air purification, International Journal of Low-Carbon Technologies 1 (2006) 47-58.
[15] C.C. Kaan, A.A. Aziz, M. Matheswaran, P. Saravanan, S. Ibrahim, Heterogeneous Photocatalytic Oxidation an Effective Tool for Wastewater Treatment-A Review, INTECH Open Access Publisher2012.
[16] R.J. Braham, A.T. Harris, Review of Major Design and Scale-up Considerations for Solar Photocatalytic Reactors, Ind. Eng. Chem. Res. 48 (2009) 8890-8905.
[17] C.A.M. Alberto E. Cassano, Rodolfo J. Brandi and Orlando M. Alfanot, Photoreactor Analysis and Design: Fundamentals and Applications, Ind. Eng. Chem. Res. 34 (1995) 2155-2201.
[18] M. Pasquali, F. Santarelli, J.F. Porter, P.L. Yue, Radiative transfer in photocatalytic systems, AlChE J. 42 (1996) 532-537.
[19] C.R. Esterkin, A.C. Negro, O.M. Alfano, A.E. Cassano, Radiation field inside a reactor of glass-fiber meshes coated with TiO_2, AlChE J. 48 (2002) 832-845.
[20] G.E. Imoberdorf, O.M. Alfano, A.E. Cassano, H.A. Irazoqui, Monte Carlo model of UV-radiation interaction with TiO_2-coated spheres, AlChE J. 53 (2007) 2688-2703.
[21] V. Tomašić, F. Jović, Z. Gomzi, Photocatalytic oxidation of toluene in the gas phase: Modelling an annular photocatalytic reactor, Catalysis Today 137 (2008) 350-356.
[22] V. Vaiano, O. Sacco, D. Pisano, D. Sannino, P. Ciambelli, From the design to the development of a continuous fixed bed photoreactor for photocatalytic degradation of organic pollutants in wastewater, Chem. Eng. Sci. 137 (2015) 152-160.
[23] M.E. Leblebici, J. Rongé, J.A. Martens, G.D. Stefanidis, T. Van Gerven, Computational modelling of a photocatalytic UV-LED reactor with internal mass and photon transfer consideration, Chem. Eng. J. 264 (2015) 962-970.
[24] A. Turolla, D. Santoro, J.R. de Bruyn, F. Crapulli, M. Antonelli, Nanoparticle scattering characterization and mechanistic modelling of UV-TiO_2 photocatalytic reactors using computational fluid dynamics, Water Res. 88 (2016) 117-126.
[25] Y. Boyjoo, H. Sun, J. Liu, V.K. Pareek, S. Wang, A review on photocatalysis for air treatment: From catalyst development to reactor design, Chem. Eng. J. 310 (2017) 537-559.
[26] G.B. Raupp, A. Alexiadis, M.M. Hossain, R. Changrani, First-principles modeling, scaling laws and design of structured photocatalytic oxidation reactors for air purification, Catal. Today 69 (2001) 41-49.
[27] R. Lakerveld, G.S.J. Sturm, A.I. Stankiewicz, G.D. Stefanidis, Integrated design of microwave and photocatalytic reactors. Where are we now?, Curr. Opin. Chem. Eng. 5 (2014) 37-41.
[28] M.F.J. Dijkstra, A. Michorius, H. Buwalda, H.J. Panneman, J.G.M. Winkelman, A.A.C.M. Beenackers, Comparison of the efficiency of immobilized and suspended systems in photocatalytic degradation, Catal. Today 66 (2001) 487-494.

[29] K. Mehrotra, G.S. Yablonsky, A.K. Ray, Kinetic Studies of Photocatalytic Degradation in a TiO_2 Slurry System: Distinguishing Working Regimes and Determining Rate Dependences, Ind. Eng. Chem. Res. 42 (2003) 2273-2281.

[30] C. McCullagh, N. Skillen, M. Adams, P.K.J. Robertson, Photocatalytic reactors for environmental remediation: a review, Journal of Chemical Technology & Biotechnology 86 (2011) 1002-1017.

[31] M.F.J. Dijkstra, H. Buwalda, A.W.F. de Jong, A. Michorius, J.G.M. Winkelman, A.A.C.M. Beenackers, Experimental comparison of three reactor designs for photocatalytic water purification, Chemical Engineering Science 56 (2001) 547-555.

[32] M.L. Satuf, R.J. Brandi, A.E. Cassano, O.M. Alfano, Photocatalytic degradation of 4-chlorophenol: A kinetic study, Appl. Catal. B 82 (2008) 37-49.

[33] R. Dillert, D. Bahnemann, H. Hidaka, Light-induced degradation of perfluorocarboxylic acids in the presence of titanium dioxide, Chemosphere 67 (2007) 785-792.

[34] P. Du, J.A. Moulijn, G. Mul, Selective photo(catalytic)-oxidation of cyclohexane: Effect of wavelength and TiO_2 structure on product yields, J. Catal. 238 (2006) 342-352.

[35] I. Izumi, F. R. F. Fan, A.J. Bard, Heterogeneous photocatalytic decomposition of benzoic acid and adipic acid on platinized titanium dioxide powder. The photo-Kolbe decarboxylative route to the breakdown of the benzene ring and to the production of butane, The Journal of Physical Chemistry 85 (1981) 218-223.

[36] W. Mu, J.-M. Herrmann, P. Pichat, Room temperature photocatalytic oxidation of liquid cyclohexane into cyclohexanone over neat and modified TiO_2, Catal. Lett. 3 (1989) 73-84.

[37] N. Ma, Y. Zhang, X. Quan, X. Fan, H. Zhao, Performing a microfiltration integrated with photocatalysis using an Ag-TiO_2/HAP/Al_2O_3 composite membrane for water treatment: Evaluating effectiveness for humic acid removal and anti-fouling properties, Water Res. 44 (2010) 6104-6114.

[38] D. Chen, A.K. Ray, Photodegradation kinetics of 4-nitrophenol in TiO_2 suspension, Water Res. 32 (1998) 3223-3234.

[39] K. Reilly, F. Taghipour, D.P. Wilkinson, Photocatalytic Hydrogen Production in a UV-irradiated Fluidized Bed Reactor, Energy Procedia 29 (2012) 513-521.

[40] L.A. Dibble, G.B. Raupp, Fluidized-bed photocatalytic oxidation of trichloroethylene in contaminated air streams, Environ. Sci. Technol. 26 (1992) 492-495.

[41] G.E. Imoberdorf, H.A. Irazoqui, A.E. Cassano, O.M. Alfano, Photocatalytic Degradation of Tetrachloroethylene in Gas Phase on TiO_2 Films: A Kinetic Study, Ind. Eng. Chem. Res. 44 (2005) 6075-6085.

[42] C. Passalía, M.E. Martínez Retamar, O.M. Alfano, R.J. Brandi, Photocatalytic Degradation of Formaldehyde in Gas Phase on TiO_2 Films: A Kinetic Study, International Journal of Chemical Reactor Engineering 8 (2010).

[43] Z.M. Wang, J. Liu, Y.C. Dai, W.Y. Dong, S.C. Zhang, J.M. Chen, Dimethyl Sulfide Photocatalytic Degradation in a Light-Emitting-Diode Continuous Reactor: Kinetic and Mechanistic Study, Ind. Eng. Chem. Res. 50 (2011) 7977-7984.

[44] Z. Zhang, W.A. Anderson, M. Moo-Young, Experimental analysis of a corrugated plate photocatalytic reactor, Chem. Eng. J. 99 (2004) 145-152.

[45] I. Salvadó-Estivill, A. Brucato, G. Li Puma, Two-Dimensional Modeling of a Flat-Plate Photocatalytic Reactor for Oxidation of Indoor Air Pollutants, Ind. Eng. Chem. Res. 46 (2007) 7489-7496.

[46] M.M. Hossain, G.B. Raupp, S.O. Hay, T.N. Obee, Three-dimensional developing flow model for photocatalytic monolith reactors, AlChE J. 45 (1999) 1309-1321.

[47] M. Singh, I. Salvadó-Estivill, G. Li Puma, Radiation field optimization in photocatalytic monolith reactors for air treatment, AlChE J. 53 (2007) 678-686.

[48] H. Lin, K.T. Valsaraj, Development of an optical fiber monolith reactor for photocatalytic wastewater treatment, Journal of Applied Electrochemistry 35 (2005) 699-708.

[49] J. Mo, Y. Zhang, Q. Xu, J.J. Lamson, R. Zhao, Photocatalytic purification of volatile organic compounds in indoor air: A literature review, Atmos. Environ. 43 (2009) 2229-2246.

[50] R.E. Marinangeli, D.F. Ollis, Photoassisted heterogeneous catalysis with optical fibers: I. Isolated single fiber, AlChE J. 23 (1977) 415-426.

[51] R.E. Marinangeli, D.F. Ollis, Photo-assisted heterogeneous catalysis with optical fibers. Part III: Photoelectrodes, AlChE J. 28 (1982) 945-955.

[52] C. McCullagh, N. Skillen, M. Adams, P.K. Robertson, Photocatalytic reactors for environmental remediation: a review, Journal of Chemical Technology and Biotechnology 86 (2011) 1002-1017.
[53] W. Choi, J.Y. Ko, H. Park, J.S. Chung, Investigation on TiO_2-coated optical fibers for gas-phase photocatalytic oxidation of acetone, Appl. Catal. B 31 (2001) 209-220.
[54] H. Lin, K. Valsaraj, Development of an optical fiber monolith reactor for photocatalytic wastewater Treatment, J. Appl. Electrochem. 35 (2005) 699-708.
[55] T.-V. Nguyen, J.C.S. Wu, Photoreduction of CO_2 in an optical-fiber photoreactor: Effects of metals addition and catalyst carrier, Appl. Catal. A 335 (2008) 112-120.
[56] P. Du, J.T. Carneiro, J.A. Moulijn, G. Mul, A novel photocatalytic monolith reactor for multiphase heterogeneous photocatalysis, Appl. Catal. A 334 (2008) 119-128.
[57] L.G. Ame´lie Queffeulou, Catherine Archambeau, Herve´ Le Gall, Paul-Marie Marquaire, and Orfan Zahraa, Kinetic Study of Acetaldehyde Photocatalytic Oxidation with a Thin Film of TiO_2 Coated on Stainless Steel and CFD Modeling Approach, Ind. Eng. Chem. Res. 49 (2010) 6890-6897.
[58] Y. Ku, C.-M. Ma, Y.-S. Shen, Decomposition of gaseous trichloroethylene in a photoreactor with TiO_2-coated nonwoven fiber textile, Appl. Catal. B 34 (2001) 181-190.
[59] G.E. Imoberdorf, A.E. Cassano, O.M. Alfano, H.A. Irazoqui, Modeling of a multiannular photocatalytic reactor for perchloroethylene degradation in air, AlChE J. 52 (2006) 1814-1823.
[60] G.E. Imoberdorf, A.E. Cassano, H.A. Irazoqui, O.M. Alfano, Optimal design and modeling of annular photocatalytic wall reactors, Catal. Today 129 (2007) 118-126.
[61] G.E. Imoberdorf, A.E. Cassano, H.A. Irazoqui, O.M. Alfano, Simulation of a multi-annular photocatalytic reactor for degradation of perchloroethylene in air: Parametric analysis of radiative energy efficiencies, Chem. Eng. Sci. 62 (2007) 1138-1154.
[62] A. Alexiadis, I. Mazzarino, Design guidelines for fixed-bed photocatalytic reactors, Chemical Engineering and Processing: Process Intensification 44 (2005) 453-459.
[63] G.B. Roupp, J.A. Nico, S. Annangi, R. Changrani, R. Annapragada, Two-flux radiation-field model for an annular packed-bed photocatalytic oxidation reactor, AlChE J. 43 (1997) 792-801.
[64] H. Al-Ekabi, N. Serpone, E. Pelizzetti, C. Minero, M.A. Fox, R.B. Draper, Kinetic studies in heterogeneous photocatalysis. 2. Titania-mediated degradation of 4-chlorophenol alone and in a three-component mixture of 4-chlorophenol, 2,4-dichlorophenol, and 2,4,5-trichlorophenol in air-equilibrated aqueous media, Langmuir 5 (1989) 250-255.
[65] K.F. Jensen, Microreaction engineering: is small better?, Chem. Eng. Sci. 56 (2001) 293-303.
[66] Y. Matsushita, S. Kumada, K. Wakabayashi, K. Sakeda, T. Ichimura, Photocatalytic Reduction in Microreactors, Chem. Lett. 35 (2006) 410-411.
[67] A.K. Ray, A.A.C.M. Beenackers, Novel photocatalytic reactor for water purification, AlChE J. 44 (1998) 477-483.
[68] R. Gorges, S. Meyer, G. Kreisel, Photocatalysis in microreactors, J. Photochem. Photobiol. A: Chem. 167 (2004) 95-99.
[69] H. Ge, G. Chen, Q. Yuan, H. Li, Gas phase catalytic partial oxidation of toluene in a microchannel reactor, Catal. Today 110 (2005) 171-178.
[70] A. Visan, D. Rafieian, W. Ogieglo, R.G.H. Lammertink, Modeling intrinsic kinetics in immobilized photocatalytic microreactors, Appl. Catal. B 150–151 (2014) 93-100.
[71] Y. Matsushita, N. Ohba, S. Kumada, K. Sakeda, T. Suzuki, T. Ichimura, Photocatalytic reactions in microreactors, Chem. Eng. J. 135, Supplement 1 (2008) S303-S308.
[72] Y. Matsushita, M. Iwasawa, T. Suzuki, T. Ichimura, Multiphase Photocatalytic Oxidation in a Microreactor, Chem. Lett. 38 (2009) 846-847.
[73] M. Krivec, K. Žagar, L. Suhadolnik, M. Čeh, G. Dražić, Highly Efficient TiO_2-Based Microreactor for Photocatalytic Applications, ACS Appl. Mater. Interfaces 5 (2013) 9088-9094.
[74] S. Sohrabi, M. Keshavarz Moraveji, D. Iranshahi, A review on the design and development of photocatalyst synthesis and application in microfluidic reactors: challenges and opportunities, Rev. Chem. Eng., 2019.
[75] N.J. Straathof, Y. Su, V. Hessel, T. Noel, Accelerated gas-liquid visible light photoredox catalysis with continuous-flow photochemical microreactors, Nat Protoc 11 (2016) 10-21.
[76] Y. Su, K. Kuijpers, V. Hessel, T. Noël, A convenient numbering-up strategy for the scale-up of gas–liquid photoredox catalysis in flow, React. Chem. Eng. 1 (2016) 73-81.

[77] K.P.L. Kuijpers, M.A.H. van Dijk, Q.G. Rumeur, V. Hessel, Y. Su, T. Noël, A sensitivity analysis of a numbered-up photomicroreactor system, React. Chem. Eng. 2 (2017) 109-115.
[78] G. Imoberdorf, M. Mohseni, Modeling and experimental evaluation of vacuum-UV photoreactors for water treatment, Chem. Eng. Sci. 66 (2011) 1159-1167.
[79] M. Motegh, J.J. Cen, P.W. Appel, J.R. van Ommen, M.T. Kreutzer, Photocatalytic-reactor efficiencies and simplified expressions to assess their relevance in kinetic experiments, Chem. Eng. J. 207 (2012) 607-615.
[80] J. Colina-Márquez, F. Machuca-Martínez, G.L. Puma, Radiation Absorption and Optimization of Solar Photocatalytic Reactors for Environmental Applications, Environ. Sci. Technol. 44 (2010) 5112-5120.
[81] G.E. Imoberdorf, F. Taghipour, M. Mohseni, Radiation field modeling of multi-lamp, homogeneous photoreactors, J. Photochem. Photobiol. A: Chem. 198 (2008) 169-178.
[82] G.E. Imoberdorf, G. Vella, A. Sclafani, L. Rizzuti, O.M. Alfano, A.E. Cassano, Radiation model of a TiO_2-coated, quartz wool, packed-bed photocatalytic reactor, AlChE J. 56 (2010) 1030-1044.
[83] A.L.L. Zazueta, H. Destaillats, G. Li Puma, Radiation field modeling and optimization of a compact and modular multi-plate photocatalytic reactor (MPPR) for air/water purification by Monte Carlo method, Chem. Eng. J. 217 (2013) 475-485.
[84] X. Lang, X. Chen, J. Zhao, Heterogeneous visible light photocatalysis for selective organic transformations, Chem. Soc. Rev. 43 (2014) 473-486.
[85] G. Li Puma, P.L. Yue, Modelling and design of thin-film slurry photocatalytic reactors for water purification, Chem. Eng. Sci. 58 (2003) 2269-2281.
[86] R.E. Bird, R.L. Hulstrom, L.J. Lewis, Terrestrial solar spectral data sets, Solar Energy 30 (1983) 563-573.
[87] R. Dillert, A.E. Cassano, R. Goslich, D. Bahnemann, Large scale studies in solar catalytic wastewater treatment, Catal. Today 54 (1999) 267-282.
[88] O.M. Alfano, D. Bahnemann, A.E. Cassano, R. Dillert, R. Goslich, Photocatalysis in water environments using artificial and solar light, Catal. Today 58 (2000) 199-230.
[89] S. Malato Rodríguez, J. Blanco Gálvez, M.I. Maldonado Rubio, P. Fernández Ibáñez, D. Alarcón Padilla, M. Collares Pereira, J. Farinha Mendes, J. Correia de Oliveira, Engineering of solar photocatalytic collectors, Solar Energy 77 (2004) 513-524.
[90] S. Malato, J. Blanco, A. Vidal, C. Richter, Photocatalysis with solar energy at a pilot-plant scale: an overview, Appl. Catal. B 37 (2002) 1-15.
[91] C. Minero, E. Pelizzetti, S. Malato, J. Blanco, Large solar plant photocatalytic water decontamination: Degradation of atrazine, Solar Energy 56 (1996) 411-419.
[92] S. Malato, J. Blanco, C. Richter, D. Curcó, J. Gimenez, Low-concentrating CPC collectors for photocatalytic water detoxification: Comparison with a medium concentrating solar collector, Water Sci. Technol. 35 (1997) 157-164.
[93] C. Minero, E. Pelizzetti, S. Malato, J. Blanco, Large solar plant photocatalytic water decontamination: Degradation of pentachlorophenol, Chemosphere 26 (1993) 2103-2119.
[94] S.M. Rodríguez, C. Richter, J.B. Gálvez, M. Vincent, Photocatalytic degradation of industrial residual waters, Solar Energy 56 (1996) 401-410.
[95] S. Malato, P. Fernández-Ibáñez, M.I. Maldonado, J. Blanco, W. Gernjak, Decontamination and disinfection of water by solar photocatalysis: Recent overview and trends, Catal. Today 147 (2009) 1-59.
[96] E.R. Bandala, C.A. Arancibia-Bulnes, S.L. Orozco, C.A. Estrada, Solar photoreactors comparison based on oxalic acid photocatalytic degradation, Solar Energy 77 (2004) 503-512.
[97] O.A. McLoughlin, S.C. Kehoe, K.G. McGuigan, E.F. Duffy, F.A. Touati, W. Gernjak, I.O. Alberola, S.M. Rodríguez, L.W. Gill, Solar disinfection of contaminated water: a comparison of three small-scale reactors, Solar Energy 77 (2004) 657-664.
[98] S. Parra, S. Malato, J. Blanco, P. Peringer, C. Pulgari, Concentrating versus non-concentrating reactors for solar photocatalytic degradation of p-nitrotoluene-o-sulfonic acid, Water Sci. Technol. 44 (2001) 219-227.
[99] D. Bahnemann, Photocatalytic water treatment: solar energy applications, Solar Energy 77 (2004) 445-459.
[100] M. van Well, R.H. Dillert, D.W. Bahnemann, V.W. Benz, M. Mueller, A novel nonconcentrating reactor for solar water detoxification, J. Sol. Energy Eng. 119 (1997) 114-119.
[101] R. Dillert, S. Vollmer, M. Schober, J. Theurich, D. Bahnemann, H.J. Arntz, K. Pahlmann, J. Wienefeld, T. Schmedding, G. Sager, Photocatalytic Treatment of an Industrial Wastewater in the Double-Skin Sheet Reactor, Chem. Eng. Technol. 22 (1999) 931-934.

[102] G. Li Puma, P.L. Yue, Comparison of the Effectiveness of Photon-Based Oxidation Processes in a Pilot Falling Film Photoreactor, Environ. Sci. Technol. 33 (1999) 3210-3216.
[103] W.-K. Jo, R.J. Tayade, New Generation Energy-Efficient Light Source for Photocatalysis: LEDs for Environmental Applications, Ind. Eng. Chem. Res. 53 (2014) 2073-2084.
[104] D.H. Chen, X. Ye, K. Li, Oxidation of PCE with a UV LED Photocatalytic Reactor, Chem. Eng. Technol. 28 (2005) 95-97.
[105] H.-W. Chen, Y. Ku, A. Irawan, Photodecomposition of o-cresol by UV-LED/TiO_2 process with controlled periodic illumination, Chemosphere 69 (2007) 184-190.
[106] J.-L. Shie, C.-H. Lee, C.-S. Chiou, C.-T. Chang, C.-C. Chang, C.-Y. Chang, Photodegradation kinetics of formaldehyde using light sources of UVA, UVC and UVLED in the presence of composed silver titanium oxide photocatalyst, J. Hazard. Mater. 155 (2008) 164-172.
[107] J.T.R. Lanfang H. Levine, and Janelle L. Coutts, Feasibility ultraviloet ligth emitting diodes as an alternative ligth source for photocatalysis, J. Air Waste Manage. Assoc. 61 (2011) 932-940.
[108] K. Natarajan, T.S. Natarajan, H.C. Bajaj, R.J. Tayade, Photocatalytic reactor based on UV-LED/TiO2 coated quartz tube for degradation of dyes, Chem. Eng. J. 178 (2011) 40-49.
[109] S. Dominguez, P. Ribao, M.J. Rivero, I. Ortiz, Influence of radiation and TiO_2 concentration on the hydroxyl radicals generation in a photocatalytic LED reactor. Application to dodecylbenzenesulfonate degradation, Appl. Catal. B 178 (2015) 165-169.
[110] S. Mosleh, M.R. Rahimi, M. Ghaedi, K. Dashtian, S. Hajati, Sonochemical-assisted synthesis of CuO/Cu_2O/Cu nanoparticles as efficient photocatalyst for simultaneous degradation of pollutant dyes in rotating packed bed reactor: LED illumination and central composite design optimization, Ultrason. Sonochem. 40 (2018) 601-610.
[111] G. Matafonova, V. Batoev, Recent advances in application of UV light-emitting diodes for degrading organic pollutants in water through advanced oxidation processes: A review, Water Res. 132 (2018) 177-189.
[112] V. Muñoz, C. Casado, S. Suárez, B. Sánchez, J. Marugán, Photocatalytic NOx removal: Rigorous kinetic modelling and ISO standard reactor simulation, Catal. Today 326 (2019) 82-93.
[113] A. Sergejevs, C.T. Clarke, D.W.E. Allsopp, J. Marugan, A. Jaroenworaluck, W. Singhapong, P. Manpetch, R. Timmers, C. Casado, C.R. Bowen, A calibrated UV-LED based light source for water purification and characterisation of photocatalysis, Photochem. Photobiol. Sci.16 (2017) 1690-1699.
[114] S. Dominguez, M.J. Rivero, P. Gomez, R. Ibañez, I. Ortiz, Kinetic modeling and energy evaluation of sodium dodecylbenzenesulfonate photocatalytic degradation in a new LED reactor, J. Ind. Eng. Chem. 37 (2016) 237-242.
[115] M. Martín-Sómer, C. Pablos, R. van Grieken, J. Marugán, Influence of light distribution on the performance of photocatalytic reactors: LED vs mercury lamps, Appl. Catal. B 215 (2017) 1-7.
[116] J.L. Zimeng Wang, Yuancan Dai, Weiyang Dong, Shicheng Zhang, Jianmin Chen, CFD modeling of a UV-LED photocatalytic odor abatement process in a continuous reactor, J. Hazard. Mater. 215-216 (2012) 25-31.
[117] R. Simons, U.E. Gabbai, M.A. Moram, Optical fluence modelling for ultraviolet light emitting diode-based water treatment systems, Water Res. 66 (2014) 338-349.
[118] C. Casado, R. Timmers, A. Sergejevs, C.T. Clarke, D.W.E. Allsopp, C.R. Bowen, R. van Grieken, J. Marugán, Design and validation of a LED-based high intensity photocatalytic reactor for quantifying activity measurements, Chem. Eng. J. 327 (2017) 1043-1055.
[119] M. Keshavarzfathy, F. Taghipour, Radiation modeling of ultraviolet light-emitting diode (UV-LED) for water treatment, J. Photochem. Photobiol. A: Chem. 377 (2019) 58-66.
[120] K.J. Buechler, R.D. Noble, C.A. Koval, W.A. Jacoby, Investigation of the Effects of Controlled Periodic Illumination on the Oxidation of Gaseous Trichloroethylene Using a Thin Film of TiO_2, Ind. Eng. Chem. Res. 38 (1999) 892-896.
[121] J.G. Sczechowski, C.A. Koval, R.D. Noble, Use of controlled periodic illumination for an improved method of photocatalysis and an improved reactor design, Google Patents, 1995.
[122] G. Stewart, M.A. Fox, The effect of dark recovery time on the photoefficiency of heterogeneous photocatalysis by TiO_2 suspended in non-aqueous media, Res. Chem. Intermed. 21 (1995) 933-938.
[123] S. Upadhya, D.F. Ollis, Simple Photocatalysis Model for Photoefficiency Enhancement via Controlled, Periodic Illumination, J. Phys. Chem. B 101 (1997) 2625-2631.

[124] K.J. Buechler, T.M. Zawistowski, R.D. Noble, C.A. Koval, Investigation of the Mechanism for the Controlled Periodic Illumination Effect in TiO_2 Photocatalysis, Ind. Eng. Chem. Res. 40 (2001) 1097-1102.

[125] C.J.G. Cornu, A.J. Colussi, M.R. Hoffmann, Quantum Yields of the Photocatalytic Oxidation of Formate in Aqueous TiO_2 Suspensions under Continuous and Periodic Illumination, J. Phys. Chem. B 105 (2001) 1351-1354.

[126] W.-M. Hou, Y. Ku, Photocatalytic decomposition of gaseous isopropanol in a tubular optical fiber reactor under periodic UV-LED illumination, J. Mol. Catal. A: Chem. 374–375 (2013) 7-11.

[127] E. Korovin, D. Selishchev, A. Besov, D. Kozlov, UV-LED TiO_2 photocatalytic oxidation of acetone vapor: Effect of high frequency controlled periodic illumination, Appl. Catal. B 163 (2015) 143-149.

Chapter 2. Model-based Optimization of a Photocatalytic Reactor with Light-Emitting Diodes

The complicated interplay between mass and photon transfer within a photocatalytic reactor calls for an integrated design approach. This work presents a model-based optimization approach for LED-based photocatalytic reactors. First, a model that describes the distribution of reactants and photons within a photocatalytic reactor is developed. Second, several design variables related to the reactor dimensions and light sources are optimized simultaneously using the photocatalytic degradation of toluene as a model system. The results demonstrate how different formulations of the problem can be used to either minimize the reactor cost or to obtain a specified concentration profile within the reactor.

Published as: F. Khodadadian, A. Poursaeidesfahani, Z. Li, J.R. van Ommen, A.I. Stankiewicz, R. Lakerveld, Model-Based Optimization of a Photocatalytic Reactor with Light-Emitting Diodes, Chem. Eng. Technol. 39 (2016) 1946-1954.

2.1 Introduction

Titania-based heterogeneous photocatalysis has great potential for the implementation of redox reactions such as water splitting to produce hydrogen [1] , reduction of carbon dioxide to hydrocarbons [2] , water and air purification [3, 4]. Consequently, the topic has raised considerable interest in recent decades. Nevertheless, the industrial application of photocatalysis has been hindered by the low overall efficiency of the process [5]. One of the main challenges is the design of a reactor in which both mass transfer and photon transfer are optimized simultaneously [6-8]. Poor photon utilization leads to a large reactor volume and, in case of using artificial light, large operational cost, which hinders practical applications.

The development of more efficient photocatalysts has seen much progress [9-12]. Moreover, many efforts have been made to improve the efficiency of photocatalytic processes by optimizing the operating conditions of photocatalytic reactors such as pH, catalyst loading, light intensity and wavelength, flow rates and reactant concentrations [13-18]. In contrast, fewer reports exist on the optimization of the photocatalytic reactor equipment [19, 20].

Mathematical models can be efficient tools for the design and optimization of photocatalytic reactors. Driven by the importance of the photon distribution within a photocatalytic reactor, several studies have considered modeling of a radiation field in combination with a reactor model [21-26]. For example, the optimal design of reactors illuminated by cylindrical UV lamps for a monolith reactor [27] and a modular multi-plate reactor [28] have been studied. The authors demonstrate how a maximum number of photons can be absorbed with a uniform irradiation on a photocatalytic surface. A Monte Carlo method was used to solve the Radiation Transport Equations (RTE) in both studies. Other factors such as fluid dynamics and reaction kinetics were not taken into account in these optimization studies. The optimal design of annular wall reactors for air treatment was investigated by choosing six different configurations. A mathematical model was used to study the effect of the physical design of the reactor on its performance [29]. Subsequently, the model was validated successfully by testing one of the configurations experimentally. In addition, the combination of models based on computational fluid dynamics (CFD) and design of experiments has been reported for the optimization of various configurations of photocatalytic reactors [30].

The photon distribution within a photocatalytic reactor depends on several factors including the type, strength and dimensions of the light sources [8]. Conventional UV-lamps such as low-pressure mercury lamp, which are rigid cylindrical lamps, may restrict the design of the reactor. Furthermore, the fragility, toxicity, potential for gas leakage and disposal issues are other known disadvantages of mercury lamps [31]. Alternatively, Light Emitting Diodes (LEDs) are promising light sources for photocatalysis applications [32-35]. LEDs are robust, energy-efficient, non-toxic and long-lasting light sources. Their spectra are narrow and available for different wavelengths. Since the commercialization of the first LEDs, significant progress has been made in their power output and packaging while their price has dropped [36]. In general, LEDs offer more flexibility for the design of photocatalytic reactors due to their small size. Wang et al. [37] developed a CFD-based model to describe the behaviour of a flat plate photocatalytic reactor, illuminated externally by an array of LEDs for air treatment. To obtain

the maximum conversion, they determined the optimal distance from the LEDs array to the catalyst surface by varying the position of the LEDs array. Anceno and Stuetz [38] developed the radiation field model of an optical fiber-coupled UV-LED lighting system and validated the model experimentally to study the impact of the light source position on the irradiated catalyst surface for the photocatalytic degradation of carbon disulphide.

The design of an array of LEDs offers several novel degrees of freedom, which affect the performance of photocatalytic reactors. In principle, each LED can be positioned flexibly within a reactor configuration due to its small size and LEDs have the ability to deliver a range of intensities, which all together introduces additional design variables. Furthermore, the reactor dimensions and operating conditions also offer various degrees of freedom for design. This combination of design decisions influences the complex interplay between mass and photon transfer within a photocatalytic reactor. Therefore, a key question is how to select the optimal combination of design variables related to light sources and reactor design simultaneously. Such simultaneous optimization of all those degrees of freedom has received less attention in the literature.

The objective of this chapter is to investigate modeling and optimization of a continuous LED-based photocatalytic reactor taking into account design decisions related to the dimensions of the reactor and spacing of the LEDs simultaneously. A mathematical approach is followed instead of trial-and-error methods for optimization. The photocatalytic degradation of toluene in the gas phase is used as the model reaction and a wall annular photocatalytic reactor has been selected as the basic reactor configuration. Two different types of objective functions are investigated. The first objective function is an economic objective function that mimics the trade-off between the capital and operational costs for a specified minimum conversion. The second objective function aims to optimize the concentration profile in the reactor by manipulating the position and number of LEDs.

2.2 Approach

2.2.1 An integrated model for a LED-based photocatalytic reactor

2.2.1.1 Transport and kinetics model

The modelled reactor consists of three concentric tubes including an inner tube to assemble the LEDs, a transparent tube in the middle, and an outer reactor shell with catalyst coating (Figure 2.1). The gas stream is evenly distributed between the middle and outer tube.

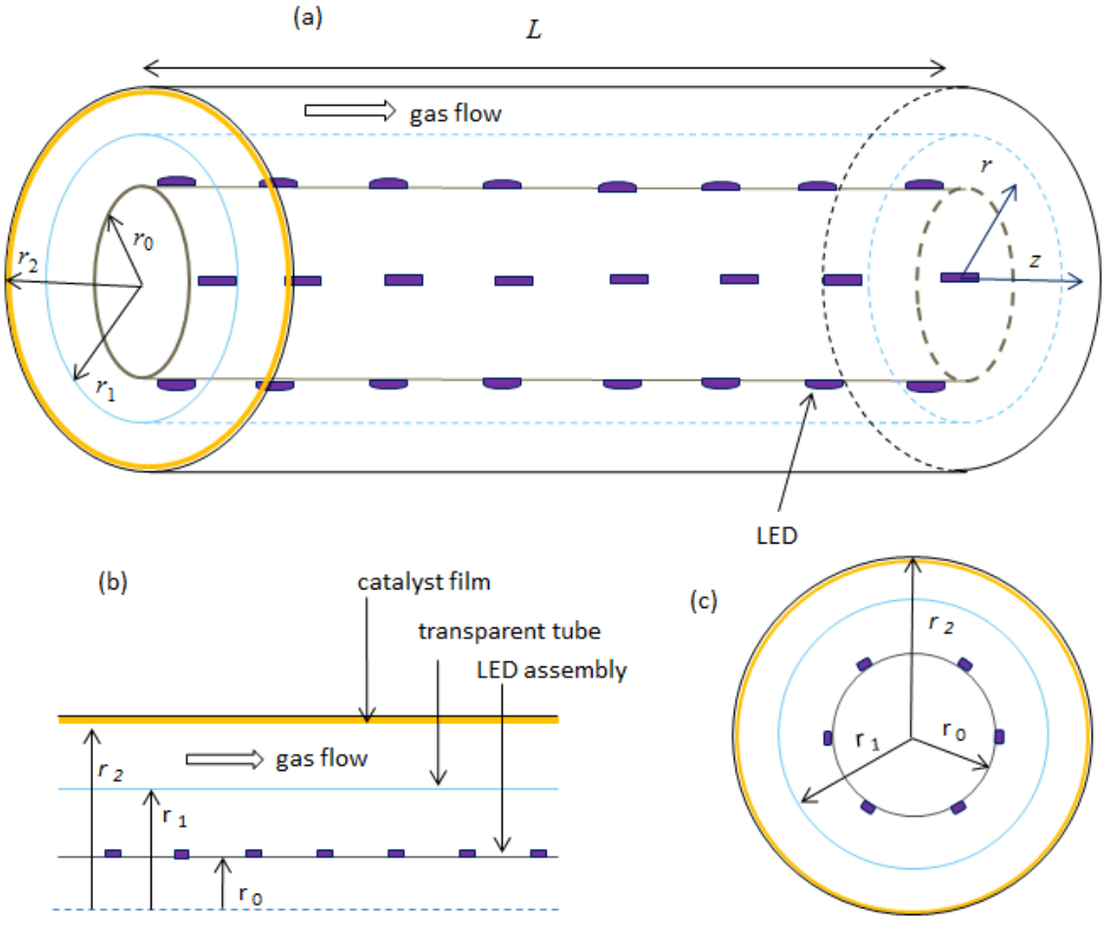

Figure 2.1 Schematic representation of the LED-based photocatalytic reactor. a) overall view, b) cross-sectional side view and c) cross-section view

The following assumptions are made to model the system: 1) Newtonian flow, 2) isothermal and isobaric conditions, 3) constant density and viscosity of the gas stream, 4) no boundary effects in the radiation field model at the inlet and outlet of the reactor, 5) steady state and, 6) azimuthal symmetry. By solving the continuity equation and momentum balance equation for a fully developed laminar flow in an annulus, the velocity profile is described by (see Appendix 2A for the derivation):

$$u(r)=2\frac{Q}{\pi r_2^2}\left[\frac{\ln\left(\frac{r_1}{r_2}\right)}{\left(1-\left(\frac{r_1}{r_2}\right)^4\right)\ln\left(\frac{r_1}{r_2}\right)+\left(1-\left(\frac{r_1}{r_2}\right)^2\right)^2}\right]\left(1-\left(\frac{r}{r_2}\right)^2-\frac{\left[1-\left(\frac{r_1}{r_2}\right)^2\right]}{\ln\left(\frac{r_1}{r_2}\right)}\ln\left(\frac{r}{r_2}\right)\right) \tag{2.1}$$

where u is the velocity of the gas (m s^{-1}), Q is the volumetric flow rate (m^3 s^{-1}), and r_2 and r_1 are the radius of outer tube and the radius of middle transparent tube (m), respectively.

Assuming that the convection in the axial direction and diffusion in the radial direction are the dominant mass transfer mechanisms, the concentration of toluene within the reactor, in cylindrical coordinates, is given by:

$$D\frac{1}{r}\frac{\partial}{\partial r}\left(r\frac{\partial C(r,z)}{\partial r}\right)-u(r)\frac{\partial C(r,z)}{\partial z}=0 \tag{2.2}$$

where C is the toluene concentration (mol m^{-3}), and D is the diffusion coefficient (m^2 s^{-1}) of toluene in the gas mixture.

Considering that the chemical reaction occurs at the catalyst surface only, the boundary conditions of equation (2.3) are given by:

$$D\frac{\partial C\left(r_2,z\right)}{\partial r}=-R \tag{2.3}$$

$$\frac{\partial C\left(r_1,z\right)}{\partial r}=0 \tag{2.4}$$

$$C\left(r,0\right)=C_{\text{in}} \tag{2.5}$$

where R is the toluene degradation rate (mol m^{-2} s^{-1}), and C_{in} is the concentration of toluene at the reactor inlet (mol m^{-3}). The average concentration of toluene (C_{out}) at the reactor outlet and conversion (X) are given by [29]:

$$C_{\text{out}}=\frac{\int_{r_1}^{r_2}C_t(r,L)u(r)rdr}{\int_{r_1}^{r_2}u(r)rdr} \tag{2.6}$$

$$\text{X}=1-\frac{C_{\text{out}}}{C_{\text{in}}} \tag{2.7}$$

where L is the reactor length (m). Similar models have been used for simulation of photocatalytic reactors for different applications [29, 39].

The Langmuir-Hinshelwood kinetic model has been widely used to describe kinetics of photocatalytic reactions [40] and has also been applied for the photocatalytic degradation of toluene [41-44]. Assuming constant water vapour concentration, Batista et al. [43] developed an intrinsic kinetic formulation for the photocatalytic degradation of toluene taking explicitly into account the rate of photon absorption:

$$R\left(r,z\right)=-\sqrt{e_{a,s}}\left(r,z\right)\frac{\alpha_1 C\left(r,z\right)}{1+\alpha_2 C\left(r,z\right)} \tag{2.8}$$

where $e_{a,s}$ is the local superficial rate of photon absorption (W m^{-2}) and α_1 and α_2 are reaction parameters. The reaction rate described by equation (2.8) was validated experimentally [43] and is used in this work to model the reaction kinetics.

2.2.1.2 Radiation field model

Integrated modeling of a photocatalytic reactor requires an emission model for the light sources. In order to calculate the effective photon absorption, the radiation contribution from each LED should be taken into account. Thus, the total radiation flux at any point on the catalyst surface is given by:

$$E(r_2,z)=\sum_{i=1}^{N}\frac{I_0\left(r_2-r_0\right)^m}{\left(\left(r_2-r_0\right)^2+\left(z-z_{0,i}(i)\right)^2\right)^{\frac{m+2}{2}}} \tag{2.9}$$

where E (W m^{-2}) is the irradiance of N number of LEDs. I_0 (W sr^{-1}) is the light intensity at a viewing angle of zero, and m is a parameter that depends on the LED packaging, which is typically determined experimentally. (r_0, z_0) and (r_2, z) refer to the coordinates of a LED and a point on the catalyst surface, respectively (see Figure 2.1). The details of the radiation field model derivation and the experimental validation of the model have been described in the Appendix 2B.

Although the wavelength of photons is one of the important factors determining the process cost, the wavelength is considered as a fixed parameter here, as the catalyst type is also fixed. In this study, LEDs with a narrow spectrum (half height width of 10 nm) and a peak wavelength at 365 nm are used and, it can be assumed that the energy of irradiated photons is proportional to the wavelength of 365 nm. A study on the impact of photon wavelengths on the efficiency of a photocatalytic process has shown that for TiO_2-based photocatalysis, a wavelength of 365 nm is the best alternative from an energy consumption point of view [18]. It is also assumed that neither the transparent tube nor the chemical species absorb photons, and thus, that all of the photons emitted by the LEDs reach the catalyst surface. Furthermore, it has been shown that a photocatalyst film typically can absorb more than 90% of the received photons [45]. In addition, some of the reflected photons can still be absorbed if they reflect back from the inner tube of the reactor towards the catalyst surface. Therefore, any loss of photons due to reflection and subsequent absorption by any material other than the photocatalyst has been neglected in this study. Moreover, the coated catalyst on the reactor wall is assumed to be sufficiently thick to absorb all photons. Therefore, the rate of photon absorption, $e_{a,s}$, is assumed to be equal to the irradiance described by equation (2.9).

2.2.1.3 Formulation of the optimization problems

Two different optimization studies are investigated:

1. Minimizing the overall cost of the reactor for a given throughput and minimum conversion by varying reactor dimensions and the spacing and number of LEDs.

2. Obtaining a specified concentration profile within the reactor by varying the spacing and number of LEDs.

For the first optimization formulation, both a simplified case (referred to as optimization problem P2.1) and a more complicated one (referred to as optimization problem P2.2) are studied.

When using artificial light sources, the costs of a photocatalytic reactor are mainly determined by the investment and operational costs for photon generation.

In a LED-based photocatalytic reactor, the light sources are discrete, and they can be arranged in different ways to optimize photon distribution on the photocatalytic surface. The minimum cost for a LED-based photocatalytic reactor is obtained by manipulating the length of the reactor and the number of LEDs:

$$\min_{L,N\in\mathbb{N}} J_1 := d_{\text{cat}}(2\pi a P_{\text{cat}} r_2 L) + d_{\text{reactor}}\rho_{\text{reactor}}\pi P_{\text{reactor}} L((r_2+t)^2) - r_2^2) + d_{\text{LED}} N P_{\text{LED}} + P_{\text{LED}} P_{\text{in}}\, N \quad \text{(P2.1)}$$

subject to equations. (2.1)- (2.5), (2.8), (2.9)

$$L \in (0,100], \quad N \le 300 \quad \text{(P2.1.1)}$$

$$r_1 = 0.020, \quad r_2 = 0.025 \quad \text{(P2.1.2)}$$

$$X \ge 0.50 \quad \text{(P2.1.3)}$$

The objective function J_1 is shaped by the electricity and investment costs for the LEDs and investment costs for catalyst and reactor equipment. The first part of the objective function J_1 represents the catalyst investment costs where d_{cat} is the catalyst depreciation factor (year^{-1}), a is the catalyst weight per unit of surface (kg m^{-2}) and P_{cat} is the catalyst price per unit of weight (\$ kg^{-1}). The second part represents the reactor equipment investment costs where d_{reactor} is the reactor depreciation factor (year^{-1}), ρ_{reactor} is the reactor material density (kg m^{-3}), t is the reactor wall thickness (m) and P_{reactor} is the reactor material cost (\$ kg). The third part represents the investment costs of the LEDs where d_{LED} is the depreciation factor of the LEDs (year $^{-1}$) and P_{LED} is the price of a single LED (\$). The last term represents the electricity cost where p_{in} is the input power of a single LED (W) and P_{elec} is the electricity price (\$ W^{-1} year^{-1}). The numerical values for the parameters included in the optimization problems are listed in Table 2.1. The case is inspired by the design of a mini-pilot plant setup that will be used for experimental validation in the next chapter.

Table 2.1 Parameters used in the cost model

Parameter	Value	Unit
D	8.4E-6	$m^2\ s^{-1}$
Q	14E-06	$m^3\ s$
C_{in}	3.9E-03	$mol\ m^{-3}$
p_{in}	0.06	W
P_{LED}	0.5	$
$P_{reactor}$	76.9	$ kg^{-1}
P_{cat}	160	$ kg^{-1}
$\dot{P}_{elec}$	0.068	$ $kW^{-1}\ h^{-1}$
d_{cat}*	12	$year^{-1}$
$d_{reactor}$**	0.2	$year^{-1}$
d_{LED}***	6	$year^{-1}$
a	0.002	$kg\ m^{-2}$
$\rho_{reactor}$	7930	$kg\ m^{-3}$
t	0.005	m
r_0	0.008	m
α_1	0.7E-3	$m^2\ W^{-0.5}$
α_2	7.1E2	$m^3\ mol^{-1}$

* depreciation factor of the catalyst is based on a typical lifetime of one month.
** depreciation factor of the reactor is based on a lifetime of 4 years.
*** depreciation factor of the LEDs is based on a lifetime of 1500 hours estimated by the supplier.

Second, an optimization similar to (P2.1) is repeated, but in this case the radiuses of the middle and outer tube of the reactor are added as additional degrees of freedom for optimization to further lower the costs:

$$\min_{L,r_1,r_2 N\in\mathbb{N}} J_1 := d_{cat}(2\pi a P_{cat} r_2 L) + d_{reactor}\rho_{reactor}\pi P_{reactor} L((r_2+t)^2) - r_2^2) + d_{LED} N P_{LED} + P_{LED} P_{in} N \quad \text{(P2.2)}$$

subject to equations (2.1)- (2.5), (2.8), (2.9)

$$L \in \left(0,100\right], \quad N \le 300 \quad \text{(P2.2.1)}$$

$$r_1 \ge r_0 + 0.002, \quad r_2 \ge r_1 + 0.002 \quad \text{(P2.2.2)}$$

$$r_2 \ge r_0 + 0.01, \quad \mathrm{Re} < 2000 \quad \text{(P2.2.3)}$$

$$X \ge 0.50 \quad \text{(P2.2.4)}$$

A number of additional constraints are added to (P2.2) compared to (P2.1). Constraints (P2.2.2) impose a minimum distance of 0.002 m between each concentric tube to facilitate easy construction. Furthermore, the constraints (P2.2.3) are added to ensure model validity. First, a minimum distance of 0.01 m between the light source and catalyst surface is required to satisfy assumptions used for derivation of the radiation field model. Second, a maximum Reynolds number (Re) is imposed to satisfy the laminar flow assumption. Both continuous (e.g., reactor dimensions) and discrete variables (e.g., number of LEDs or existence of LED) are present in the formulated optimization problems. The problems (P2.1) and (P2.2) were solved using two methods: 1) mixed-integer non-linear programing (MINLP) considering number of LEDs as an integer variable and, 2) non-linear-programing (NLP) considering number of LEDs as a continuous variable.

In the second type of optimization study, we aim to obtain a specified concentration profile within the reactor by varying the spacing and the number of LEDs. In contrast to conventional UV-lamps, LEDs are local light sources. Therefore, by varying the location of the LEDs, one is able to manipulate the irradiance profile throughout the reactor and thus the local reaction rates. In general, photocatalytic reactions may include chain reactions resulting in the formation of different intermediates and by-products. For example, in some cases of air and water treatment, the complete mineralization of parent pollutants does not happen and instead the compounds are degraded to some intermediates and by-products which are more harmful and toxic than the parent compounds [46-48]. Manipulating local reaction rates might help to improve selectivity when detailed knowledge on kinetics is available for specific cases. Judicious placement of LEDs within a photocatalytic reactor may enable regions with different irradiation intensities within the reactor to manipulate local reaction rates, which is mimicked by the following optimization problem:

$$\min_{y} J_2 := \sqrt{\frac{\sum_{i=1}^{n_z}\left(C_{ave,i}-C_{des,i}\right)^2}{n_z}} \tag{P2.3}$$

subject to equations (2.1)- (2.5), (2.8), (2.9)

$$E(r_2,z,y_i)=\sum_{i=1}^{500} y_i \frac{I_0\left(r_2-r_0\right)^m}{\left(\left(r_2-r_0\right)^2+(z-z_{0,i})^2\right)^{\frac{m+2}{2}}} \tag{P2.3.1}$$

$$y_i \in \{0,1\} \;\forall\; i = 1,2,\ldots,500 \tag{P2.3.2}$$

$$L=5, \quad r_1=0.016, \quad r_2=0.018 \tag{P2.3.3}$$

where

$$C_{ave}\left(z\right)=\frac{\int_{r_1}^{r_2} C_t(r,L)u(r)rdr}{\int_{r_1}^{r_2} u(r)rdr} \tag{P2.3.4}$$

$$C_{des}\left(z\right)=\begin{cases} C_{in}\left(1-\dfrac{z}{3L}\right) & \text{if } z\in\left[0,\dfrac{L}{2}\right] \\ C_{in}\left(\dfrac{5}{6}-\dfrac{2z-L}{3L}\right) & \text{if } z\in\left(\dfrac{L}{2},L\right] \end{cases} \tag{P2.3.5}$$

In optimization problem (P2.3), a desired concentration profile of toluene (C_{des}) within the reactor is defined in (P2.3.5) arbitrarily. However, this arbitrary concentration profile has been set in such a way that the required reaction rate is guaranteed to be achievable. In particular, the maximum reaction rate is obtained when the light intensity is maximized, which forms together with the chosen desired concentration profile the basis for choosing a maximum of 500 possible LEDs in (P2.3.2). The maximum light intensity is achieved when all the elements of vector y are equal to one. The objective function (J_2) describes the difference between the desired

concentration profile and the simulated average concentration of toluene (C_{ave}) as defined by (P2.3.4). The optimization problem aims to minimize the difference between the desired and simulated concentration profile by manipulating the positions of LEDs within the reactor. Note that both the desired and simulated concentration profiles are discretized over n_z points in the axial direction for implementation. Furthermore, instead of directly introducing the existence and positions of each LED as degrees of freedom, a fixed number of LEDs (500) has been evenly distributed over the reactor length and binary variables are introduced to represent the state of each LED (on or not-existent). Therefore, equation (2.9) from the model presented in Section 2 has been replaced with equation (P2.3.1) to account for the variable contribution of each LED to the total irradiation at each point on the catalyst surface. The optimization algorithm was implemented in MATLAB R2013b (The MathWorks Inc., USA).

2.2.2 Numerical implementation

Both continuous (e.g., reactor dimensions) and discrete variables (e.g., number of LEDs or existence of LED) are present in the formulated optimization problems. Such optimization problems can be classified as mixed-integer non-linear programming (MINLP) problems. For optimization problems (P2.1) and (P2.2), two approaches are explored. In the first approach, the integer variable that represents the number of LEDs is replaced by a continuous variable and the final solution is rounded to the nearest integer. This so-called relaxed optimization problem is a non-linear programing (NLP) problem, which is typically easier to solve. In the second approach, the original formulation is maintained and an MINLP solver is used to solve optimization problems (P2.1) and (P2.2). Both problems are implemented in General Algebraic Modeling System (GAMS) Release 24.4.6. (GAMS Development Corporation, Washington, DC, USA, 2015). To do so, equation. (2.2) is written as a set of algebraic equations using finite differences and a discretization scheme in the radial and axial direction. In particular, a backward finite differences method with 1,000 nodes is used in the axial direction and a central finite differences method with 100 nodes is used in the radial direction. As the initial guess for the concentration at each node, we assume within the reactor a linear decreasing concentration from the inlet concentration to a concentration corresponding to 50% conversion at the outlet in the axial direction and a uniform concentration in the radial direction. Furthermore, the number of additions in equation (2.9) is determined by the number of LEDs, which is a decision variable itself and, therefore, complicates optimization. To circumvent a variable number of additions in equation (2.9) during optimization, for both approaches, the summation is implemented by the addition of a constant and high number of LEDs (typically, $N_{\max} = 300$). Consequently, the decision variable that is being optimized is the number of LEDs that is present inside the reactor, which can either be implemented as a continuous or as an integer variable. The remaining LEDs are positioned outside the reactor, which, obviously, only exist in the mathematical model. Since all of the LEDs contribute to the local intensity on the catalyst surface within the reactor (i.e., the number of additions in equation (2.9) is constant), a small mathematical bias is created by the LEDs that are positioned outside the reactor, which would physically not exist, but still contribute to the local irradiation of the catalyst surface inside the reactor within the model. Nevertheless, since the aspect ratio of reactor is high (i.e., the length of the reactor is typically two orders of magnitude larger than the outer radius), the effect of LEDs far away from a point on the catalyst surface is considered to be negligibly small. A

possible exception is the catalyst area that is very close to the outlet of the reactor, but this boundary effect is considered to be small and, therefore, assumed to be zero in our model. The resulting NLP problems are solved with GAMS/CONOPT3 [49] and the MINLP problems are solved with GAMS/DICOPT [50], both with default settings, on a desktop PC equipped with 32-bit Windows 7, an Intel® Core™ i5-3470 3.20 GHz CPU and 4.0GB RAM.

Optimization problem (P2.3) involves a large number of binary variables (500), which makes it challenging to solve. Therefore, we decomposed the problem into a series of smaller optimization problems, which avoids the need to optimize all of the variables simultaneously. This can be done because the LEDs are local light sources within a narrow tube. LEDs that are far away from a given point have a limited influence on the local reaction rate. In other words, instead of summing over all potential LED positions in equation (P2.3.1), summation is done only over the nearest neighbours for a candidate LED position. Since the objective function of (P2.3) can also be computed locally, the optimization problem can be decomposed into a series of smaller optimization problems that involve each a lower number of variables. In this way, the required CPU time is reduced significantly. The smaller optimization problems are considered consecutively starting from the inlet of the reactor, using a moving window along the reactor towards the end of the reactor. In each step, decisions are made regarding the existence of LEDs at any of the possible LED positions within the moving window. Subsequently, the moving window is moved one LED position towards the outlet of the reactor. If the size of the moving window is too small, the influence of the neighbouring LEDs might be considerable. By increasing the size of the moving window, the number of possible LED positions within the moving window increases and, therefore, the total required CPU time increases. To find a reasonable window length, the changes in the optimal value of objective function (J_2) as a function of the window size were investigated. It was found that when more than five LED positions are considered within the moving window, the improvements in the optimal value of objective function (J_2) with an increasing window size are very limited. Therefore, a moving window that includes only five possible LED positions has been chosen for this study. Since the optimization problem at each step only involves 5 binary variables, the whole domain for each individual optimization problem is quite small and an exhaustive enumeration of all possible values of the local objective function is computationally tractable. In case the number of possible LEDs that has to be considered for each window would have been larger, branch-and-bound mixed-integer optimization could be explored to reduce the time required to solve the optimization problems for each position of the moving window compared to an exhaustive enumeration to reduce computational load. The optimization algorithm was implemented in MATLAB R2013b (The MathWorks Inc., USA). Similar methods have been used for other applications as well [51, 52].

2.3 Results and discussion

The solutions obtained for optimization problem (P2.1) for different initial guesses are given in Table 2.2. The results demonstrate that different optimal solutions are found for the tested initial guesses.

Table 2.2 Solution of optimization problem (P2.1) for different initial guesses. The costs are reported as reactor and operating costs ($J1$) divided by the consumption of toluene.

Initial guess		Optimal solution		Objective function	Method
N [-]	L [m]	N [-]	L [m]	Cost [\$ mol^{-1}]	
100	1	120	3.09	840.73	NLP
150	2	120	3.09	840.73	NLP
250	2	120	3.09	840.73	NLP
50	5	105	3.55	845.49	NLP
100	5	105	3.55	845.49	NLP
112	5	112	3.32	840.73	NLP
200	5	120	3.09	840.73	NLP
100	10	105	3.55	845.49	NLP
200	10	120	3.09	840.73	NLP
200	5	120	3.09	840.73	MINLP
200	5	120	3.09	840.73	MINLP

The optimization aims to find a trade-off between the reactor equipment costs (residence time) and the LED investment and operating costs (reaction rate), which results in solutions that either have a shorter reactor and more LEDs or a longer reactor with less LEDs. Since the optimization problem (P2.1) involves only two decision variables, the changes of the reactor cost with changing reactor length and number of LEDs can be visualized (Figure 2.2). The reactor length illustrated in Figure 2.2 was found by solving optimization problem (P2.1) but with the number of LEDs as a fixed parameter. In such case, the optimization algorithm simply finds the reactor length required to obtain the minimum required conversion. A relatively flat region for the minimum cost as a function of number of LEDs can be seen, which might explain why the optimization code converges at different points for different initial guesses. In general, local minima can also be expected since the model presented in Section 2.1. is highly nonlinear. Therefore, a multi-start optimization method in which a number of initial guesses are generated is recommended to find the lowest costs for the modelled LED-based photocatalytic reactor. Finally, when comparing the solutions obtained with an NLP and MINLP formulation, it can be seen that the optimization results for both formulations give the same result (Table 2.2). However, as expected, using an NLP formulation with relaxed integer variable requires a shorter CPU time (about 15 times) compared to solving the original MINLP formulation. Furthermore, the MINLP algorithm did not converge for all the tested initial guesses, whereas the NLP algorithm did.

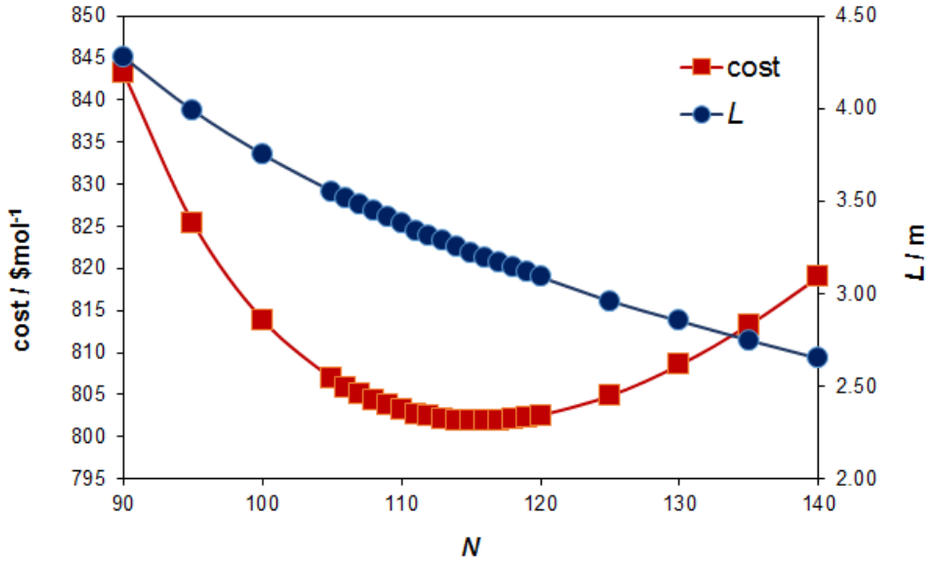

Figure 2.2 Reactor and operating cost (J_1), divided by the consumption of toluene, and minimum reactor length as a function of number of LEDs for reaching 50% conversion of toluene.

Optimization problem (P2.2) extends on (P2.1) by introducing additional decision variables related to the dimensions of the reactor: the radiuses of middle and outer tubes. The results for optimization problem (P2.2) as obtained for a number of initial guesses are presented in Table 2.3.

Table 2.3 Solution of optimization problem (P2.2) for different initial guesses. The costs are reported as reactor and operating costs (J_1) divided by the consumption of toluene.

Initial guess				Optimal solution				Objective function	Method
N	L	r_1	r_2	N	L	r_1	r_2	Cost	
[-]	[m]	[m]	[m]	[-]	[m]	[m]	[m]	[$ mol^{-1}]	
75	5	0.015	0.025	96	4.2	0.021	0.023	847	NLP
75	5	0.01	0.025	96	4.2	0.021	0.023	847	NLP
100	5	0.015	0.025	123	3.5	0.016	0.018	790	NLP
100	5	0.018	0.019	100	4.16	0.019	0.021	833	NLP
150	5	0.015	0.017	134	3.12	0.016	0.018	796	NLP
150	5	0.15	0.16	96	4.2	0.021	0.023	847	NLP
200	5	0.015	0.017	134	3.12	0.016	0.018	796	NLP
250	5	0.01	0.025	128	3.33	0.016	0.018	791	NLP
250	5	0.015	0.025	134	3.12	0.016	0.018	796	NLP
100	10	0.015	0.025	101	4.14	0.019	0.021	833	NLP
150	10	0.015	0.025	116	3.82	0.016	0.018	795	NLP
250	10	0.015	0.025	134	3.12	0.016	0.018	796	NLP
150	5	0.015	0.017	135	3.1	0.016	0.018	797	MINLP
150	10	0.015	0.025	116	3.81	0.016	0.018	795	MINLP
250	5	0.010	0.025	128	3.33	0.016	0.018	791	MINLP

Optimization problem (P2.2) is much more challenging compared to optimization problem (P2.1) since the additional decision variables are present in non-linear terms in both the model and objective function. Nevertheless, the proposed optimization approach is capable to find optimum values for all of the decision variables related to reactor dimensions and number of

LEDs simultaneously. The required time to reach convergence did depend strongly on the initial guess ranging from a few minutes for the fastest cases and up to 2.5 hours for the slowest NLP cases. The CPU time for the MINLP method was typically about 4-5 hours. Similar as for optimization problem (P2.1), it was found that the optimization results depend on the initial guess. Broadly speaking, two types of solutions were found. The lowest values for the objective function were found when both the radius of the middle and outer tube were at the constraints (P2.2.2) and (P2.2.3). The found number of LEDs was high and reactor length was short for those cases. The other type of solution corresponds to a longer reactor, lower number of LEDs and an inner and outer radius that is not constrained and has a higher objective function value. Similar as for optimization (P2.1), in optimization (P2.2) the results from the NLP and MINLP method correspond well to each other (Table 2.3). Therefore, solving the relaxed optimization problem only by treating the number of LEDs as a continuous variable is justified based on our tested cases, which simplifies the optimization.

To further investigate the differences between the solutions found, the irradiance distribution within the reactor is analysed in more detail for three cases. The reaction kinetics is coupled to the irradiance distribution from the light source on the catalyst surface as described by equation (2.8). Figure 2.3 illustrates the irradiance on the catalyst surface in the first part of the reactor for three different solutions from Table 2.4. One solution corresponds to a case with a longer reactor length (4.20 m) and a smaller number of LEDs (96). Another solution corresponds to a case with a shorter reactor length (3.12 m) and a higher number of LEDs (134). The last case corresponds to an intermediate reactor length (3.50 m) and intermediate number of LEDs (123), which gives the lowest value of the objective function among the initial guesses that were tested.

Table 2.4 Average irradiance, standard deviation and residence time for three selected solutions of optimization problem (P2.2).

N [-]	L [m]	r_1 [m]	r_2 [m]	E_{mean} [W m^{-2}]	Residence time [s]	Cost [\$ mol^{-1}]
96	4.2	0.0205	0.023	2.58	85.1	846
134	3.12	0.016	0.018	7.04	49.9	795
123	3.5	0.016	0.018	5.77	56	789

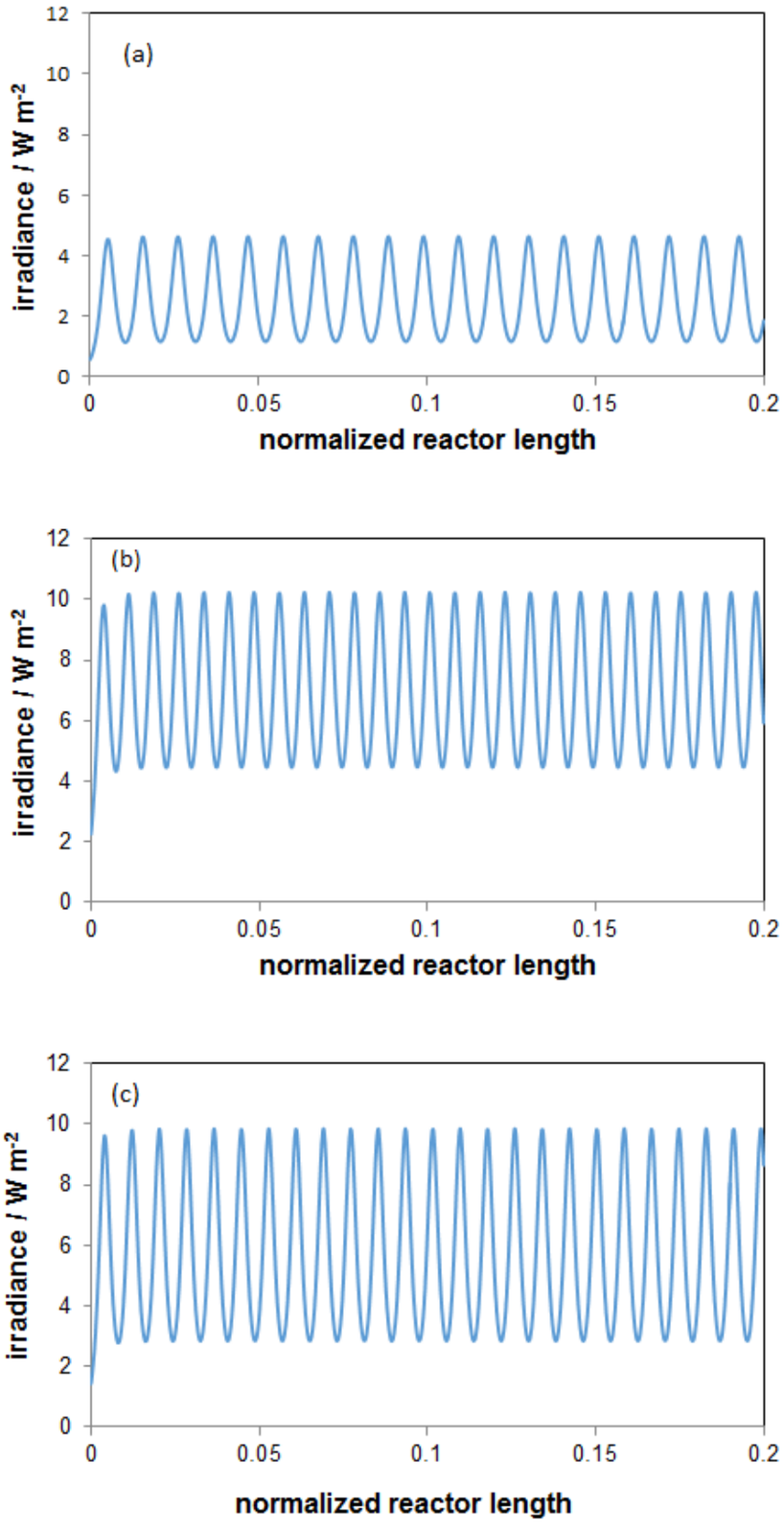

Figure 2.3 Irradiance patterns of different optimum design variables: a) N=96, L=4.2 m, r_1=0.0205 m and r_2=0.0225 m; b) N=134, L=3.12 m, r_1=0.016 m and r_2=0.018 m; c) N=123, L=3.5 m, r_1=0.016 m and r_2=0.018 m.

In a shorter reactor with higher number of LEDs (Figure 2.3(b)), the irradiance pattern is affected more by overlapping light between neighbouring LEDs resulting in a more uniform irradiance distribution with higher peak values. Furthermore, the smaller value for the outer radius generates a more intense field since irradiance is inversely proportional to the square of the distance from the light source to the catalyst surface. In addition, the smaller the distance between the catalyst surface and the light source is, the more of a non-uniform irradiance pattern is created on the catalyst surface area. The combined effect is the reason why the irradiance in Figure 2.3(b) is the highest. Non-uniformity depends on both the LED-to-LED distance and distance of catalyst surface from the light source. A larger LED-to-LED distance and a shorter distance of the catalyst from the light source each result in a more non-uniform irradiance distribution. The mean value of an irradiance pattern directly influences the reaction rate at the catalyst surface. Residence time is another factor that affects conversion, which is proportional to the reactor volume. Therefore, both reactor length and dimensions of the concentric tubes impact conversion. Finally, the distance between the middle and outer tube will influence the mass transfer of reactant to the catalyst surface through diffusion, which is another factor with an impact on conversion. In general, this complicated interplay between all those factors in LED-based photocatalytic reactors makes its design not trivial and warrants the use of mathematical optimization techniques to find optimal trade-offs. It is possible that the different solutions found for optimization correspond to different trade-offs that are optimal locally, which could explain the dependency of the final solution on the initial guess.

The average irradiance and residence time for the three selected solutions are shown in Table 2.4 as well. It is clear that a uniform light distribution is not achieved for the optimal solutions (Figure 2.3). A more uniform distribution would need either more LEDs or a larger outer radius, which means increased costs for our studied case. Therefore, optimization involves a trade-off between the residence time, mass transfer limitations and average irradiance.

In general, the photocatalytic reaction rate increases linearly for lower irradiance levels since the consumption of generated electrons-hole pairs by the chemical reaction is faster than their recombination. However, upon a further increase in irradiance, the rate of electron-hole recombination becomes significant and may surpass the consumption by the chemical reaction [36]. Although the recombination of electron-hole pairs is included empirically in our kinetic model, it seems that for the optimal solutions the reaction rate corresponds to the linear regime with respect to the irradiance [34]. Therefore, there is no penalty for a highly non-uniform light distribution and the mean intensity of the irradiance is the key property that is driving our optimization results. Experimental validation is important to further strengthen that conclusion. Therefore, a LED-based photocatalytic reactor set-up has been developed in our laboratory, facilitating the future validation of the radiative model of the reactor that is presented in Chapter 3.

In optimization problem (P2.3), the optimal position of LEDs was found to achieve a desired concentration profile. A comparison between the simulated and the desired concentration profile after optimization is illustrated in Figure 2.4, which shows a close correspondence between both profiles. An optimum number of 111 LEDs was found with distribution as illustrated in Figure 2.5. Although this particular profile is chosen arbitrarily, this optimization

illustrates the capability of LED-based photocatalytic reactors to control the reaction rate as a function of the reactor length. However, engineering of the photon distribution within solar- or lamp-based photocatalytic reactors is difficult to achieve. This feature of LED-based photocatalytic reactors facilitates controlling the process for example by using a sensor measuring the concentrations within the reactor.

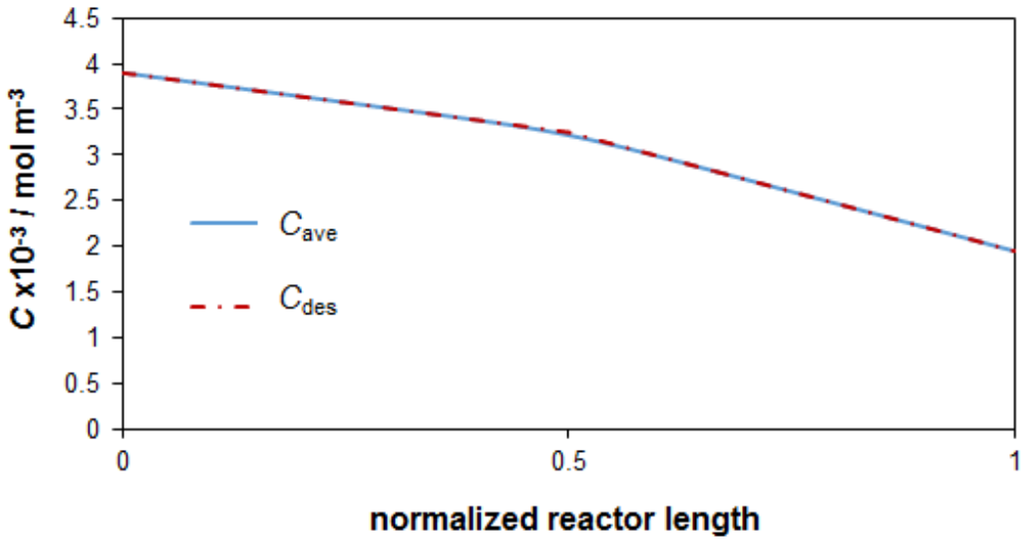

Figure 2.4 Desired and simulated concentration profile along the reactor obtained from solving optimization problem (P2.3).

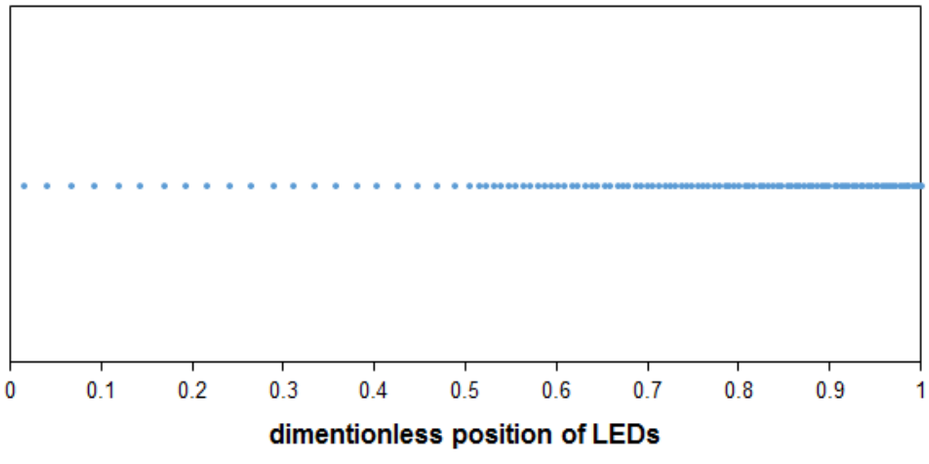

Figure 2.5 The optimized positions of 111 LEDs to reach the desired concentration profile obtained from solving optimization problem (P2.3).

2.4 Conclusions

The mathematical optimization of a LED-based photocatalytic reactor involving both decision variables related to reactor dimensions and light sources is presented. Two types of optimization problems were solved successfully. First, an economic objective function involving equipment and operational costs was minimized. Simultaneous optimization of the length, radiuses of concentric tubes and number of LEDs for an annular LED-based photocatalytic reactor was successfully achieved for the case of toluene degradation. The results suggest that different local minima exist. Therefore, to obtain the design with the lowest cost, a multi-start

optimization method, using several initial guesses, is recommended. The full optimization problem involved both integer variables (number of LEDs) and continuous variables (length, diameters) with a highly non-linear model, which is challenging to solve. However, when implementing the number of LEDs as a continuous variable and using an NLP solver, the same solution was found compared to solving the full optimization problem with a dedicated MINLP solver. The optimal irradiance profile on the catalyst surface is found to be non-uniform, which is influenced by a low rate of recombination of electron-hole pairs in the assumed kinetic model. Creating a non-uniform irradiance profile turned out to be economically more favorable compared to a design with a more uniform light distribution on the catalyst surface when taking into account the investment and operational costs of the studied case.

Second, we studied the optimization of the required number and position of LEDs for obtaining a selected concentration profile in the reactor. An optimal number of 111 LEDs with optimal positions to reach a desired concentration profile within the reactor was found. This method is a basic illustration how LEDs can be placed flexibly within a photocatalytic reactor to manipulate reaction rates locally, which could potentially be used to obtain a desired selectivity when detailed kinetics are known. Further study, focusing on the experimental validation of the proposed approach and the optimization results, is required to support the conclusions.

References:

[1] A. Fujishima, K. Honda, Electrochemical Photolysis of Water at a Semiconductor Electrode, Nature 238 (1972) 37-38.

[2] T. Inoue, A. Fujishima, S. Konishi, K. Honda, Photoelectrocatalytic reduction of carbon dioxide in aqueous suspensions of semiconductor powders, Nature 277 (1979) 637-638.

[3] M.R. Hoffmann, S.T. Martin, W. Choi, D.W. Bahnemann, Environmental Applications of Semiconductor Photocatalysis, Chem. Rev. 95 (1995) 69-96.

[4] J.M. Herrmann, Heterogeneous photocatalysis: state of the art and present applications In honor of Pr. R.L. Burwell Jr. (1912–2003), Former Head of Ipatieff Laboratories, Northwestern University, Evanston (Ill), Top. Catal. 34 (2005) 49-65.

[5] T. Van Gerven, G. Mul, J. Moulijn, A. Stankiewicz, A review of intensification of photocatalytic processes, Chemical Engineering and Processing: Process Intensification 46 (2007) 781-789.

[6] G.B. Roupp, J.A. Nico, S. Annangi, R. Changrani, R. Annapragada, Two-flux radiation-field model for an annular packed-bed photocatalytic oxidation reactor, AlChE J. 43 (1997) 792-801.

[7] R. Lakerveld, G.S.J. Sturm, A.I. Stankiewicz, G.D. Stefanidis, Integrated design of microwave and photocatalytic reactors. Where are we now?, Curr. Opin. Chem. Eng. 5 (2014) 37-41.

[8] M. Dijkstra, H. Buwalda, A. De Jong, A. Michorius, J. Winkelman, A. Beenackers, Experimental comparison of three reactor designs for photocatalytic water purification, Chem. Eng. Sci. 56 (2001) 547-555.

[9] U.I. Gaya, A.H. Abdullah, Heterogeneous photocatalytic degradation of organic contaminants over titanium dioxide: A review of fundamentals, progress and problems, J. Photochem. Photobiol. 9 (2008) 1-12.

[10] S. Sato, T. Arai, T. Morikawa, K. Uemura, T.M. Suzuki, H. Tanaka, T. Kajino, Selective CO_2 conversion to formate conjugated with H_2O oxidation utilizing semiconductor/complex hybrid photocatalysts, J. Am. Chem. Soc. 133 (2011) 15240-15243.

[11] T. Tachikawa, M. Fujitsuka, T. Majima, Mechanistic Insight into the TiO_2 Photocatalytic Reactions: Design of New Photocatalysts, J. Phys. Chem. C 111 (2007) 5259-5275.

[12] A.M. Huerta-Flores, J.M. Mora-Hernández, L.M. Torres-Martínez, E. Moctezuma, D. Sánchez-Martínez, M.E. Zarazúa-Morín, B. Wickman, Extended visible light harvesting and boosted charge carrier dynamics in heterostructured zirconate–FeS_2 photocatalysts for efficient solar water splitting, JJ. Mater. Sci. Mater. Electron. 29 (2018) 18957-18970.

[13] D. Vildozo, C. Ferronato, M. Sleiman, J.M. Chovelon, Photocatalytic treatment of indoor air: Optimization of 2-propanol removal using a response surface methodology (RSM), Appl. Catal. B 94 (2010) 303-310.
[14] F. Shahrezaei, Y. Mansouri, A.A.L. Zinatizadeh, A. Akhbari, Process modeling and kinetic evaluation of petroleum refinery wastewater treatment in a photocatalytic reactor using TiO_2 nanoparticles, Powder Technol. 221 (2012) 203-212.
[15] M.N. Chong, B. Jin, C.W.K. Chow, C.P. Saint, A new approach to optimise an annular slurry photoreactor system for the degradation of Congo Red: Statistical analysis and modelling, Chem. Eng. J. 152 (2009) 158-166.
[16] D. Vildozo, C. Ferronato, M. Sleiman, J.M. Chovelon, Photocatalytic treatment of indoor air: Optimization of 2-propanol removal using a response surface methodology (RSM), Appl. Cata. B 94 (2010) 303-310.
[17] G. Camera-Roda, F. Santarelli, M. Panico, Study and optimization of an annular photocatalytic slurry reactor, Photochem. Photobiol. Sci.8 (2009) 712-718.
[18] M. Martín-Sómer, B. Vega, C. Pablos, R. van Grieken, J. Marugán, Wavelength dependence of the efficiency of photocatalytic processes for water treatment, Appl. Catal. B 221 (2018) 258-265.
[19] J. Taranto, D. Frochot, P. Pichat, Modeling and optimizing irradiance on planar, folded, and honeycomb shapes to maximize photocatalytic air purification, Catal. Today 122 (2007) 66-77.
[20] M. Motegh, J.J. Cen, P.W. Appel, J.R. van Ommen, M.T. Kreutzer, Photocatalytic-reactor efficiencies and simplified expressions to assess their relevance in kinetic experiments, Chem. Eng. J. 207 (2012) 607-615.
[21] C.A.M. Alberto E. Cassano, Rodolfo J. Brandi and Orlando M. Alfanot, Photoreactor Analysis and Design: Fundamentals and Applications, Ind. Eng. Chem. Res. 34 (1995) 2155-2201.
[22] A.E. Cassano, O.M. Alfano, Reaction engineering of suspended solid heterogeneous photocatalytic reactors, Catal. Today 58 (2000) 167-197.
[23] C.A. Martin, G. Camera-Roda, F. Santarelli, Effective design of photocatalytic reactors: influence of radiative transfer on their performance, Catal. Today 48 (1999) 307-313.
[24] C. Passalía, O.M. Alfano, R.J. Brandi, A methodology for modeling photocatalytic reactors for indoor pollution control using previously estimated kinetic parameters, J. Hazard. Mater. 211–212 (2012) 357-365.
[25] M. Motegh, J.R. van Ommen, P.W. Appel, M.T. Kreutzer, Scale-Up Study of a Multiphase Photocatalytic Reactor: Degradation of Cyanide in Water over TiO_2, Environ. Sci. Technol. 48 (2013) 1574-1581.
[26] F. Machuca-Martínez, M.A. Mueses, J. Colina-Márquez, G.L. Puma, CHAPTER 16. Photocatalytic Reactor Modeling, (2016) 388-424.
[27] M. Singh, I. Salvadó-Estivill, G. Li Puma, Radiation field optimization in photocatalytic monolith reactors for air treatment, AlChE J. 53 (2007) 678-686.
[28] A.L.L. Zazueta, H. Destaillats, G. Li Puma, Radiation field modeling and optimization of a compact and modular multi-plate photocatalytic reactor (MPPR) for air/water purification by Monte Carlo method, Chem. Eng. J. 217 (2013) 475-485.
[29] G.E. Imoberdorf, A.E. Cassano, O.M. Alfano, H.A. Irazoqui, Modeling of a multiannular photocatalytic reactor for perchloroethylene degradation in air, AlChE J. 52 (2006) 1814-1823.
[30] J.E. Duran, M. Mohseni, F. Taghipour, Design Improvement of Immobilized Photocatalytic Reactors Using a CFD-Taguchi Combined Method, Ind. Eng. Chem. Res. 50 (2011) 824-831.
[31] W.-K. Jo, R.J. Tayade, New Generation Energy-Efficient Light Source for Photocatalysis: LEDs for Environmental Applications, Ind. Eng. Chem. Res. 53 (2014) 2073-2084.
[32] D.H. Chen, X. Ye, K. Li, Oxidation of PCE with a UV LED Photocatalytic Reactor, Chem. Eng. Technol. 28 (2005) 95-97.
[33] J.T.R. Lanfang H. Levine, and Janelle L. Coutts, Feasibility ultraviloet ligth emitting diodes as an alternative ligth source for photocatalysis, J. Air Waste Manage. Assoc. 61 (2011) 932-940.
[34] T.S.N. Kalithasan Natarajan, H.C. Bajaj, Rajesh J. Tayade, Photocatalytic reactor based on UV-LED/TiO_2 coated quartz tube for degradation of dyes, Chem. Eng. J. 178 (2011) 40-49.
[35] K. Song, M. Mohseni, F. Taghipour, Application of ultraviolet light-emitting diodes (UV-LEDs) for water disinfection: A review, Water Res. 94 (2016) 341-349.
[36] R.V. Steele, The story of a new light source, Nat Photon 1 (2007) 25-26.
[37] J.L. Zimeng Wang, Yuancan Dai, Weiyang Dong, Shicheng Zhang, Jianmin Chen, CFD modeling of a UV-LED photocatalytic odor abatement process in a continuous reactor, J. Hazard. Mater. 215-216 (2012) 25-31.

[38] A.J. Anceno, R.M. Stuetz, Photocatalytic odor abatement by platinized TiO_2 under optically transmitted LED–UV light, Appl. Catal. B 181 (2016) 661-671.
[39] M.J. Muñoz-Batista, A. Kubacka, M.N. Gómez-Cerezo, D. Tudela, M. Fernández-García, Sunlight-driven toluene photo-elimination using CeO_2-TiO_2 composite systems: A kinetic study, Appl. Catal. B 140–141 (2013) 626-635.
[40] J.-M. Herrmann, Heterogeneous photocatalysis: fundamentals and applications to the removal of various types of aqueous pollutants, Catal. Today 53 (1999) 115-129.
[41] A. Bouzaza, C. Vallet, A. Laplanche, Photocatalytic degradation of some VOCs in the gas phase using an annular flow reactor: Determination of the contribution of mass transfer and chemical reaction steps in the photodegradation process, J. Photochem. Photobiol. 177 (2006) 212-217.
[42] S.B. Kim, S.C. Hong, Kinetic study for photocatalytic degradation of volatile organic compounds in air using thin film TiO_2 photocatalyst, Appl. Catal. B 35 (2002) 305-315.
[43] M.J. Munoz-Batista, M.N. Gomez-Cerezo, A. Kubacka, D. Tudela, M. Fernandez-Garcia, Role of Interface Contact in CeO_2-TiO_2 Photocatalytic Composite Materials, Acs Catalysis 4 (2014) 63-72.
[44] V. Tomašić, F. Jović, Z. Gomzi, Photocatalytic oxidation of toluene in the gas phase: Modelling an annular photocatalytic reactor, Catal. Today 137 (2008) 350-356.
[45] M.L.S. Silvia M. Zacarías, María C. Vaccari, and Orlando M. Alfano, Efficiency Evaluation of Different TiO_2 Coatings on the Photocatalytic Inactivation of Airborne Bacterial Spores, Ind. Eng. Chem. Res. 51 (2012) 13599−13608.
[46] W. Wang, Y. Ku, Photocatalytic degradation of gaseous benzene in air streams by using an optical fiber photoreactor, J. Photochem. Photobiol. 159 (2003) 47-59.
[47] J. Jeong, K. Sekiguchi, W. Lee, K. Sakamoto, Photodegradation of gaseous volatile organic compounds (VOCs) using TiO_2 photoirradiated by an ozone-producing UV lamp: decomposition characteristics, identification of by-products and water-soluble organic intermediates, J. Photochem. Photobiol. 169 (2005) 279-287.
[48] Y. Liu, Y. Zhu, J. Xu, X. Bai, R. Zong, Y. Zhu, Degradation and mineralization mechanism of phenol by BiPO4 photocatalysis assisted with H2O2, Appl. Catal. B 142–143 (2013) 561-567.
[49] A. Drud, CONOPT: A GRG code for large sparse dynamic nonlinear optimization problems, Math. Program. 31 (1985) 153-191.
[50] M. Duran, I. Grossmann, An outer-approximation algorithm for a class of mixed-integer nonlinear programs, Math. Program. 36 (1986) 307-339.
[51] J.-H. Jiang, R.J. Berry, H.W. Siesler, Y. Ozaki, Wavelength Interval Selection in Multicomponent Spectral Analysis by Moving Window Partial Least-Squares Regression with Applications to Mid-Infrared and Near-Infrared Spectroscopic Data, Anal. Chem. 74 (2002) 3555-3565.
[52] S. Dosen, D.B. Popovic, Moving-window dynamic optimization: design of stimulation profiles for walking, Biomedical Engineering, IEEE Transactions on 56 (2009) 1298-1309.

Appendix 2A: Velocity profile in section 2.2.1.1

To find the velocity profile in the annulus, the continuity and momentum balance equations need to be evaluated. Assuming one-dimensional flow, the continuity equation is simplified to:

$$\frac{\delta u}{\delta z} = 0$$

$$u_r = u_\theta = 0 \qquad (2A.1)$$

$$u_z = u$$

Assuming a linear pressure drop over the length of the reactor, the momentum balance in cylindrical coordinates is:

$$\mu\left[\frac{1}{r}\frac{\delta}{\delta r}\left(r\frac{\delta u}{\delta r}\right)\right] = \frac{\Delta p}{L} \qquad (2A.2)$$

The boundary conditions are:

$$u(r_1) = 0 \qquad (2A.3)$$

$$u(r_2) = 0 \qquad (2A.4)$$

Integrating equation (2A.2) and by considering the boundary conditions, the velocity profile is:

$$u = \frac{\Delta p}{4\mu L} r^2 + c_1 \ln r + c_2 \qquad (2A.5)$$

$$c_1 = \frac{\Delta p\left(r_2^2 - r_1^2\right)}{4\mu L \ln\left(\frac{r_2}{r_1}\right)} \qquad (2A.6)$$

$$c_2 = \frac{\Delta p}{4\mu L}\left[r_2^2 - \frac{\left(r_2^2 - r_1^2\right)\ln r_2}{\ln\left(\frac{r_2}{r_1}\right)}\right] \qquad (2A.7)$$

The volumetric flow rate, Q can be defined as:

$$Q = \int_A u dA = \int_{r_1}^{r_2} u 2\pi r dr \cdot \qquad (2A.8)$$

Substituting equation (2A.5,) (2A.6), (2.A7) in equation. (2A.8), and integrating equation (2A.8), the volumetric flow rate can be defined by:

$$Q = \frac{\pi \Delta p r_2^2}{8\mu L}\left[-1 + \left(\frac{r_1}{r_2}\right)^4 + \frac{\left(1 - \left(\frac{r_1}{r_2}\right)^2\right)^2}{\ln\left(\frac{r_2}{r_1}\right)}\right] \qquad (2A.9)$$

Finally, by substituting equation (2A.6), (2A.7) and (2A.9) in equation (2A.5,) the velocity profile is described by:

$$u(r)=2\frac{Q}{\pi r_2^{\,2}}\frac{\ln\left(\frac{r_1}{r_2}\right)}{\left[\left(1-\left(\frac{r_1}{r_2}\right)^4\right)\ln\left(\frac{r_1}{r_2}\right)+\left(1-\left(\frac{r_1}{r_2}\right)^2\right)^2\right]}\left(1-\left(\frac{r}{r_2}\right)^2-\frac{\left[1-\left(\frac{r_1}{r_2}\right)^2\right]}{\ln\left(\frac{r_1}{r_2}\right)}\ln\left(\frac{r}{r_2}\right)\right) \quad (2A.10)$$

Appendix 2B: Radiation field model in section 2.2.1.2

2B.1 Radiation field model derivation

2B.1 Radiation field model derivation

Integrated modeling of a photocatalytic reactor requires an emission model for the light sources. The irradiance of a single LED at any point on a surface is described as follows [1]:

$$E=\frac{I}{d^2} \quad (2B.1)$$

where E is the irradiance (W m^{-2}) of a single LED , d is the distance from the LED to the catalytic surface (m). I is the light intensity (W sr^{-1}), which is a function of the viewing angle, Θ (degree) as follows [1]:

$$I\left(\theta\right)=I_0 cos^m\left(\theta\right) \quad (2B.2)$$

where I_0 is the light intensity at a viewing angle of zero, and m is a parameter that depends on the LED packaging, which is typically determined experimentally.

Regarding equation (2B.1), to model the radition field, it is needed to calculate the distance of a LED from a point on the catalyst surface and also the viewing angle from the point. Regarding the reactor geometery, it is assumed that the i^{th} LED is positioned at $\left(r_0,\varphi_{0,i},z_{0,i}\right)$ and an arbitarary point on the catalyst surface is descibed by $P\left(r_2,\varphi,z\right)$ in cylindrical coordinates. In order to to calculate the distance of a LED from point P, the cylindrical coordinates are converted into cartesian coordinates.

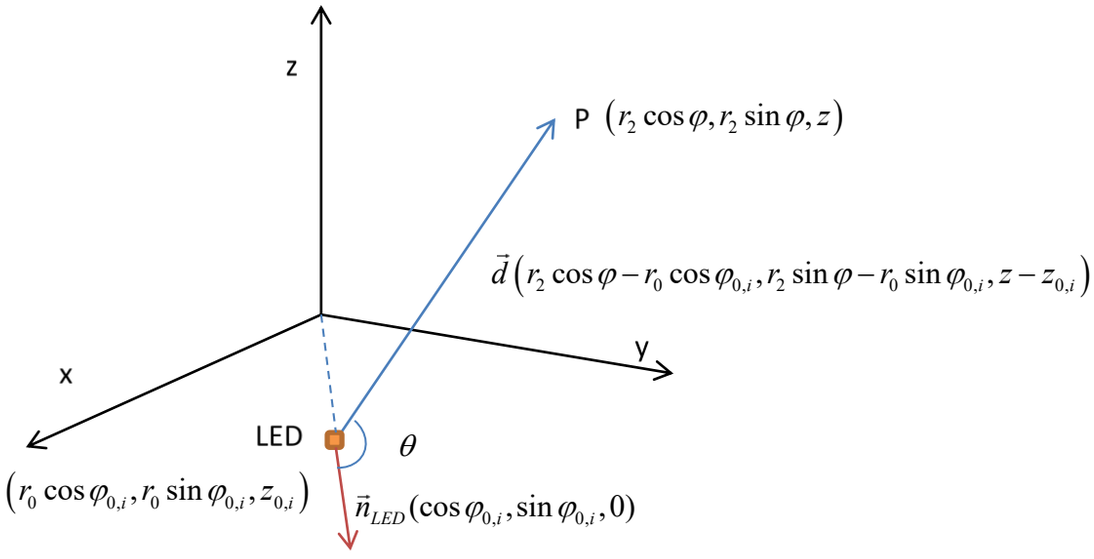

Figure 2B.1. Coordinate system for a single LED and an arbitrary point (P) on the catalytic surface.

In cartesian coordinates, the LED and P positions are desribed by $(r_0\cos\varphi_{0,i}, r_0\sin\varphi_{0,i}, z_{0,i})$ and $(r_2\cos\varphi, r_2\sin\varphi, z)$. Therfore, the distance of a LED to a point P is equal to the norm of the vector $\vec{d} = (r_2\cos\varphi - r_0\cos\varphi_{0,i}, r_2\sin\varphi - r_0\sin\varphi_{0,i}, z - z_{0,i})$ that connects the LED position to (see Figure 2B.1):

$$\left\|\vec{d}\right\| = \sqrt{r_2^2 + r_1^2 - 2r_2r_1\cos\left(\varphi - \varphi_{0,i}\right) + (z - z_{0,i})^2} \tag{2B. 3}$$

We also need to calculate the viewing angle, which is an angle between $\vec{n}_{LED} = (\cos\varphi_{0,i}, \sin\varphi_{0,i}, 0)$,

a normal vector of LED, and the vector that connects the LED position to *P*, $\vec{d}$.

From the dot product of the two vectors, the viewing angle can be found:

$$\vec{n}_{LED}\cdot\vec{d} = \left\|\vec{d}\right\|\left\|\vec{n}_{LED}\right\|\cos\theta \tag{2B.4}$$

$$\cos\theta = \frac{r_2\cos\left(\varphi - \varphi_{i,0}\right) - r_0}{d} \tag{2B.5}$$

Substituting equation (2B. 2), d and $\cos\theta$ into equation. (2B.1) and using cylindrical coordinates, the irradiance of a single LED on a point on the catalyst surface in the modelled tubular reactor can be found as follows:

$$E\left(r_2,\varphi,z\right) = \frac{I_O\left(r_2\cos\left(\varphi - \varphi_{0,i}\right) - r_0\right)^m}{\left(r_2^2 + r_0^2 - 2r_2r_0\cos\left(\varphi - \varphi_{0,i}\right) + (z - z_{0,i})^2\right)^{\frac{m+2}{2}}} \tag{2B.6}$$

where (r_0, φ_0, z_0) and (r_2, φ, z) refer to the coordinates of a LED and a point on the catalyst surface, respectively (see Figure 2B.1).

In order to calculate the effective photon absorption, the radiation contribution from each LED should be taken into account. Thus, the total radiation flux at any point on the catalyst surface is given by:

$$E\left(r_2,\varphi,z\right)=\sum_{i=1}^{N}E_i \tag{2B. 7}$$

where E_i is the irradiance of i^{th} LED and N is the total number of LEDs.

Assuming that all LEDs have the same emission characteristics, the total irradiance on the catalyst surface can be found by combining equation (2B.6) and equation (2B.7):

$$E(r_2,\varphi,z)=\sum_{i=1}^{N}\frac{I_0\left(r_2\cos\left(\varphi-\varphi_{i,0}\right)-r_0\right)^m}{\left(r_2^2+r_0^2-2r_2r_0\cos\left(\varphi-\varphi_{i,0}\right)+(z-z_{0,i})^2\right)^{\frac{m+2}{2}}} \tag{2B.8}$$

For simplicity, it is assumed that there is no irradiance gradient in angular direction. Therefore, equation (2B.8) can be simplified as follows:

$$E(r_2,z)=\sum_{i=1}^{N}\frac{I_0\left(r_2-r_0\right)^m}{\left(\left(r_2-r_0\right)^2+(z-z_{0,i}(i))^2\right)^{\frac{m+2}{2}}} \tag{2B.9}$$

2B.2 Validation of the radiation field model

2B.2.1 Radiation field model validation for a single LED

In order to validate the radiation field model of a single LED (equation (2B. 2), the actual UV output of a LED (Nichia Co., model NSSU100C, Japan) was determined using a so-called goniometric method at a forward current of 20 mA using a dedicated experimental set-up (Figure 2B.2). This method has also been used successfully to evaluate the emission model of a conventional lamp [2]. The method comprises a series of intensity measurements along an arc with fixed radius from the centre of the LED. The light intensity W sr^{-1} of a LED was measured at different angles using a calibrated spectroradiometer (Avaspec-ULS2048) at constant electrical current of 20 mA. The UV-LEDs used for this study have a central wavelength of 365 nm and irradiance angle of 110 degrees. The model parameters were estimated using a non-linear regression method (Table 2B.1). In Figure 2B.2, the irradiance profiles as predicted by the model are compared with the experimental data. The results demonstrate that the proposed model is well capable of describing the experiments.

Table 2B.1. Values for radiation field model parameters equation (2B. 2) fitted from experimental data.

I_0 [Wsr^{-1}]	1910E-6
m [-]	1.54

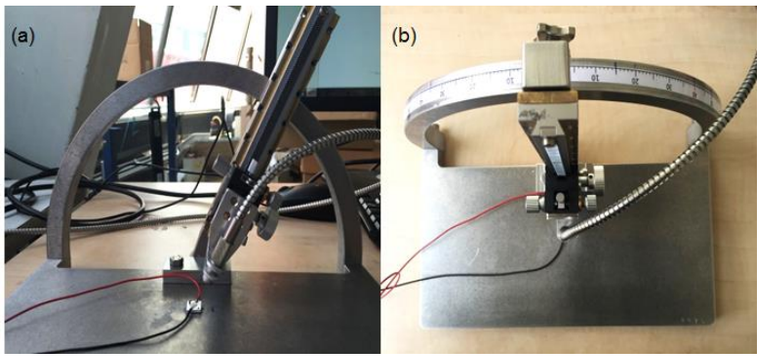

Figure 2B.2. a) Front view and b) top view of the experimental setup used to validate the radiation field model of a single LED by goniometric method.

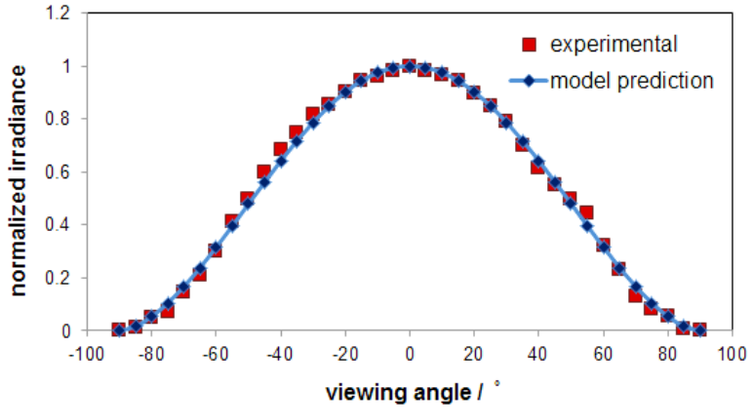

Figure 2B.2. Comparison of the measured and modelled irradiance of a single LED.

2B.2.2 Radiation field model validation for the LED assembly

In order to validate the radiation model from the LEDs configuration, a LED assembly was made in our laboratory. The individual LEDs were mounted into an array of 41 (in lateral direction) × 6 (in angular direction), forming a LED assembly including 246 LEDs in total (see Figure 2B.3 (a)). Also, a photocatalytic reactor that consists of a reactor shell of 0.6 m in length and with a 0.025 m inner radius was made. The catalyst was coated on the inner wall of the reactor shell. Therefore, to measure the irradiance on the catalytic surface, a tube with several holes at different lengths and angles was used (see Figure 2B.3 (b)) . The tube had the same dimensions as the reactor shell. The LED assembly was placed inside the tube to resemble the radiation on the catalyst surface. Afterwards, the spectroradiometer probe was inserted in the holes to measure the flux of irradiated photons on the catalytic surface at different lengths and angles. Figure 2B.4 and 2B.5 compare the irradiance obtained from the model and experimental measurement for different viewing angles and different reactor lengths. The experimental results confirm the capability of the radiation field model

to predict the flux of received photons on the catalytic surface.

Figure 2B.3. (a) LED assembly (b) the tube with the exact size of the reactor shell and the holes for irradiance measurement

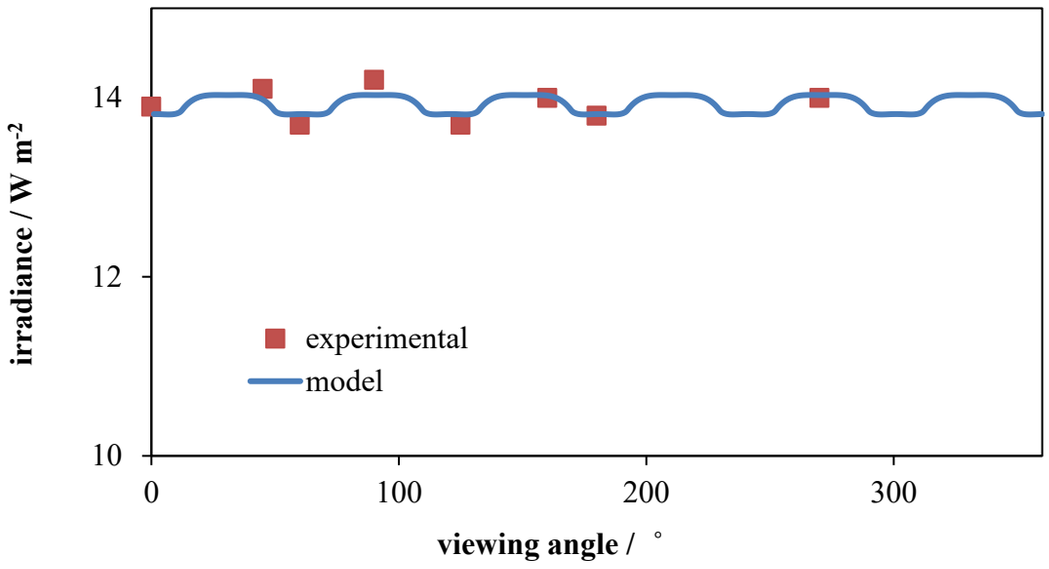

Figure 2B.4. Comparison of the modelled and measured irradiance at different viewing angles and at the same lengths (32.5 cm) for the LED assembly

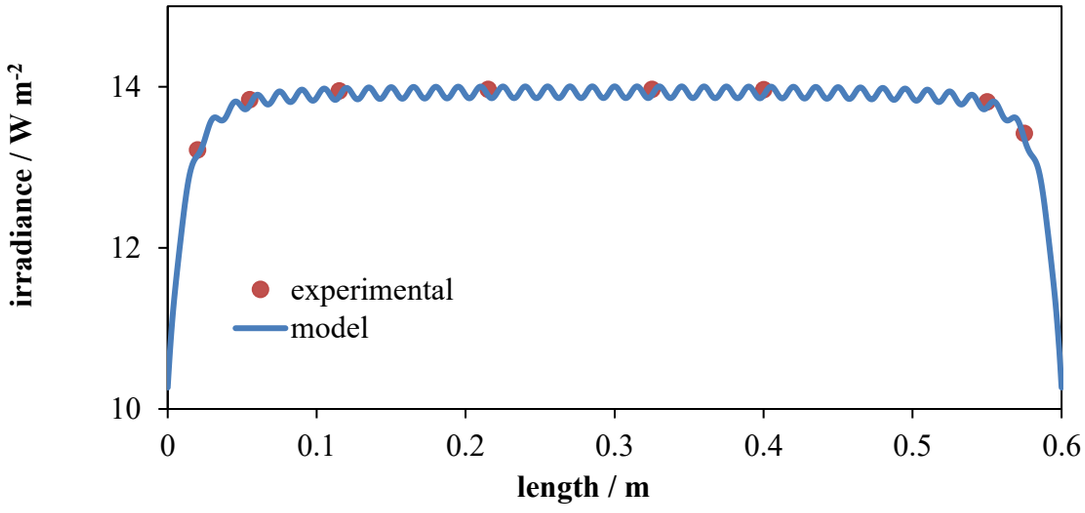

Figure 2B.5 Comparison of the modelled and measured irradiance at different lengths and at the same viewing angle (0°) for the LED assembly

References

[1] I. Moreno, M. Avendano-Alejo, R.I. Tzonchev, Appl Opt 2006, 45 (10), 2265-2272. Doi:10.1364/Ao.45.002265

[2] J.E. Duran, F. Taghipour, M. Mohseni, Journal of Photochemistry and Photobiology a-Chemistry 2010, 215 (1), 81-89. Doi:10.1016/j.jphotochem.2010.07.02

Chapter 3. Design, Characterization and Model Validation of a LED-Based Photocatalytic Reactor for Gas Phase Applications

The design and operation of reactors for photocatalytic degradation of organic pollutants remains challenging due to the complex interplay of photon, mass, and heat transfer. An integrated process model including a radiation field, reaction kinetics, and material balances of an annular LED-based photocatalytic reactor for photocatalytic degradation of toluene is validated using experimental data from a mini-pilot plant. A particular emphasis is on the effect of water on reaction kinetics, toluene conversion, mineralization, and catalyst deactivation, which is currently not well understood. The results from parameter estimation demonstrate that a competitive reaction rate model describes the experimental data with varying water concentration best. Furthermore, experimental trends demonstrate that toluene conversion is highest at low water concentrations, however mineralization and catalyst lifetime are enhanced by the presence of water. The validation of the integrated process model and understanding of the role of water allow for improved design and operation of future photocatalytic reactors.

Published as: F. Khodadadian, M.W. de Boer, A. Poursaeidesfahani, J.R. van Ommen, A.I. Stankiewicz, R. Lakerveld, Design, characterization and model validation of a LED-based photocatalytic reactor for gas phase applications, Chem. Eng. J. 333 (2018) 456-466.

3.1 Introduction

Heterogeneous photocatalysis has great potential for many applications involving either a liquid or a gas phase [1-5]. Photocatalysis uses a semiconductor, often TiO_2, to generate catalytic active sites by absorbing photons that are typically in the UV range. Recently, much attention has been paid to the capability of this technology for remediation of water and air because of its ability to degrade a broad range of organic pollutants at very low concentrations [6-9]. However, photocatalysis still lacks broad industrial adoption due its low overall efficiency despite its promising applications and intensive research during the last decades.

The main challenges to improve the efficiency of photocatalytic processes include the development of more efficient photocatalysts as well as the design of efficient photocatalytic reactors. The latter is complicated by the lack of knowledge on kinetic reaction mechanisms and by the need to optimize mass, heat, and photon transfer simultaneously [10, 11]. Especially, if artificial light sources are used, an efficient utilization of photons within the reactor is of great importance to lower operational costs while still achieving optimal illumination of the catalyst. Furthermore, efficient mass transfer of reactants and products is required. Therefore, the scale-up and efficient operation of photocatalytic reactors remains challenging, which may hinder commercial development [10].

Mathematical models based on first principles can be efficient tools for design, scale-up and optimization studies since process models provide an understanding about optimal performance and limitations of a process. For photocatalytic processes, such models should include mass, momentum and radiation balances coupled via reaction kinetics. Several studies have been dedicated to modeling of photocatalytic systems for different applications [12-19]. Tomasic et al. [13] compared one (1-D) and two-dimensional (2-D) models of a continuous annular photocatalytic reactor for toluene degradation in air, where TiO_2 was coated on the inner wall of the reactor shell and illuminated internally by a fluorescent backlight blue lamp. They concluded that a 2-D model is superior to a 1-D model when comparing experiments to simulations. Lopes et al. [14] modelled a continuous tubular photocatalytic reactor, under simulated solar irradiation assuming a uniform light distribution on the catalytic surface, for degradation of perchloroethylene over TiO_2 in the gas phase by solving mass and momentum balances. They combined the mathematical model with different reaction rate expressions and fitted to the experimental results from a lab-scale set-up to find the mechanism that described the reaction best. In general, the irradiance over the catalyst surface might not be uniform leading to differences in local reaction rates. Therefore, a radiation field model predicting the local photon flux within the reactor is important to improve models of photocatalytic processes [15, 18]. Hossain et al. [17] developed a three-dimensional model for a pilot-plant monolith photocatalytic reactor, which was illuminated from the front and backsides by low pressure mercury lamps. The model included mass, momentum and radiation balances and was validated experimentally for degradation of formaldehyde and toluene. A monolith reactor provides a large catalytic surface area; however, the photon utilization within such a reactor can be poor. In order to provide a bigger catalytic surface area and more efficient photon utilization, Imoberdorf et al. [16] proposed a multi-annular photocatalytic reactor, where TiO_2 is coated on the reactor walls. They studied models and experiments of the reactor for perchloroethylene

photocatalytic degradation in air. A tubular UV lamp was placed at the center of the reactor and the lamp emission profile was modelled and coupled to intrinsic reaction rates to close material balances and a momentum balance. The experimental data corresponded well to the model. In another study, Batista et al. [19] modelled the performance of a non-steady state annular photocatalytic reactor, illuminated externally by four cylindrical daylight fluorescent lamps. The model was validated by experimental results for toluene degradation over CeO_2-TiO_2. Experimental results confirmed the results from the model.

Conventional lamps, which are frequently applied for photocatalysis studies, are normally rigid cylindrical lamps constraining the reactor design due to their fixed shape and size. In addition, they exhibit a relatively short life span, high toxicity, risk for gas leakage and disposal issues, and a relatively high-energy consumption and heat production [20]. When using artificial light sources, the operational costs of a photocatalytic process are mainly determined by photon generation. Therefore, an inefficient photon generation and utilization within a reactor may limit economic viability. Alternatively, Light emitting diodes (LEDs) are feasible light sources for TiO_2 assisted-photocatalytic applications [21, 22]. Compared to conventional lamps, LEDs are more robust, energy efficient, cheap, non-toxic, long-lasting and compact. Moreover, cost might be favoured by a non-uniform illumination, which cannot be achieved easily with a conventional lamp [23]. Finally, LEDs are small, which offers flexibility for design and, therefore, require a systematic design approach when used in photocatalytic reactors.

Modeling of a LED-based photocatalytic reactor including an emission model for LEDs to derive the local rate of photon absorption is important for design and optimization, but only few studies exist on this topic. Wang et al. [24] modelled an externally illuminated flat plate photocatalytic reactor for degradation of dimethyl sulphide. A flat array of 3×9 LEDs, whose dimension matched the TiO_2 catalytic plate inside the reactor, was chosen as the light source in this study. A LED emission model was coupled with reaction kinetics and computational fluid dynamics (CFD) to model the degradation of dimethyl sulphide in air, which showed good agreement with experiments. Most of the experimental studies on modeling and validation of photocatalytic processes have been done using lab-scale photocatalytic reactors. However, considering the complicated scale dependency of photon and mass transfer within photocatalytic reactors, studies on the modeling and experimental validation of larger scale LED-based photocatalytic reactors are also needed.

The objective of this chapter is to validate experimentally an integrated process model of a LED-based photocatalytic reactor on a mini-pilot plant scale. An experimental setup involving an internally illuminated annular LED-based photocatalytic reactor was designed and constructed for the current model validation study using the photocatalytic degradation of toluene, a typical indoor air pollutant, in the gas phase as model system. Toluene is one of the most common indoor pollutants, which has recently raised many concerns regarding human health [4, 25-27]. The process model has been described and optimized in earlier work [23] and includes mass transfer, reaction kinetics, and a LED emission model. The mass transfer model and radiation field model allow for local concentrations of chemical species and photon absorption to be calculated when kinetics of toluene degradation are fully understood. In addition to toluene and oxygen, water will likely be part of the feed mixture of any practical

system. However, although the role of water in degradation of toluene has been investigated extensively [28-35], water remains a controversial subject of debate. Some studies showed that in the absence of water, no photocatalytic degradation of toluene occurs [30-34], while other studies proposed only a minor role of hydroxyl radicals originated from water in the photocatalytic degradation of toluene [28, 29, 35]. The effect of water on the process behaviour of a LED-based photocatalytic reactor needs to be fully understood to develop reliable process models for engineering purposes such as design, control, and optimization. Therefore, this study aims to improve the prediction of the effect of water by operating the system at different relative humidity and fitting various kinetics models to the data from the new mini-pilot plant. Furthermore, a focus will be on the experimental trends regarding conversion and full mineralization of toluene and catalyst deactivation as function of water content. Catalyst deactivation has been reported frequently in related studies at high toluene concentrations [30, 36]. Finally, the effect of other variables such as toluene inlet concentration, residence time, and irradiance will be investigated to better understand process trends and to create a data set that is sufficiently rich for parameter estimation and validation of the integrated process model.

3.2 Materials and methods

3.2.1 Catalysts preparation and characterization

TiO_2 was used to prepare a catalytic film on a stainless steel sheet of 0.1 mm thickness as support following the method proposed by Lee et al. [37]. Before coating, the rectangle sheet of 0.157 m width (the sheet width matches with the perimeter of a circle of 0.05 m diameter) and 0.6 m length was washed with ethanol and dried at 80 ℃ for 15 minutes. 1.2 g of TiO_2 powder (P25 by Evonik; particle size of 21-30 nm; BET surface area of 50 m^2 g^{-1}) was mixed with 0.4 g of acetyl acetone (Sigma-Aldrich). The mixture was added to a solution of 6.0 ml of deionized water and 0.24 g of polyethylene oxide (M.W. 1000, Sigma-Aldrich) and 0.24 g of polyethylene glycol (M.W. 8000, Sigma-Aldrich). Subsequently, the obtained paste was sonicated for 8 hours and coated uniformly on the stainless steel sheet by a doctor blade method. The sheet coated with catalyst was annealed with air at 550 ℃ for 4 hours. Finally, the catalytic sheet was rolled to form a cylinder and was placed on the inner wall of the reactor shell.

The phase change between the anatase and rutile crystal form of TiO_2 after annealing at 550℃ was investigated by X-ray diffraction (XRD) analysis (see Figure 3A.1 in Appendix 3A). The used TiO_2 is a combination of anatase (≈80%) and rutile (≈20%). The photocatalytic activity of anatase is superior to rutile [38]. It is well known that at high temperatures the anatase phase of TiO_2 converts to the rutile phase. Different temperatures have been reported for this transition [39]. Our XRD analysis showed that the anatase to rutile transition for P25 was negligible and reached only around 3% after being heated to 550℃. The catalyst film thickness was measured by a profilometer (Dektak 8 Profiler, Veeco GmbH) at several locations on the catalytic sheet, which was found to be 25 ± 6 μm.

The fraction of photons reflected by the catalytic film was measured as function of wavelength using a spectroradiometer equipped with an integrating-sphere attachment (Perkin Elmer Lambda 900) with 150 mm integrating sphere. Figure 3.1 shows the fraction of light reflected

at different wavelengths of light. For the dominant wavelength used in this study (365 nm), the fraction of light reflected is 25%. Considering that there is no transmission of light in our catalytic system, the fraction of light absorbed is about 75%.

The fraction of light transmitted through the catalytic film and substrate material is assumed to be zero, because of the optically thick catalytic film and chosen substrate material [40]. Taking into account the closed and tubular reactor configuration and the possibility of re-absorption of reflected photons, any loss of photons due to reflection and subsequent absorption by any material other than the photocatalyst has been neglected when modeling the photocatalytic reactor. Therefore, any kinetic effects of photon reflection will be taken into account indirectly when fitting model parameters of reaction kinetics. In addition, the fraction of absorbed photons depends on the photon wavelength as depicted in Figure 3.1. Therefore, for a polychromatic field, the monochromatic rate of photon absorption in the reaction kinetics is calculated by integration of photon absorption rates for different photon wavelengths over the catalytic surface. However, in this study due to the very narrow spectra of LEDs, the rate of photon absorption is approximated as a monochromatic radiation source of 365 nm wavelength.

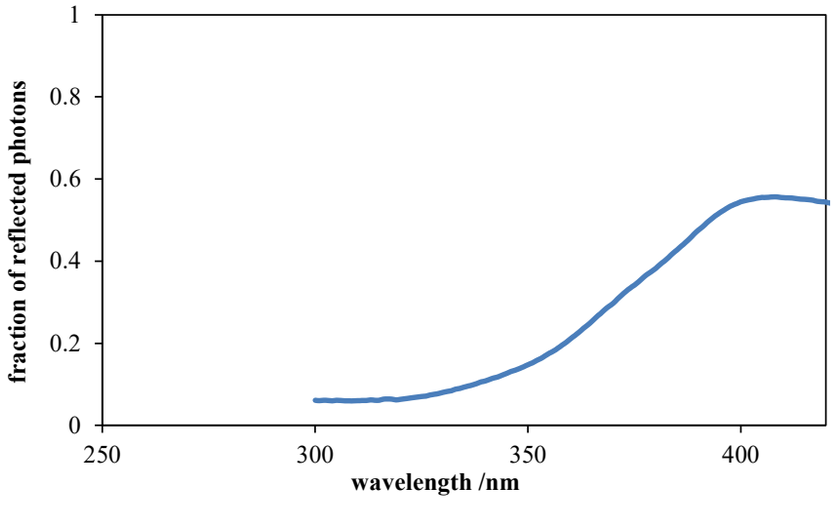

Figure 3.1 Fraction of photons reflected by the catalytic sheet versus emitted photons wavelength

3.2.2 Experimental set-up and method

A mini-pilot plant experimental set-up (Figure 3.2) was designed and constructed. The set-up is composed of three main parts: a feed preparation system, a tubular LED-based photocatalytic reactor and a product sampling and analysis system.

The carrier gas in this study is a mixture representing air with N_2 (78%) and O_2 (22%). The reactor feed is generated by mixing three gas streams: a stream of carrier gas containing toluene, a humid stream of carrier gas with water vapor and a stream of carrier gas for dilution. Liquid toluene is used to generate toluene vapour in the carrier gas. First, regulated flows of pure N_2 and O_2 are mixed via two mass flow controllers (MFC) (F-201CV-1K0-RAD, Bronkhorst, the Netherlands) at a desired ratio to generate the carrier gas. The liquid toluene (anhydrous 99.8%, Sigma-Aldrich) is pressurized by helium in a stainless steel vessel of which the outlet flow is controlled by the MFC. The liquid toluene and the carrier gas flow into a Controlled Evaporator

Mixer (E-7110-04-33-01-RAA, Bronkhorst, the Netherlands) where toluene is heated, vaporized and mixed with the carrier gas. A similar Controlled Evaporator Mixer system is used to obtain carrier gas humidified with water. The two carrier gas streams (toluene feed and humidified carrier gas) are mixed and further diluted with a third feed stream of carrier gas to provide the reactor feed of desired toluene concentration and relative humidity. Consequently, the initial toluene concentration and relative humidity of the resulting mixture can be varied in the range of 20-85 ppmv and 0-70%, respectively, before entering the reactor. The relative humidity of the feed is monitored at the reactor inlet and outlet using on-line thermohygrometer (model HC2-IE102, Rotronic). The photocatalytic degradation of toluene at the surface of a TiO_2 film is known to be more effective at room temperature rather than at elevated temperature [41]. Therefore, all experiments were performed at 30℃. The reactor shell has a jacket through which water of 30℃ flows to keep the reactor temperature at this desired value. Furthermore, all of the conduits are made of stainless steel and are heat traced to keep the gas flow at 30℃.

The standard configuration of the LED-based photocatalytic reactor consists of three concentric cylinders of the same length. The used UV-LEDs (NSSU100CT, Nichia, Japan) have a maximum spectral intensity at 365 nm and 10 nm half height width and a directivity of 55˚at 50% of irradiance. 246 LEDs are mounted evenly on the inner cylinder and distributed in such a way that they provide almost a uniform illumination pattern on the catalytic surface [23]. The irradiance emitted by the LEDs can be manipulated using current-control mode since irradiance of LEDs is linearly proportional to the applied current. Depending on the applied current, the power consumption of LEDs varied from 0.81 to 3.6 W in this study. The photon flux from the LEDs received by the catalytic film is measured by a calibrated spectroradiometer (Avaspec-ULS2048). The LEDs are separated from the reacting medium by a quartz cylinder in the middle, which is transparent to UV radiation. The outer cylinder is made of stainless steel and is used as the reactor shell to support the catalyst film. The catalytic sheet is placed on the inner wall of the reactor shell. A flow distributor with several small orifices is used at the reactor inlet to achieve a fully developed velocity profile at the cross section of the reactor. The system is characterized in terms of toluene conversion, mineralization, and catalyst deactivation for different reactor lengths and operational variables including toluene inlet concentration, relative humidity, volumetric flow rate and irradiance. The experimental details including reactor geometry and operational conditions are summarized in Table 3.1. Every experiment in this study has been repeated at least once. The uncertainty of the experimental results has been reported as the 90% confidence interval.

A back pressure controller (P-702CV-6K0A-RAD, Bronkhorst, the Netherlands) keeps the reactor pressure at slightly above ambient pressure (1.09 bar) and the pressure of the system is measured using a pressure meter (P-502C-6K0A-RAD, Bronkhorst, the Netherlands) located before the reactor inlet. A part of the reactor effluent flows into an on-line Gas Chromatograph (GC) (GC-7890B, Agilent Technologies) with a constant flow rate, which is measured with a mass flow controller (F-201CV-1K0-RAD, Bronkhorst, the Netherlands). The remaining part of the reactor effluent flows into a vent. The GC is equipped with a methane convertor, two Flame Ionization Detectors (FID, one for hydrocarbons and another one for CO_2 concentrations lower than 50 ppmv detection) and two Thermal Conductivity Detectors (TCD, one for N_2 and

O_2 and another one for CO_2 detection). Gasses such as CO and CO_2 are separated with PPQ/Molseive columns. After the chromatographic separation has taken place, CO and CO_2 are converted to CH_4 using hydrogen on a nickel catalyst and measured as CH_4 with the FID detector. The advantage of using the FID detector is the much higher sensitivity and stability of FID compared to TCD. Although the GC configuration used in this study was designed and calibrated to detect a wide range of by-products from photocatalytic degradation of toluene such as benzaldehyde and benzoic acid, no by-product was detected in the reactor effluent gas.

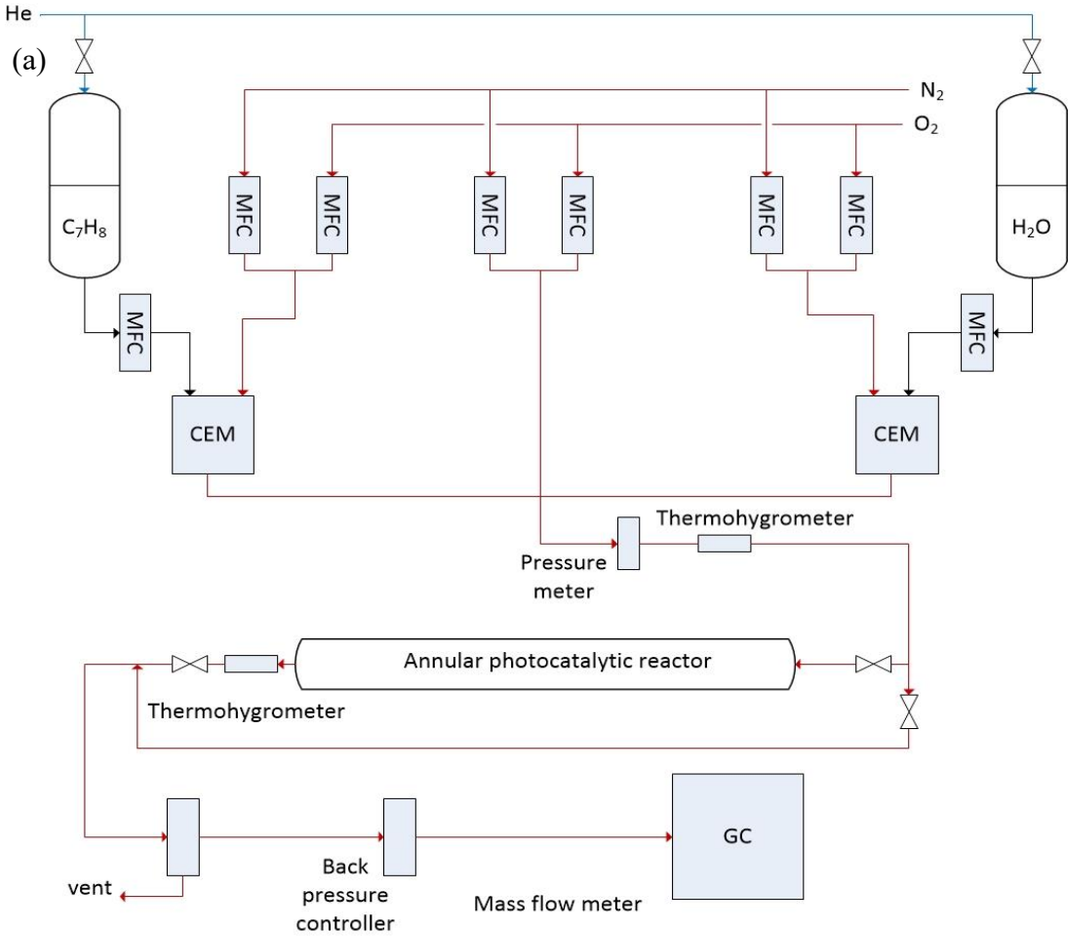

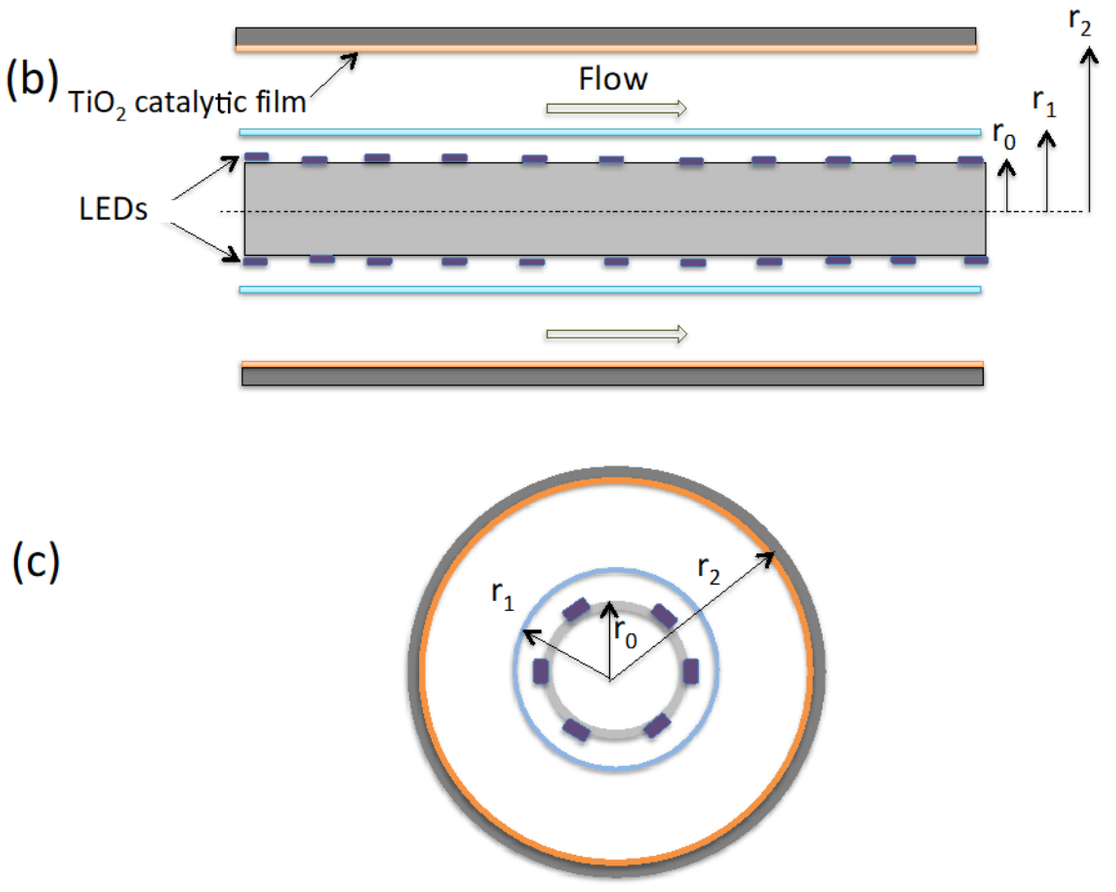

Figure 3.2(a) Schematic diagram of experimental set-up; (b) schematic representation of the cross-sectional side view of the LED-photocatalytic reactor, and (c) schematic representation of the cross-sectional view of the LED-photocatalytic reactor.

Before starting a catalytic test, the reactor feed is injected into the GC via a bypass line to analyse the feed composition. Subsequently, the reactor is purged for 2 hours with feed without illumination to reach the equilibrium state. Finally, the illumination is started and the concentrations of the various species in the reactor effluent are measured every 20 minutes. All the experimental data are obtained using the same catalytic film to prevent any bias resulting from differences in catalyst surface and thickness. However, due to catalyst deactivation, the catalyst was regenerated rigorously before conducting a new experiment.

To investigate the catalyst deactivation, experiments are carried out for a period of 240 minutes. It has been reported that O_2 molecules are necessary for faster catalyst regeneration since the humidified N_2 stream cannot efficiently regenerate the catalyst activity [42]. Therefore, before every experiment, the photocatalyst is regenerated by using an 800 ml min^{-1} humidified air (55% RH) stream with 13 W m^{-2} of UV irradiance for 8 hours. Only the first 30 minutes of every experiment have been considered to determine the steady state, because the catalyst activity decreased over longer periods for some experiments. Catalyst deactivation is not included in the steady-state process model described in the next section.

Table 3.1 Reactor dimensions and operating conditions

Photocatalytic reactor geometry		
L	reactor length [m]	0.12 - 0.6
r_0	LEDs tube radius [m]	0.008
r_1	quartz tube radius [m]	0.02
r_2	reactor shell radius [m]	0.025

Operation conditions				
Experiment no.	Relative Humidity (RH) %	Irradiance (E) [W m^{-2}]	Toluene inlet concentration ($C_{t,in}$) [ppmv]	Volumetric flow rate (Q) [ml min^{-1}]
#1	40	13	19	1250
#2	40	13	30	1250
#3	40	13	42	1250
#4	40	13	52	1250
#5	40	13	70	1250
#6	40	13	80	1250
#7	40	13	42	500
#8	40	13	42	800
#9	40	13	42	1000
#10	40	13	42	1500
#11	0	13	42	800
#12	10	13	42	800
#13	25	13	42	800
#14	55	13	42	800
#15	70	13	42	800
#16	40	3	42	800
#17	40	5	42	800
#18	40	7	42	800
#19	40	9	42	800
#20	40	11	42	800

3.2.3 Reactor modeling and validation

The reactor model is based on material, momentum and radiation balance equations. The internal mass transfer within the catalytic film has been neglected since the catalyst film is thin and non-porous. Biard et al. [43] found that the internal mass transfer is negligible for a similar system as used in this study, which justifies our assumption. The model used in this chapter and its assumptions have been described in detail in Chapter 2; however, it has been extended in the present chapter to consider different effects of water on the reaction kinetics.

The Langmuir-Hinshelwood (L-H) mechanism has been widely applied to describe the reaction rate at the initial step of photocatalytic reaction [6, 44, 45] including the photocatalytic degradation rate of toluene [31, 46]. Since the by-products and intermediates are normally formed in trace amounts and could not be detected at the reactor outlet during our experimental tests despite the used GC configuration that was calibrated to detect typical by-products from toluene degradation, their effects on the reaction rate are ignored:

$$R \propto \theta_t \tag{3.1}$$

where θ_t is the toluene coverage on the catalytic surface.

A photocatalytic reaction rate can often be described by a power law in association with the rate of photon absorption [47]. The details of the radiation field model of an array of LEDs are given in Appendix 2B. Furthermore; the radiation field model has been validated for the reactor used here in Chapter 2. The reaction rate is proportional to irradiance:

$$R \propto E^{\gamma} \tag{3.2}$$

where the exponent γ has a value between 1 and 0, which can typically be estimated using non-linear data fitting. At low irradiance, the reaction rate is proportional to irradiance since the limiting step is electron-hole generation. When further increasing the irradiance, the electron-hole generation rate surpasses the reactant consumption rate, stimulating charge recombination processes, which causes a transition from a first order to a square root dependency with respect to irradiance. Finally, at the light-saturated regime, the reaction rate becomes independent of irradiance since the reaction is limited by mass transfer [7, 48, 49].

In several studies, photocatalytic degradation of toluene has been described successfully by a simple uni-molecular L-H, considering only toluene adsorption on the catalytic surface [13, 28, 31, 46, 50]:

$$R = -E^{\gamma} k \frac{KC_t}{1 + KC_t} \tag{3.3}$$

where k and K are the rate constant and adsorption equilibrium constant, respectively. C_t is toluene concentrations on the catalyst surface. However, it may be needed to include the effect of water concentration in the reaction rate expression [32]. Humidity can play a significant role in a photocatalytic oxidation mechanism via transformation of water into hydroxyl radicals on the catalyst surface, which are highly reactive oxidants. In addition, water can also supress electron-hole recombination [31]. On the other hand, the surface of TiO_2 is hydrophilic, which results in competitive adsorption between the reactants and water on the catalytic sites [29]. Consequently, increasing the water content may decrease toluene adsorption on TiO_2 active sites, affecting toluene coverage on the catalytic surface and, therefore, reaction rate. To better predict the effect of water on the process behavior, a competitive bi-molecular L-H reaction rate model, described by

$$R = -E^{\gamma} k \frac{K_t C_t}{1 + K_w C_w + K_t C_t} \tag{3.4}$$

is investigated as an alternative to simple L-H kinetics described by equation (3.3). In equation (3.4), K_t and K_w are the toluene and water adsorption equilibrium constant and C_w is the water concentration. Four series of experiments are conducted at identical operating conditions except for the toluene and water inlet concentrations, irradiances and volumetric flow rates (see Table 3.1) to compare the performance of both models for reaction kinetics within the overall process model when describing the experimental data.

When neglecting any volume changes for different toluene concentrations that have low values in this study, the average concentration of toluene ($C_{t,out,mod}$) at the reactor outlet and toluene conversion (X) are given by:

$$C_{t,\text{out,mod}} = \frac{\int_{r_1}^{r_2} C_t(r,L)u(r)rdr}{\int_{r_1}^{r_2} u(r)rdr} \tag{3.5}$$

$$\text{X} = 1 - \frac{C_{t,\text{out}}}{C_{t,\text{in}}} \tag{3.6}$$

where L is the reactor length and r_1 and r_2 are the inner and outer annulus radius. $C_{t,in}$ and $C_{t,out}$ are toluene concentrations at the reactor inlet and outlet. Toluene mineralization is defined as the ratio of toluene moles converted to form CO_2 to the total moles of toluene converted (complete oxidization of 1 mole toluene results in the formation of 7 moles of CO_2), and described as follows [28]:

$$\text{mineralization} = \frac{1}{7}\frac{\text{mole}_{CO_2,\text{formed}}}{\text{mole}_{\text{toluene,converted}}} \tag{3.7}$$

The reactor model is solved using Matlab R2014b. An optimization algorithm is used for fitting the model parameters to experimental data by minimizing the following error function:

$$\text{err} = \sum_{i}^{M}\left(C_{t,\text{out,exp}}(i) - C_{t,\text{out,mod}}(i)\right)^2 \tag{3.8}$$

where M is the number of data points obtained from multiple identical experiments and $C_{t,out,exp}$ and $C_{t,out,mod}$ are the toluene outlet concentrations from the experiments and the model, respectively.

The differential equation (2.2) is solved via discretization along the axial and radial directions using finite difference approximations. In particular, a first-order upwind scheme is used to produce $N_R \times N_L$ algebraic equation (where N_R is the number of grid points in the radial direction and N_L is the number of grid points in the axial direction), which are solved simultaneously.

3.3 Results and Discussion

3.3.1 Model validation and parameter estimation

3.3.1.1 Mass transfer limitations

A number of experiments were conducted to study any mass transfer limitation in the reactor. Changing the volumetric feed flow rate will change both the residence time as well as the flow conditions inside the reactor when reactor length is constant. Therefore, for a fair comparison, a series of experiments were conducted at different volumetric flow rates, but with the same residence time, toluene inlet concentration, irradiance and RH. To be able to keep the residence time constant at different flow rates, the modular design of the reactor was used by controlling the illumination in each of the 5 identical modules of 0.12 m in length independently. Considering the fact that there is no photocatalytic reaction at darkness, it is possible to vary the reaction length by either switching on or off the LED arrays in each module. In this study, the illumination edge effect on the adjacent dark module was neglected due to the high aspect ratio of the studied system. The results show that the volumetric flow rate has no significant influence on the toluene conversion at different volumetric flow rates (Figure 3.3). Therefore, it can be concluded that at least under the operating conditions applied in this study, mass transfer limitations are small compared to limitations in reaction rate. In case volumetric flow rates would become much higher compared to the values applied in this study, our assumption of a fully developed laminar flow would be violated. In such case, a film model should be used to describe the mass transfer in the system.

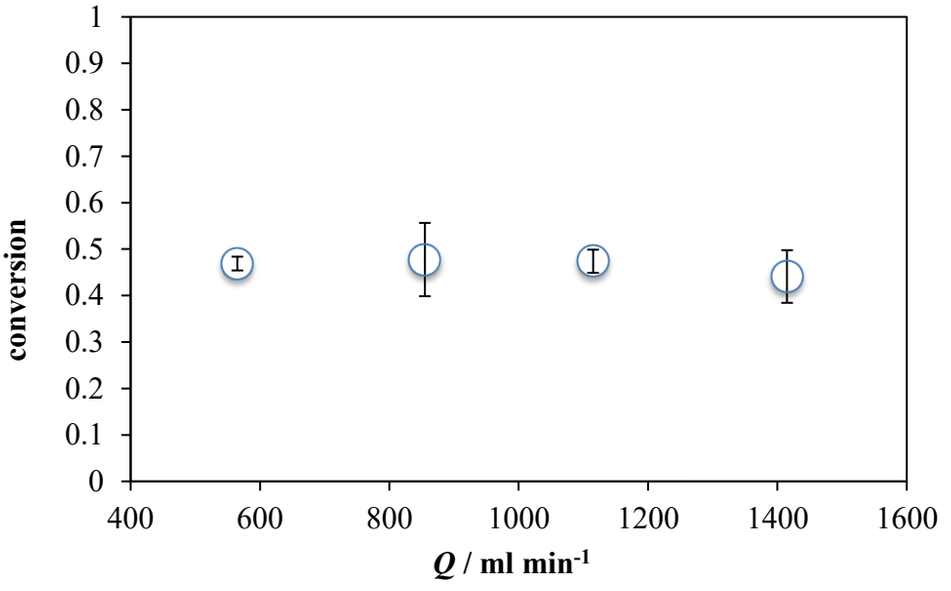

Figure 3.3 Toluene photocatalytic conversion versus volumetric flow rate for $C_{t,in}$≈29 ppmv, residence time= 18 s, E=13 Wm^{-2} and RH=40%.

3.3.1.2 Kinetic model

The integrated process model describes the toluene conversion reasonably well (see Figure 3B.1(a) in Appendix 3B for the parity plot) when using a simple uni-molecular L-H reaction rate equation (equation (3.3)) at a fixed RH of 40% after parameter estimation. However, the model with uni-molecular L-H kinetics failed to describe the toluene conversion when parameter estimation was based on the full data set including experiments at different RH, which was indicated by an error function value that was about 5 times higher compared to the case at constant RH (see Figure 3B. 1(b) in Appendix 3B for the parity plot). The estimated parameter values and error function values for both cases are given in Table 3.2. It is clear that the influence of water should be included in the reaction rate equation to describe the experimental data well.

The estimated parameters and error function value for the model including equation (3.4) are also reported in Table 3.2 (see Figure 3.B2 in Appendix 3B). It can be seen that the competitive bi-molecular L-H reaction rate explains the experimental data satisfactorily in the studied range for all experiments. Therefore, it is concluded that for varying water concentrations, the competitive bi-molecular L-H reaction rate offers a more suitable description of the system behaviour. The reaction rate can be simplified to the simple uni-molecular L-H only if the water concentration does not change, which would simplify modeling and optimization.

When comparing the estimated parameters for equation (3.4) in this study and literature, it can be seen that the estimated parameters are very comparable with the values reported in some studies, where the applied catalysts, operating conditions and the reaction rate are similar [51]. However, the reported values for kinetics parameters are different from other studies but still in the same order of magnitude. The observed differences can be attributed to the difference in different catalyst properties as well as the reactor system, operating conditions and the reaction rate [32, 52].

Table 3.3.2 Kinetic and adsorption equilibrium parameters obtained from parameter estimation when using the reaction rate expressions (3.3) and (3.4) in the reactor model including objective function value (err) of the found minimum.

Rate expression	Parameters	Values	Units	err	Remark
$R = -E^{\gamma} k \frac{KC_t}{1+KC_t}$ (3.3)	k	1.64E-7	mol m^{-1} s^{-1} $W^{-0.5}$		For the experimental results at fixed RH of 40%
	K	692	m^3 mol^{-1}	0.0014	
	γ	0.5	-		
$R = -E^{\gamma} k \frac{KC_t}{1+KC_t}$ (3.3)	k	8.9 E-8	mol m^{-1} s^{-1} $W^{-0.5}$		For all the experimental results including all tested water concentrations
	K	1160	m^3 mol^{-1}	0.0060	
	γ	0.5			
$R = -E^{\gamma} k \frac{K_t C_t}{1+K_w C_w + K_t C_t}$ (3.4)	k	1.04E-7	mol m^{-1} s^{-1} $W^{-0.5}$		For all the experimental results including all tested water concentrations
	K_t	2089	m^3 mol^{-1}	0.0027	
	K_w	3.32	m^3 mol^{-1}		
	γ	0.5	-		

3.3.2 Experimental characterization of reactor performance

No degradation of toluene was found under either dark conditions or in absence of catalyst. Carbon dioxide was the main product of the photocatalytic experiments and no intermediates or by-products other than a trace amount of benzene (≈ 0.2 ppmv) were identified by GC/FID. In case of complete oxidization of toluene to carbon dioxide, it is expected that 7 moles of carbon dioxide to be formed per mole of toluene converted. However, a carbon balance showed only a partial oxidation of toluene to carbon dioxide, which varied from 22 to 87 % depending on the operating conditions. By-products could have been adsorbed on the catalytic surface, as it has been reported by other researchers as well [29] or remained undetected in the GC/FID analysis. Adsorption of by-products is most likely since catalyst deactivation was observed for several experiments.

3.3.2.1 The effect of toluene and water inlet concentration

The effect of toluene inlet concentration on the toluene conversion and mineralization to CO_2 is shown in Figure 3.4. It can be seen that both toluene conversion and mineralization decrease by increasing toluene inlet concentration, which may be explained by the toluene degradation kinetics according to a L-H mechanism. When increasing the toluene inlet concentration, although the reaction rate is expected to increase, conversion decreases (see equations (3.4) and (3.6)). The toluene degradation could be limited by the number of catalyst active sites [39, 45]. In addition, increasing the toluene inlet concentration may result in a more dominant role of

mass transfer compared to photon transfer. The reason is that the number of toluene molecules adsorbed on the catalytic surface surpasses the number of generated electron-hole pairs by photon absorption on the catalytic surface. As a result, the electron-hole pairs on the catalytic surface may become insufficient to initiate a chemical reaction with the adsorbed reactants. Thus, photon delivery from the light source to the catalytic surface and subsequent charge generation becomes the reaction controlling factor.

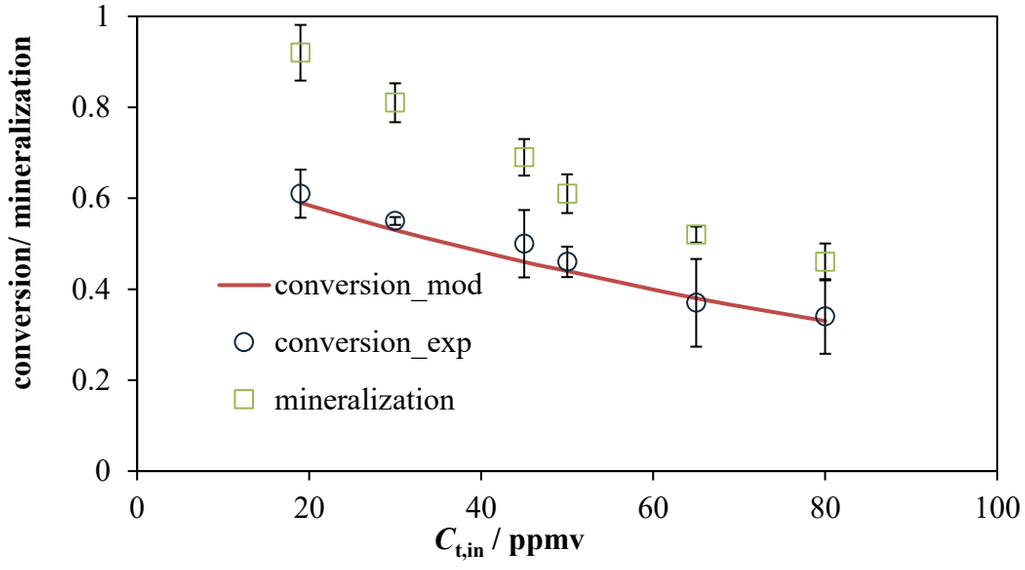

Figure 3.4 Effect of toluene inlet concentration on the conversion and mineralization of toluene for Q= 1270 ml min^{-1}, E=13 W m^{-2}, RH=40% (see Table 3.1). Error bars indicate the 90% confidence interval.

According to equation (3.4), by increasing the toluene concentration at the inlet, although the fractional conversion decreases, the absolute number of moles of toluene that are converted increases. However, the number of CO_2 moles formed remains almost constant by varying toluene inlet concentration. Therefore, according to equation (3.7), toluene mineralization decreases when increasing the toluene inlet concentration. This decreasing mineralization can be attributed to the fact that at the very first step, toluene is converted to intermediates. In the next steps, the intermediates undergo subsequent surface reactions producing the final product (CO_2), which is apparently not affected by the toluene inlet concentration but possibly by other factors such as water concentration. In fact, at a fixed molar flow of water, the number of moles of CO_2 formed remains constant, which results in a decrease in mineralization when the toluene feed molar flow rate increases. Therefore, it is concluded that CO_2 formation mainly depends on the water molar flow rate.

To investigate the effect of the water content in the feed on the photocatalytic degradation of toluene, experiments were carried out at different relative humidity values. The maximum conversion was obtained at low water concentrations (Figure 3.5), which is in agreement with some studies [28, 29] and in contrast to other studies where no toluene degradation was reported in the absence of water [30-34]. Different reaction paths have been suggested for toluene degradation on UV-illuminated TiO_2 [28, 35, 53]. d'Hennezel et al. [35] proposed that the OH radical is not the dominant reactive agent in gas phase photocatalytic oxidation of many volatile

organic compounds (VOCs) including toluene, which can explain the high conversion at no or very low water concentrations in the present study. When increasing the water content, conversion decreases gradually which can be caused by the competition between water and toluene adsorption on the catalyst active sites as it has been expressed in the reaction rate (equation (3.4)) that gave the best model fit to our data.

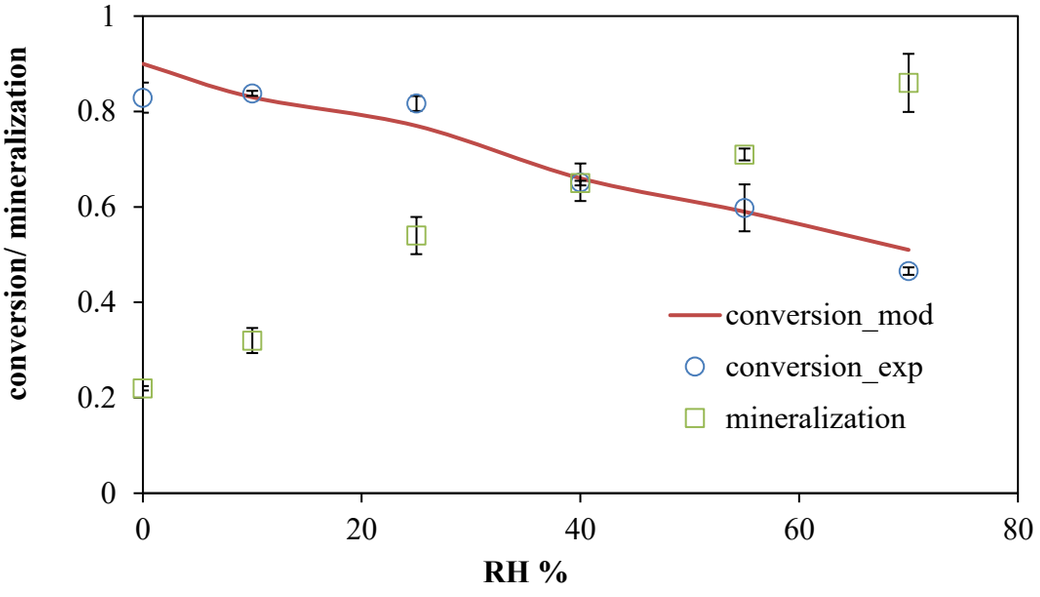

Figure 3.5 Effect of relative humidity on the conversion and mineralization of toluene for $C_{t,in}$≈45 ppmv, Q=812 ml min^{-1} and E=13 W m^{-2}. Error bars indicate the 90% confidence interval.

In contrast to toluene conversion, mineralization increased significantly by increasing the water content of the feed (Figure 3.5), which can be explained by the involved reaction steps. Toluene conversion is determined by the initial step of the degradation reaction sequence where mass and photon transfer to the catalytic surface and the availability of catalyst active sites are dominant factors in contrast to relative humidity and hydroxyl radicals, which may play minor roles. On the other hand, the role of hydroxyl radicals becomes possibly more dominant when converting intermediates, formed in initial step of degradation, to CO_2 for our experimental conditions. Consequently, by increasing the water content in the feed, the number of hydroxyl radicals on the catalytic surface increases leading to increased toluene mineralization.

3.3.2.2 The effect of irradiance

The effect of irradiance on the toluene conversion and mineralization is illustrated in Figure 3.6 in the range of 0-13 W m^{-2}. It can be seen that by increasing irradiance, the toluene conversion increases approximately by the square root of the irradiance for all tested irradiance levels, which implies that the rate of photon transfer surpasses the rate of mass transfer leading to charge recombination. Furthermore, when increasing the irradiance, mineralization increases. The electron-hole pairs generated on the catalytic surface may either react with water to form hydroxyl radicals needed for mineralization or directly with adsorbed intermediates on the catalyst surface which both can enhance CO_2 formation and thus mineralization. In term of energy consumption, the LED-based reactor is able to convert 0.15 to 0.80 mole of toluene per KWh consumed depending on the operating conditions.

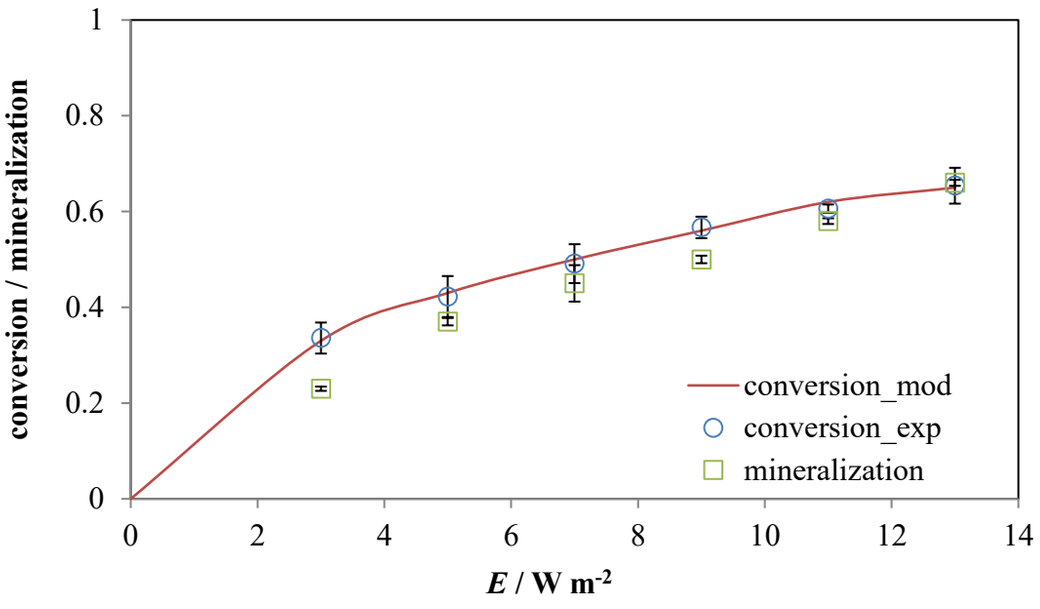

Figure 3.6 Effect of the average irradiance on the toluene conversion for $C_{t,in}$≈45 ppmv, Q=800 ml min^{-1} and RH=40%. Error bars indicate the 90% confidence interval.

3.3.2.3 The effect of residence time

The effect of residence time in the range of 16-50 s (corresponding to volumetric flow rates of 500 to 1500 ml min^{-1}) on the toluene conversion and mineralization is shown in Figure 3.7. An increase in volumetric flow rate, and consequently a decrease in residence time, results in a conversion drop as it was observed in other studies as well [28, 54]. For a surface catalytic reaction, a decrease in contact time between reactants and a catalytic surface should result in a conversion drop. In addition, toluene binds relatively weak with TiO_2, suggesting enhanced effectiveness of contact time on the reactor performance [28]. As demonstrated earlier, changes in the volumetric feed flow rate at constant contact time do not improve the mass transfer of reactant from the bulk to the catalytic surface significantly. Furthermore, the integrated process model, which does not include enhanced mass transfer at higher flow rates, describes the experimental data well. Therefore, it is concluded that the contact time between catalyst and reactant is the most dominant factor for the conditions studied in this work.

Toluene mineralization remains essentially unchanged when varying the volumetric flow rate and, consequently, the residence time. A possible reason for this observation is the fixed toluene to water molar ratio for these experiments. As discussed above, toluene conversion is a function of contact time and mass transfer for which volumetric flow rate plays a significant role. However, CO_2 is a product of multiple surface reaction steps involving various intermediates [28, 35]. The OH radicals are an important oxidation agent to achieve full mineralization. Therefore, the number of CO_2 moles formed to the number of toluene moles converted may remain constant at a fixed toluene to water molar ratio.

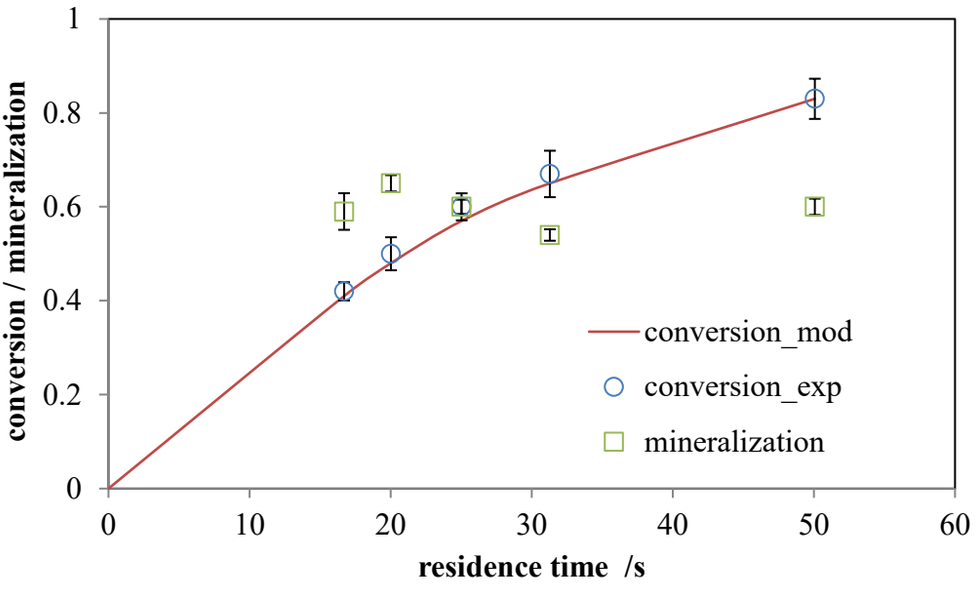

Figure 3.7 Effect of residence time (derived from volumetric flow rate and reactor volume) on the toluene conversion and mineralization for $C_{t,in}$≈45 ppmv, RH=40%, E=13 W m^{-2}. Error bars indicate the 90% confidence interval.

3.3.3 Catalyst deactivation and regeneration

Catalyst activity dropped under various operating conditions over the course of several hours (Figure 3. 8). This catalyst deactivation is most likely caused by partial oxidation of toluene to intermediates, which can accumulate on the catalyst surface when time progresses [55]. Larson et al. [56] found that toluene is converted to less-reactive intermediates in the initial step of degradation, which make stronger bonds to TiO_2 compared to toluene. Thus, those intermediates may block the catalyst active sites, which inhibits adsorption of toluene molecules and deactivates the catalyst.

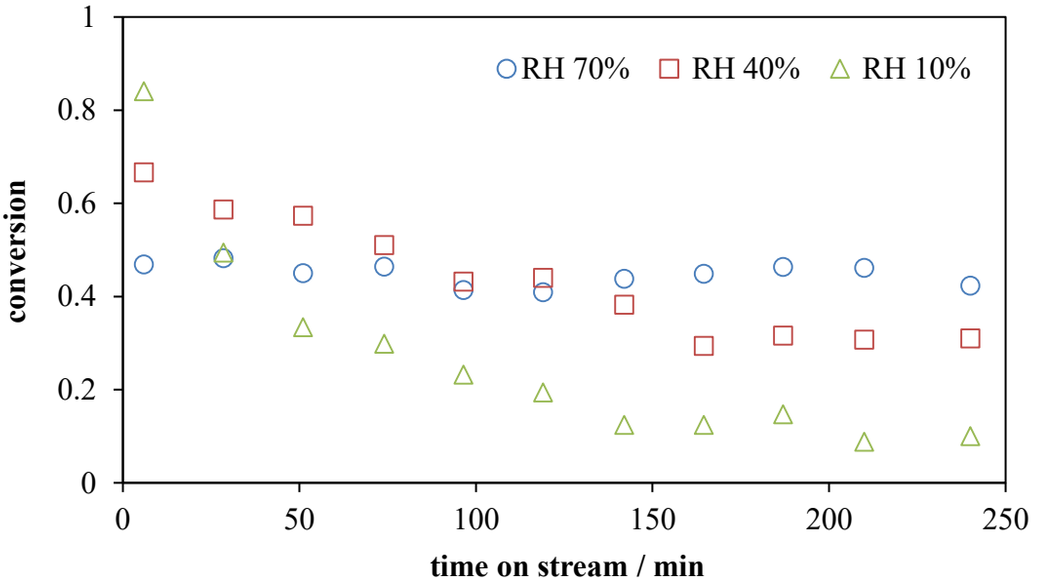

Figure 3.8 Toluene conversion versus time for three different relative humidity values for $C_{t,in}$≈45 ppmv, Q=812 ml min^{-1} and E=13 W m^{-2}.

The effects of relative humidity and toluene inlet concentration on the catalyst deactivation are shown in Figure 3.9. It can be seen that water plays a significant role in maintaining catalyst activity (Figure 3.9 (a)). Most probably, hydroxyl radicals formed after water adsorption on the TiO_2 active sites react with strongly adsorbed intermediates, which release from the catalyst surface in the form of CO_2. As a result, mineralization enhances while the catalyst maintains its activity as discussed before. At the lowest tested toluene concentration (19 ppmv) no catalyst deactivation was observed at a fixed relative humidity of 40% while toluene degradation reduced to less than half after 4 hours of operation when increasing the toluene inlet concentration to 30 ppmv. Upon further increasing the toluene inlet concentration to 80 ppmv, a slight decrease in toluene degradation can be observed (Figure 3. 9 (b)). A higher toluene inlet concentration results in a higher number of toluene moles converted to intermediates. Therefore, the required water content to prevent significant catalyst deactivation is correlated to the toluene inlet concentration. However, after a certain toluene concentration, the rate of catalyst deactivation becomes less sensitive to the toluene inlet concentration, which may be explained by saturation of the catalyst surface. No significant trend in the rate of catalyst deactivation was observed by changing irradiance or residence time at fixed water to toluene molar flow ratio (data not shown).

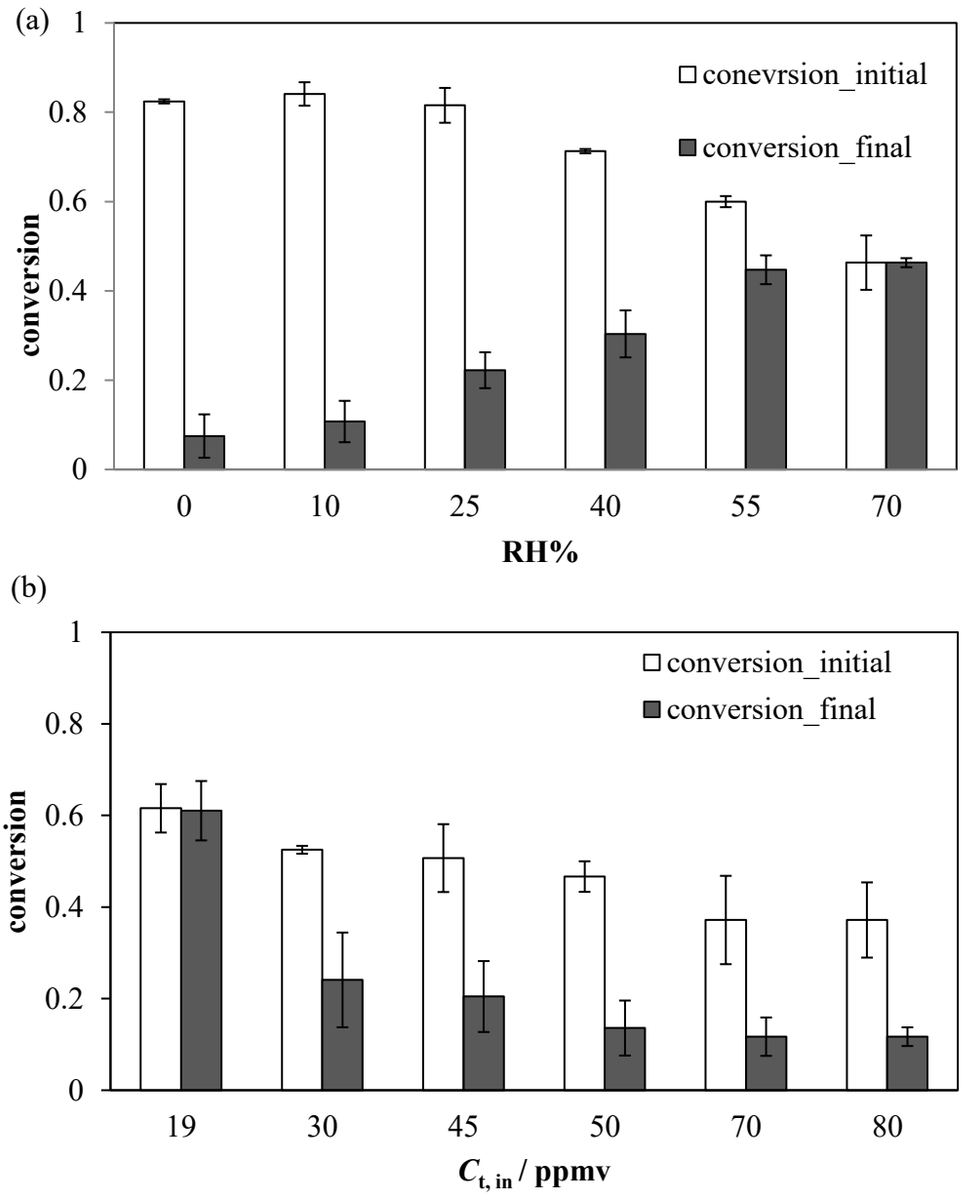

Figure 3.9 Initial (after 6 minutes) and final (after 4 hours) conversion as a function of (a) relative humidity ($C_{t,in}$≈45 ppmv, Q=812 ml min^{-1} and E=13 W m^{-2}) and (b) toluene inlet concentration (RH=40%, Q=1270 ml min^{-1} and E=13 Wm^{-2}). Error bars indicate the 90% confidence interval.

To better predict the effect of water on catalyst activity, the rate of change of the toluene conversion over time as function of relative humidity is shown in Figure 3.10. It can be seen that the rate of catalyst deactivation decreases linearly with RH. Furthermore, the rate of catalyst deactivation was relatively low compared to the other dynamics of the system. Therefore, a correction factor as a function of relative humidity could be included in the process model to predict the rate of catalyst deactivation under pseudo steady–state conditions.

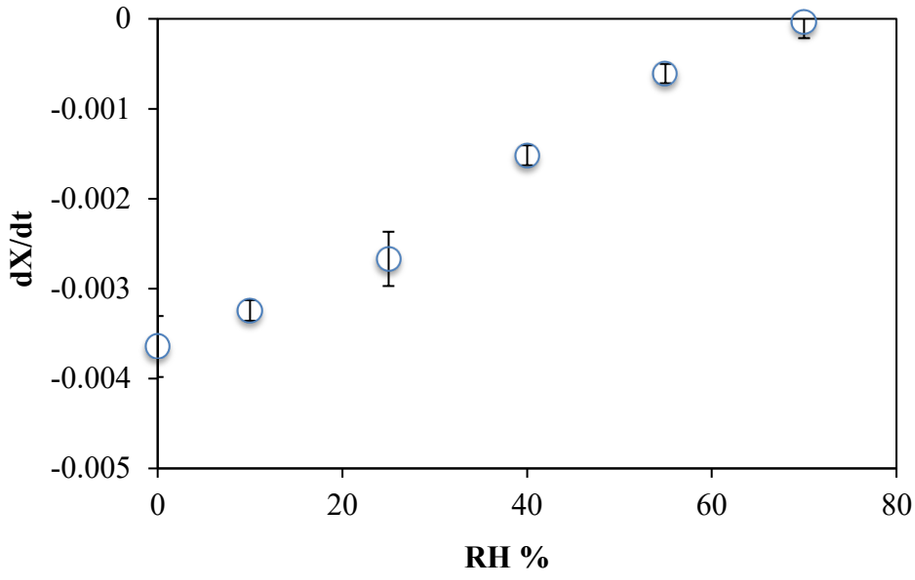

Figure 3.10 The rate of catalyst deactivation vs. RH %.

Finally, to test the regeneration of the catalyst, the toluene outlet concentrations versus time for three experiments with identical conditions for the same catalyst are compared in Figure 3.11. The three experiments show very comparable results. Therefore, it is concluded that, although catalyst deactivation clearly occurs for certain experiments, full recovery of catalyst activity is obtained after applying the regeneration process described in Section 3.2. At the first minutes of the regeneration process, typically a high concentration of CO_2 is detected in the reactor effluent, which decreases by time as the catalyst regeneration proceeds until no CO_2 is detected after 6-8 hours indicating full recovery of catalyst activity.

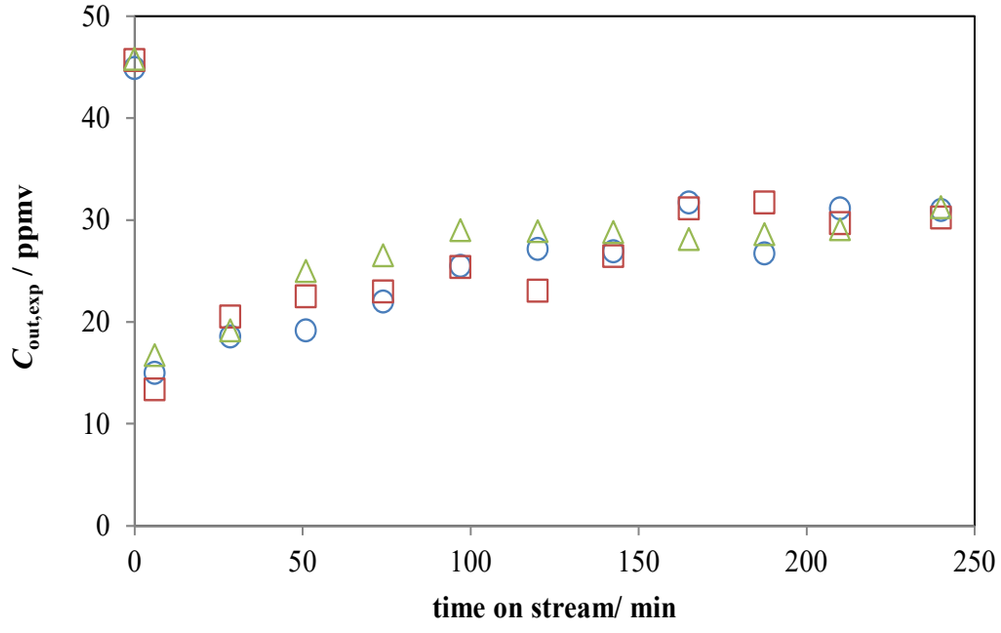

Figure 3.11 Toluene outlet concentrations for three experiments with identical conditions

3.4 Conclusion

An integrated process model describing an annular LED-based photocatalytic reactor including a radiation field model from LEDs, reaction kinetics, and mass transfer is successfully validated experimentally for a broad range of operating conditions. A special focus is on the role of water. Parameter estimation based on experimental data demonstrates that including competitive water adsorption enhances model prediction significantly compared to simple uni-molecular Langmuir-Hinshelwood kinetics.

Experimental characterization of a mini-pilot plant setup shows that a rise in toluene inlet concentration from 19 to 80 ppmv results in a decrease of toluene conversion, which is likely caused by an increasing mass transfer rate as opposed to the photon transfer rate. In the absence of water or at very low water concentrations, toluene conversion is maximized indicating a limited role of water in the first step of toluene degradation. Toluene conversion decreases gradually when increasing the relative humidity to 70%, which can be caused by the competition among toluene and water for adsorption on the catalyst active sites. Furthermore, toluene degradation varies by the square root of irradiance when increasing irradiance from 3 to 13 W m^{-2}. Thus, it can be concluded that mass transfer resistant becomes dominant, leading to charge recombination for the studied operating conditions. Increasing the volumetric flow rate of the feed from 500 to 1500 ml min^{-1} results in a decrease in toluene conversion due to a decrease of the reactants and catalyst contact time.

Toluene mineralization to CO_2 is a strong function of the ratio of water to toluene molar flow rate. Toluene mineralization decreases when increasing the toluene inlet concentration or when decreasing the ratio of water to toluene molar flow rates. Therefore, it is concluded that hydroxyl radicals originating from water are the dominant species for conversion of reaction intermediates to CO_2. At fixed water to toluene molar flow, an increase in irradiance enhances toluene mineralization which can be explained by an increase in the formation of hydroxyl radicals from the increased irradiance. On the other hand, at a fixed toluene to water molar flow rate and irradiance, mineralization remains constant when changing volumetric flow rate.

For conditions with low relative humidity, significant catalyst deactivation occurred over time, which was likely due to strong adsorption of reaction intermediates on the catalyst active site. Relative humidity plays an important role in the reaction of the intermediates, releasing them in the form of CO_2 from the catalyst surface and maintaining catalyst activity. Full recovery of the catalyst activity can be achieved by using humidified air in the presence of UV-illumination for 6-8 hours.

Even though the integrated model of a LED-based photocatalytic reactor was successfully validated by this experimental study under fully developed laminar flow condition, the practical limitation of the experimental set-up hindered the investigation of the effect of volumetric flow rates higher than 1500 ml min^{-1}. However, higher volumetric flow rates may be applied for certain practical cases, where different mass transfer mechanisms may play a role due to the change in flow regime. Therefore, future works should focus on the effect of higher volumetric flow rates and the required model modification to account for the different flow regime and mass transfer mechanism.

References:

[1] A. F. Tooru Inoue, Satoshi Konishi, Kenichi Honda, photoelectrocatalytic reduction of carbon dioxide in aqueus suspension of semiconductor powders, Nature 277 (1979) 2.

[2] S. Banerjee, D.D. Dionysiou, S.C. Pillai, Self-cleaning applications of TiO_2 by photo-induced hydrophilicity and photocatalysis, Appl. Catal. B 176–177 (2015) 396-428.

[3] C. Hu, Y. Lan, J. Qu, X. Hu, A. Wang, Ag/AgBr/TiO_2 Visible Light Photocatalyst for Destruction of Azodyes and Bacteria, J. Phys. Chem. B 110 (2006) 4066-4072.

[4] G. Marcì, M. Addamo, V. Augugliaro, S. Coluccia, E. García-López, V. Loddo, G. Martra, L. Palmisano, M. Schiavello, Photocatalytic oxidation of toluene on irradiated TiO_2: comparison of degradation performance in humidified air, in water and in water containing a zwitterionic surfactant, J. Photochem. Photobiol. A: Chem. 160 (2003) 105-114.

[5] A. Fujishima, K. Honda, Electrochemical Photolysis of Water at a Semiconductor Electrode, Nature 238 (1972) 37-38.

[6] M.A. Fox, M.T. Dulay, Heterogeneous photocatalysis, Chem. Rev. 93 (1993) 341-357.

[7] D.F. Ollis, E. Pelizzetti, N. Serpone, Photocatalyzed destruction of water contaminants, Environ. Sci. Technol. 25 (1991) 1522-1529.

[8] M.R. Hoffmann, S.T. Martin, W. Choi, D.W. Bahnemann, Environmental Applications of Semiconductor Photocatalysis, Chem. Rev. 95 (1995) 69-96.

[9] J. Zhao, X. Yang, Photocatalytic oxidation for indoor air purification: a literature review, Build. Environ. 38 (2003) 645-654.

[10] T. Van Gerven, G. Mul, J. Moulijn, A. Stankiewicz, A review of intensification of photocatalytic processes, Chem. Eng. Process. 46 (2007) 781-789.

[11] R. Lakerveld, G.S.J. Sturm, A.I. Stankiewicz, G.D. Stefanidis, Integrated design of microwave and photocatalytic reactors. Where are we now?, Curr. Opin. Chem. Eng. 5 (2014) 37-41.

[12] M. Motegh, J.R. van Ommen, P.W. Appel, M.T. Kreutzer, Scale-up study of a multiphase photocatalytic reactor--degradation of cyanide in water over TiO_2, Environ. Sci. Technol. 48 (2014) 1574-1581.

[13] V. Tomasic, F. Jovic, Z. Gomzi, Photocatalytic oxidation of toluene in the gas phase: Modeling an annular photocatalytic reactor, Catal. Today 137 (2008) 350-356.

[14] F.V.S. Lopes, S.M. Miranda, R.A.R. Monteiro, S.D.S. Martins, A.M.T. Silva, J.L. Faria, R.A.R. Boaventura, V.J.P. Vilar, Perchloroethylene gas-phase degradation over titania-coated transparent monoliths, Appl. Catal. B 140–141 (2013) 444-456.

[15] A.E. Cassano, C.A. Martin, R.J. Brandi, O.M. Alfano, Photoreactor Analysis and Design - Fundamentals and Applications, Ind. Eng. Chem. Res. 34 (1995) 2155-2201.

[16] G.E. Imoberdorf, A.E. Cassano, O.M. Alfano, H.A. Irazoqui, Modeling of a multiannular photocatalytic reactor for perchloroethylene degradation in air, AlChE J. 52 (2006) 1814-1823.

[17] M.M. Hossain, G.B. Raupp, S.O. Hay, T.N. Obee, Three-dimensional developing flow model for photocatalytic monolith reactors, AlChE J. 45 (1999) 1309-1321.

[18] M. Moazzem Hossain, G.B. Raupp, Radiation field modeling in a photocatalytic monolith reactor, Chem. Eng. Sci. 53 (1998) 3771-3780.

[19] M.J. Munoz-Batista, A. Kubacka, M.N. Gomez-Cerezo, D. Tudela, M. Fernandez-Garcia, Sunlight-driven toluene photo-elimination using CeO_2-TiO_2 composite systems: A kinetic study, Appl. Catal. B 140 (2013) 626-635.

[20] W.-K. Jo, R.J. Tayade, New Generation Energy-Efficient Light Source for Photocatalysis: LEDs for Environmental Applications, Ind. Eng. Chem. Res. 53 (2014) 2073-2084.

[21] D.H. Chen, X. Ye, K. Li, Oxidation of PCE with a UV LED Photocatalytic Reactor, Chem. Eng. Technol. 28 (2005) 95-97.

[22] T.S.N. Kalithasan Natarajan, H.C. Bajaj, Rajesh J. Tayade, Photocatalytic reactor based on UV-LED/TiO_2 coated quartz tube for degradation of dyes, Chem. Eng. J. 178 (2011) 40-49.

[23] F. Khodadadian, A. Poursaeidesfahani, Z. Li, J.R. van Ommen, A.I. Stankiewicz, R. Lakerveld, Model-Based Optimization of a Photocatalytic Reactor with Light-Emitting Diodes, Chem. Eng. Technol. 39 (2016) 1946-1954.

[24] Z. Wang, J. Liu, Y. Dai, W. Dong, S. Zhang, J. Chen, CFD modeling of a UV-LED photocatalytic odor abatement process in a continuous reactor, J. Hazard. Mater. 215-216 (2012) 25-31.
[25] Z. Pengyi, L. Fuyan, Y. Gang, C. Qing, Z. Wanpeng, A comparative study on decomposition of gaseous toluene by O_3/UV, TiO_2/UV and O_3/TiO_2/UV, J. Photochem. Photobiol. A: Chem. 156 (2003) 189-194.
[26] Y.-p. Zhang, R. Yang, Q.-j. Xu, J.-h. Mo, Characteristics of Photocatalytic Oxidation of Toluene, Benzene, and Their Mixture, J. Air Waste Manage. Assoc. 57 (2007) 94-101.
[27] P.C. Yao, S.T. Hang, C.W. Lin, D.H. Hai, Photocatalytic destruction of gaseous toluene by porphyrin-sensitized TiO_2 thin films, J. Taiwan Inst. Chem. Eng. 42 (2011) 470-479.
[28] M. Sleiman, P. Conchon, C. Ferronato, J.M. Chovelon, Photocatalytic oxidation of toluene at indoor air levels (ppbv): Towards a better assessment of conversion, reaction intermediates and mineralization, Appl. Catal. B 86 (2009) 159-165.
[29] L.X. Cao, Z. Gao, S.L. Suib, T.N. Obee, S.O. Hay, J.D. Freihaut, Photocatalytic oxidation of toluene on nanoscale TiO_2 catalysts: Studies of deactivation and regeneration, J. Catal. 196 (2000) 253-261.
[30] Y. Luo, D.F. Ollis, Heterogeneous Photocatalytic Oxidation of Trichloroethylene and Toluene Mixtures in Air: Kinetic Promotion and Inhibition, Time-Dependent Catalyst Activity, J. Catal. 163 (1996) 1-11.
[31] S.B. Kim, S.C. Hong, Kinetic study for photocatalytic degradation of volatile organic compounds in air using thin film TiO_2 photocatalyst, Appl. Catal. B 35 (2002) 305-315.
[32] C.A. Korologos, C.J. Philippopoulos, S.G. Poulopoulos, The effect of water presence on the photocatalytic oxidation of benzene, toluene, ethylbenzene and m-xylene in the gas-phase, Atmos. Environ. 45 (2011) 7089-7095.
[33] T.N. Obee, R.T. Brown, TiO_2 Photocatalysis for Indoor Air Applications: Effects of Humidity and Trace Contaminant Levels on the Oxidation Rates of Formaldehyde, Toluene, and 1,3-Butadiene, Environ. Sci. Technol. 29 (1995) 1223-1231.
[34] T. Ibusuki, K. Takeuchi, Toluene oxidation on UV-irradiated titanium dioxide with and without O_2, NO_2 OR H2O at ambient temperature, Atmos. Environ. 20 (1986) 1711-1715.
[35] O. d'Hennezel, P. Pichat, D.F. Ollis, Benzene and toluene gas-phase photocatalytic degradation over H_2O and HCL pretreated TiO_2: by-products and mechanisms, J. Photochem. Photobiol. A: Chem. 118 (1998) 197-204.
[36] T. Guo, Z. Bai, C. Wu, T. Zhu, Influence of relative humidity on the photocatalytic oxidation (PCO) of toluene by TiO2 loaded on activated carbon fibers: PCO rate and intermediates accumulation, Appl. Catal. B 79 (2008) 171-178.
[37] D.M. Lee, H.J. Yun, S. Yu, S.J. Yun, S.Y. Lee, S.H. Mang, J. Yi, Design of an efficient photocatalytic reactor for the decomposition of gaseous organic contaminants in air, Chem. Eng. J. 187 (2012) 203-209.
[38] A. Sclafani, J.M. Herrmann, Comparison of the Photoelectronic and Photocatalytic Activities of Various Anatase and Rutile Forms of Titania in Pure Liquid Organic Phases and in Aqueous Solutions, J. Phys. Chem. 100 (1996) 13655-13661.
[39] D.A. Hanaor, C.C. Sorrell, Review of the anatase to rutile phase transformation, Journal of Materials science 46 (2011) 855-874.
[40] N. Padoin, C. Soares, An explicit correlation for optimal TiO_2 film thickness in immobilized photocatalytic reaction systems, Chem. Eng. J. 310, Part 2 (2017) 381-388.
[41] S.B. Kim, W.S. Cha, S.C. Hong, Photocatalytic degradation of gas-phase methanol and toluene using thin-film TiO2 photocatalyst II. Kinetic study for the effect of initial concentration and photon flux, J. Ind. Eng. Chem. 8 (2002) 162-167.
[42] J. Jeong, K. Sekiguchi, K. Sakamoto, Photochemical and photocatalytic degradation of gaseous toluene using short-wavelength UV irradiation with TiO_2 catalyst: comparison of three UV sources, Chemosphere 57 (2004) 663-671.
[43] P.-F. Biard, A. Bouzaza, D. Wolbert, Photocatalytic Degradation of Two Volatile Fatty Acids in an Annular Plug-Flow Reactor; Kinetic Modeling and Contribution of Mass Transfer Rate, Environ. Sci. Technol. 41 (2007) 2908-2914.
[44] J.-M. Herrmann, Photocatalysis fundamentals revisited to avoid several misconceptions, Appl. Catal. B 99 (2010) 461-468.
[45] C.S. Turchi, D.F. Ollis, Photocatalytic degradation of organic water contaminants: Mechanisms involving hydroxyl radical attack, J. Catal. 122 (1990) 178-192.

[46] A. Bouzaza, C. Vallet, A. Laplanche, Photocatalytic degradation of some VOCs in the gas phase using an annular flow reactor - Determination of the contribution of mass transfer and chemical reaction steps in the photodegradation process, J. Photochem. Photobiol. A 177 (2006) 212-217.

[47] M. Motegh, J.J. Cen, P.W. Appel, J.R. van Ommen, M.T. Kreutzer, Photocatalytic-reactor efficiencies and simplified expressions to assess their relevance in kinetic experiments, Chem. Eng. J. 207 (2012) 607-615.

[48] J.C. D'Oliveira, G. Al-Sayyed, P. Pichat, Photodegradation of 2- and 3-chlorophenol in titanium dioxide aqueous suspensions, Environ. Sci. Technol. 24 (1990) 990-996.

[49] Z.M. Wang, J. Liu, Y.C. Dai, W.Y. Dong, S.C. Zhang, J.M. Chen, Dimethyl Sulfide Photocatalytic Degradation in a Light-Emitting-Diode Continuous Reactor: Kinetic and Mechanistic Study, Ind. Eng. Chem. Res. 50 (2011) 7977-7984.

[50] R.M. Alberici, W.F. Jardim, Photocatalytic destruction of VOCs in the gas-phase using titanium dioxide, Appl. Catal. B 14 (1997) 55-68.

[51] C. Passalía, O.M. Alfano, R.J. Brandi, Modeling and Experimental Verification of a Corrugated Plate Photocatalytic Reactor Using Computational Fluid Dynamics, Ind. Eng. Chem. Res., 50 (2011) 9077-9086.

[52] M.J. Muñoz-Batista, A. Kubacka, M. Fernández-García, Effective Enhancement of TiO_2 Photocatalysis by Synergistic Interaction of Surface Species: From Promoters to Co-catalysts, ACS Catal. 4 (2014) 4277-4288.

[53] F. Zhang, X. Zhu, J. Ding, Z. Qi, M. Wang, S. Sun, J. Bao, C. Gao, Mechanism Study of Photocatalytic Degradation of Gaseous Toluene on TiO2 with Weak-Bond Adsorption Analysis Using In Situ Far Infrared Spectroscopy, Catal. Lett. 144 (2014) 995-1000.

[54] J. Jeong, K. Sekiguchi, W. Lee, K. Sakamoto, Photodegradation of gaseous volatile organic compounds (VOCs) using TiO_2 photoirradiated by an ozone-producing UV lamp: decomposition characteristics, identification of by-products and water-soluble organic intermediates, J. Photochem. Photobiol. A: Chem. 169 (2005) 279-287.

[55] R. Méndez-Román, N. Cardona-Martínez, Relationship between the formation of surface species and catalyst deactivation during the gas-phase photocatalytic oxidation of toluene, Catal. Today 40 (1998) 353-365.

[56] S.A. Larson, J.L. Falconer, Initial reaction steps in photocatalytic oxidation of aromatics, Catal. Lett. 44 (1997) 57-65.

Appendix 3A: XRD pattern of the catalyst used in this study

The X-ray diffraction (XRD) pattern of the sample was measured via Bruker D8 Advance diffractometer (CuKα radiation) Bragg-Brentano geometry and Lynxeye position sensitive detector (Divergence slit 0.5°, scatter screen height 5 mm, 45 kV, 40 mA, Sample spinning). As it is shown in Figure 3A.1, the XRD pattern of the sample used in this study is comparable with XRD pattern of P25 [1].

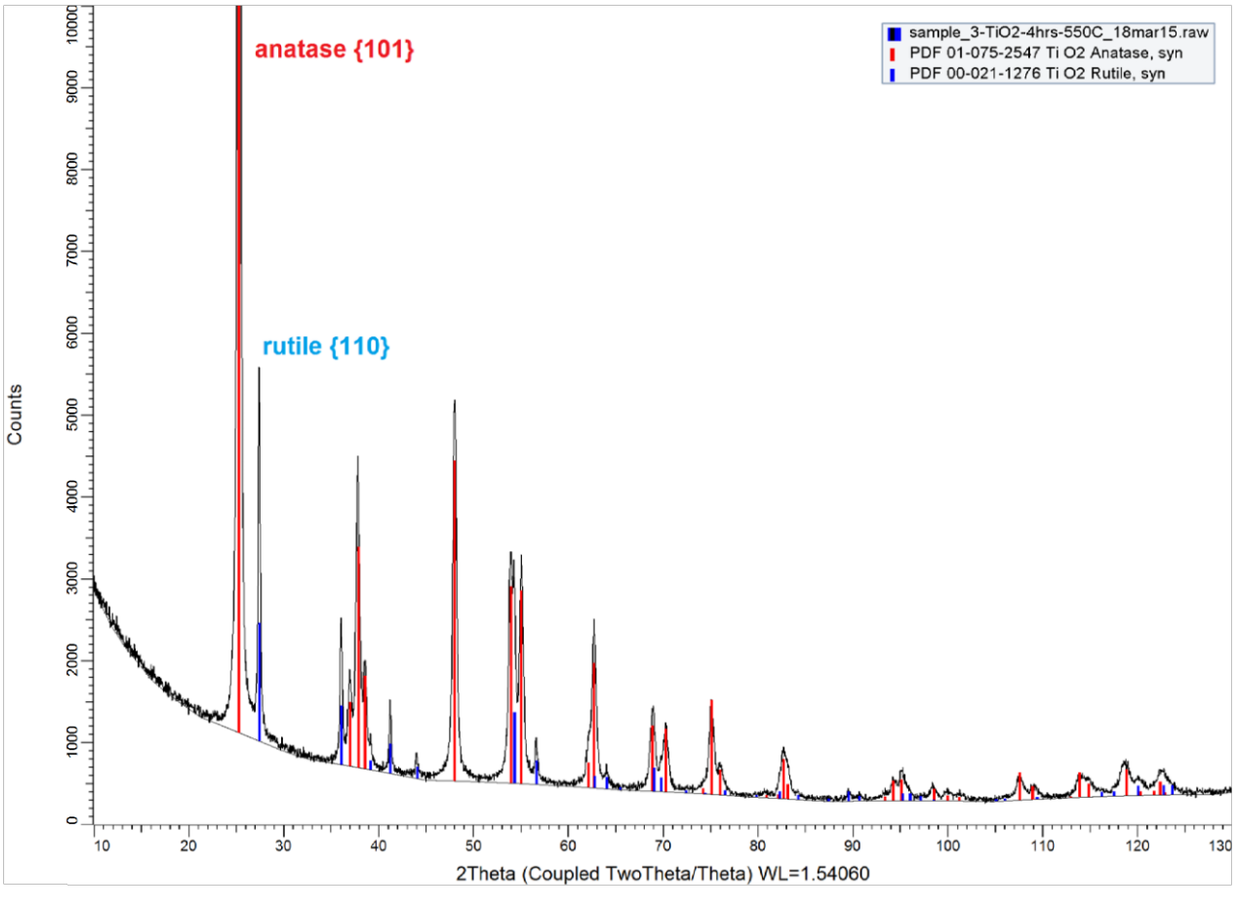

Figure 3A. 1. XRD pattern of the catalyst used in this study.

Appendix 3B: parity plot of experimental data vs. the reactor model prediction

The parity plots of the experimentally measured toluene outlet concentration and model prediction when the reaction kinetics does not include (equation 3.3) and includes competition from water adsorption (equation (3.4)) are shown in Figure 3B.2 and Figure 3B.3.

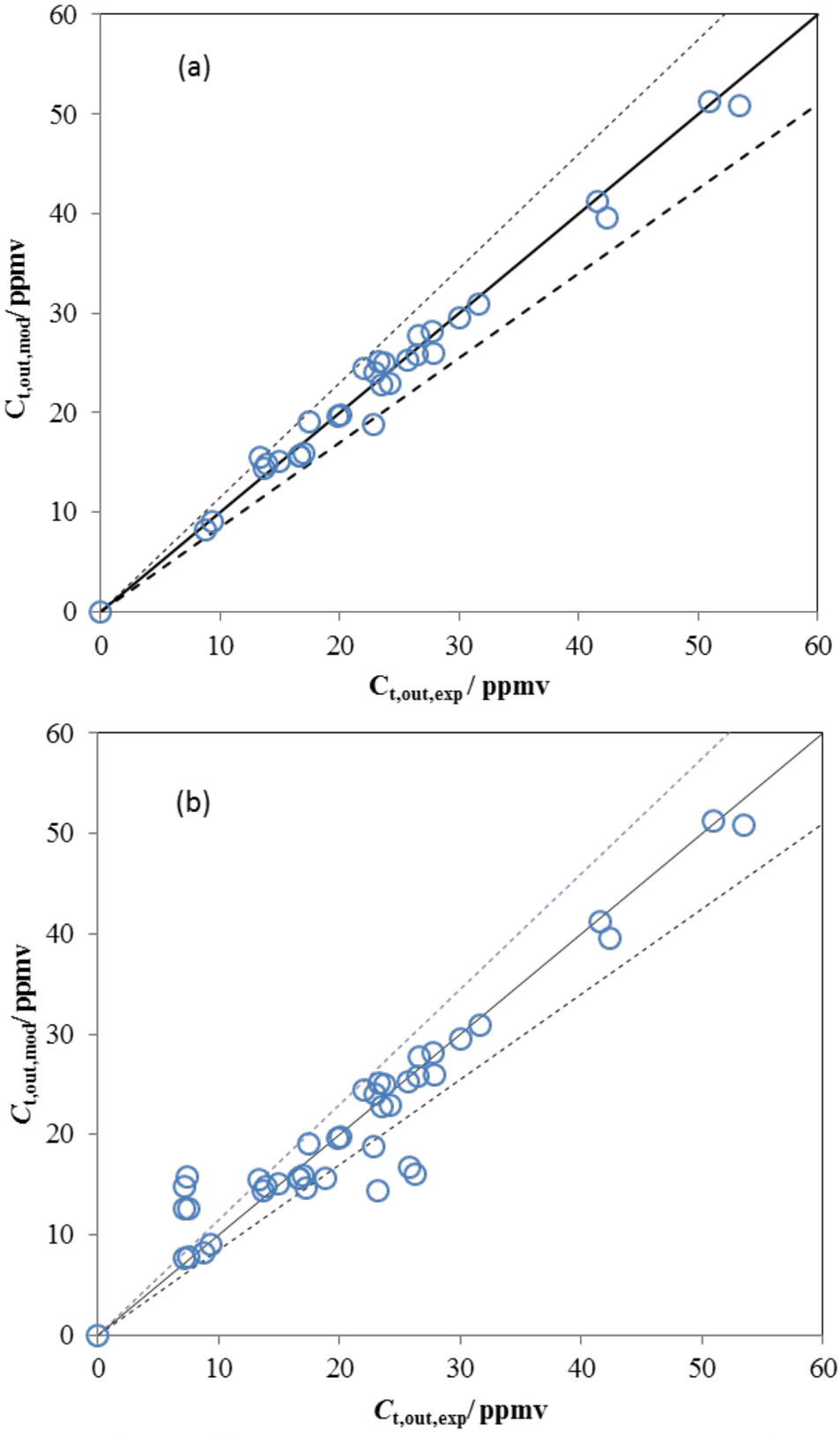

Figure 3B.1. Parity plot of the predicted toluene outlet concentration by the model versus the experimentally measured one when using a simple uni-molecular L-H reaction rate (a) for the experimental results obtained at fixed RH of 40%; (b) for all the experimental results. Dashed lines represent a 10% deviation.

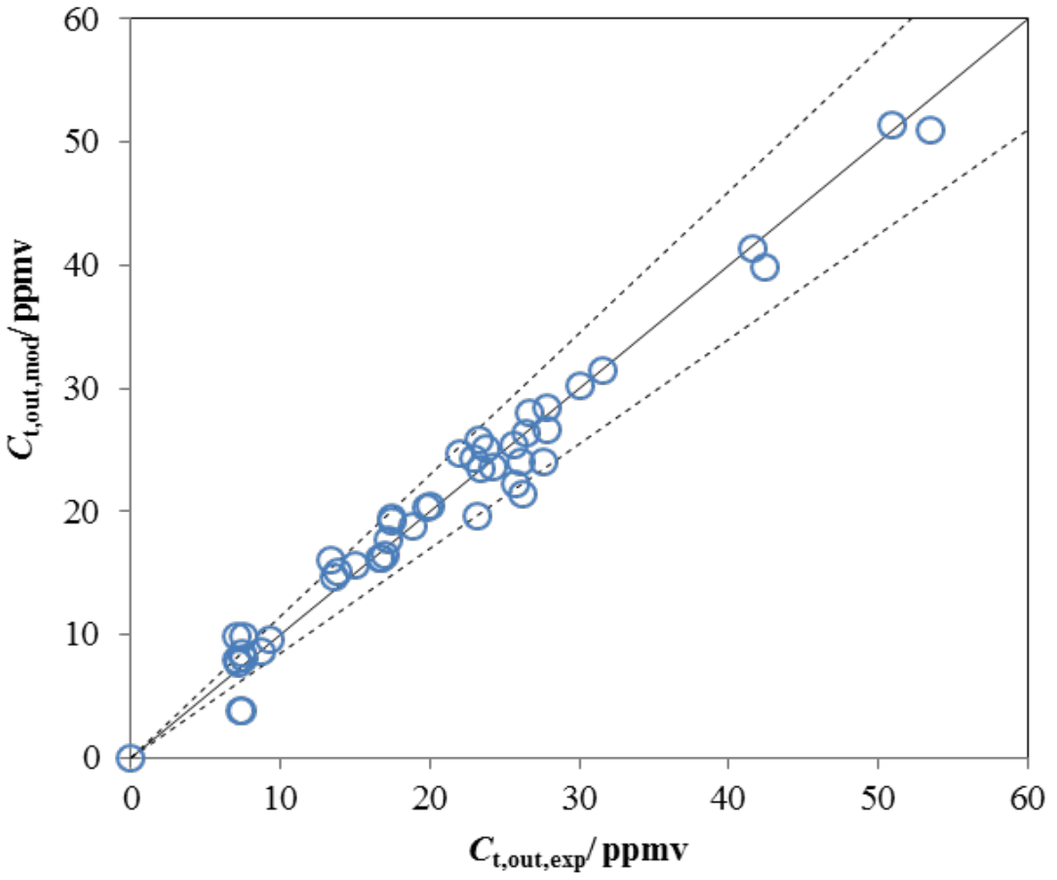

Figure 3B. 2. Partiy plot of the predicted toluene outlet concentration by the model versus the experimentally measured one when using a competetive uni-molecular L-H reaction rate model. Dashed lines represent a 10% deviation.

Calculation of the initial toluene concentration:

$$C_{in} = ppmv \frac{P}{RT} \times 10^{-6}$$

where C_{in} is toluene inlet concentration (mol m^{-3}), P the pressure (N m^{-2}), T is the temperature (K), R is the gas global constant (J K^{-1} mol^{-1}) and ppmv is the partial volume of toluene per 1 million volume of gas mixture.

References:

[1] B. Ohtani, O.O. Prieto-Mahaney, D. Li, R. Abe, What is Degussa (Evonik) P25? Crystalline composition analysis, reconstruction from isolated pure particles and photocatalytic activity test, J. Photochem. Photobiol. A: Chem. 216 (2010) 179-182.

Chapter 4. Periodical Illumination Impact on Photon Utilization in a LED-Based Photocatalytic Reactor

The impact of periodical illumination of LED's on the photonic efficiency in photocatalytic degradation of toluene in the gas phase was studied. The light/dark period and duty cycle were varied in this study. The effect of period was studied in the range of 0.05 to 10 s at a fixed duty cycle of 0.5 s. The experimental results showed no transition or change in the photonic efficiency by moving from short to long light/dark time at a fixed duty cycle. The photonic efficiency was found to be comparable under Controlled Periodic Illumination (CPI) and continuous illumination of equivalent average irradiance indicating that the reaction was photon limited. Furthermore, the results of experiments at two different periods of 0.5 and 1 s showed an increase in photonic efficiency with decrease in the duty cycle. However, the photonic efficiency under CPI, no matter of the duty cycle, was found to be similar to that under continuous illumination at equivalent average irradiance, suggesting no mass transfer limitation in the system.

4.1 Introduction

Photocatalysis is a phenomenon where a semiconductor, as the photocatalyst, absorbs photons with the energy equal or higher than its band gap energy. The photon absorption results in migration of electrons valance band to conductive band and consequently, generation of electron-hole charges and migration of them to the semiconductor surface. Subsequently, the generated electron-hole may either be recombined or undergo redox reactions. Despite the broad application of this technology, especially in the field of organic compounds oxidation, inefficient usage of photons within the reactor results in low efficiency of the process and ultimately hinders commercialization [1]. In addition, full mineralization of an organic compound includes a complicated chain of reactions where many one-electron transfers are required and reaction intermediates compete for primary oxidizing species resulting in an inefficient degradation reaction [2, 3].

Controlled Periodic illumination (CPI) is based on a series of alternate light (t_{ON}) and dark periods (t_{OFF}), and avoids the continuous introduction of photons, as it is illustrated in Figure 4.1. CPI is one of the reported methods to improve the photonic efficiency [4-8]. The main variables in CPI are the period, which refers to the time taken for a complete light and dark time cycle, i.e., period = t_{ON} + t_{OFF}, and the duty cycle (β), which is the fraction of the period with light, i.e.,

$$\beta = \frac{t_{on}}{t_{on} + t_{off}}$$

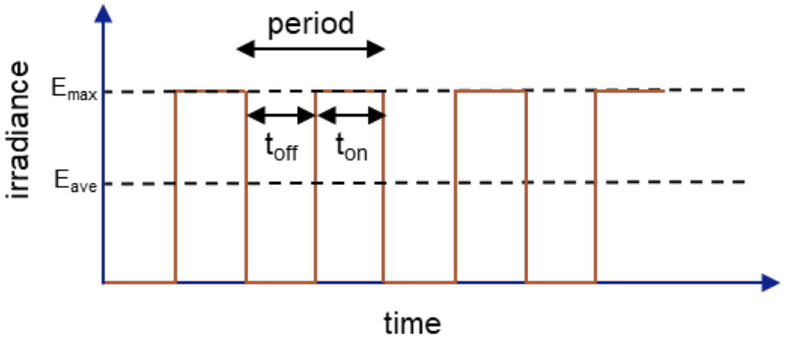

Figure 4.1 time profile of controlled periodic illumination pulses

In the early work done by Sczechowski et al. [5], the effect of the CPI duty cycle on the photonic efficiency of formate oxidation in a slurry reactor was studied. Their experimental results showed a 5-fold increase in the photonic efficiency of the process under CPI compared to continuous illumination. The authors suggested that continuous introduction of photons promotes a build-up of charges and photo-generated intermediates and, consequently, electron-hole recombination, which is inhibited by periodic illumination. However, Buechler et al. [6,9], investigated further the mechanism of the CPI effect for TiO_2 photocatalysis both in the gas and liquid phase and suggested that the apparent improvement of the process efficiency is either due to the mass transfer limitation or to slow adsorption/reaction steps.

The mentioned studies tried to explain the photonic efficiency under CPI due to its impact on electron-hole recombination rate or mass transfer limitations. However, when comparing the photonic efficiencies obtained from the CPI and continuous illuminations, they did not take into account that the variation in duty cycle means variation of radiation flux [11], as:

$$E_{ave} = \beta E_{max} \tag{4.1}$$

where E_{max} and E_{ave} are the irradiance during the light periods and the average irradiance under CPI, respectively. In their next studies, Buechler [10] and Cornu [2] showed that, photonic efficiency under a sufficiently high-frequency periodic illumination approached the photonic efficiency under continuous illumination at the same average absorbed photon flux. Therefore, other studies focused on the effect of CPI periods (or frequency) at fixed duty cycles. Cornu et al. [2] investigated the time scales of redox intermediates at different pH under periodic illumination for the degradation of methyl orange. Their results revealed a transition in photonic efficiency by moving from the long to the short light time. They attributed this transition to the change in the carrier recombination rate. They suggested that for chain reactions in the kinetic control regime, the average concentrations of the rate-determining intermediates will affect the photonic efficiency.

Recent advances in LED technology have made them a more reliable light source compared to conventional UV-lamps for photocatalytic applications [12]. Particularly, LEDs can be controlled electronically to deliver rectangular impulses of on/off periods in the order of milliseconds while conventional UV-lamps requires complicated mechanical shutters to obtain similar on/off time profiles [13]. In 2007, Chen et al. [13] studied the effect of controlled periodic illumination using LEDs on the photodecomposition of *o*-cresol and found that, the photonic efficiency achieved under CPI at sufficient intermittence was lower but advanced towards those under continuous illumination at equivalent irradiance level. Tokode et al. [14] investigated the effect of CPI on the photonic efficiency of the methyl orange degradation in a UV-LED based photocatalytic reactor. Their results showed an increase in photonic efficiency with reducing duty cycle. They also investigated the individual effect of light and dark times. They showed that photonic efficiency was mainly a function of duty cycle rather than the light or dark time, which indicated that the reaction was not limited by mass transfer or by the adsorption or desorption of chemical species. In addition, they concluded, that there is no enhancement in photonic efficiency due to CPI at an average intensity equal to the maximum intensity under continuous illumination as previous studies indicated [2, 13]. Hou et al. [15] studied decomposition of gaseous isopropanol in a continues tubular optical fiber reactor under periodic UV-LED illumination. Their results showed that by decreasing the duty cycle and increasing the frequency of periodic illumination, the apparent quantum yield increased. They concluded that the application of periodic illumination provided the opportunity to renew the active sites on the surface of the catalyst, which subsequently enhanced the decomposition rate and the overall removal efficiency and photonic efficiency.

Korovin et al. [16] investigated the effect of CPI on the degradation of acetone vapour in an LED-based photocatalytic reactor for a broad period range of 0.001 to 120 s. They demonstrated that photonic efficiency improves with the increase of the frequency of light pulses and decrease

of the duty cycle. Nevertheless, they concluded that at equivalent average UV light intensities, photonic efficiency under CPI is always lower than or equal to that of continuous illumination.

For over two decades, the mechanism and the effect of CPI on the photonic efficiency have been a controversial subject of research. The original hypothesis [5] for the enhancement of photonic efficiency through CPI has been proved to be valid for some initial studies [4, 7, 8] and challenged by other subsequent studies [2, 9, 14, 16]. Subsequent studies concluded that the enhancement in photonic efficiency was due to mass transfer limitations and not necessarily to a decrease in electron-hole recombination. In addition, the impact of CPI on the reactor performance have been mainly studied for the reactions in the liquid phase while the number of reports for the gas phase studies is limited [6, 15, 16]. In Chapter 3, it was shown that the reaction rate is proportional to the square root of the irradiance for all tested irradiance levels, suggesting electron-hole recombination becomes predominant (competes with electron-hole separation) in the system. In addition, it was concluded that at least under the operating conditions applied in this set-up, mass transfer limitations are small compared to limitations in reaction rate. Therefore, this chapter investigates whether application of LEDs periodical illumination can optimize photon utilization of a LED-based photocatalytic reactor in the gas phase by reducing carrier recombination in absent of mass transfer limitation. The photocatalytic oxidation of toluene within a continuous annular LED-based photocatalytic reactor is used as a model system, which has been studied extensively in previous chapters. In this study, photonic efficiency is measured under CPI where the irradiance at the light time (E_{max}) and duty cycle are kept constant, while the light time is varied within the range of 0.05 to 10 s to understand the reactor response on the way that the same amount of energy is provided. In addition, the effect of duty cycle at different periods is investigated. Finally, the photonic efficiencies from CPI and continuous illumination were compared under the same average irradiance (or power).

4.2 Materials & method

The experimental set-up and the catalyst preparation method, used for this study, have been described in detail in Chapter 3. The UV-LEDs (NSSU100CT, Nichia, Japan) light and impulses in this study are controlled with programmable power supplies (Aim TTi model PLH120-P). Before initiating the photocatalytic test, the reactor feed is bypassed and analyzed by GC to determine the composition. Subsequently, the reactor is purged with the feed stream at dark condition to reach an equilibrium state. Finally, the reactor is illuminated for 2 hours to conduct the photocatalytic experiment. GC analyzes the reactor effluent every 20 minutes. The same catalytic film has been used for each experiment to avoid obtaining biased results due to the different properties of the catalytic sheets from different batches. After every test, the catalyst was regenerated before conducting the next test. The shortest illumination period was/is 0.05 s. At light periods, the irradiance is set to its maximum (E_{max}) of 1.35 mW cm^{-2}; hence, for an experiment under CPI, the average irradiance (E_{avg}) is calculated by equation (4.1). All the experiments are performed for toluene inlet concentration of 30 ppmv, relative humidity of 40% and volumetric flow rate of 1400 ml min^{-1}, while the reactor temperature and pressure are kept constant at 30 °C and 1.1 bar. The experimental details and operational conditions are summarized in Table 4.1.

In order to study the effect of CPI on the photocatalytic degradation of toluene in the UV-based annular reactor, the photonic efficiency was defined as the degraded moles of toluene to the moles of photon absorbed by the catalytic surface [15]:

$$\text{photonic efficiency} = \frac{\text{moles of toluene degraded (mol s}^{-1})}{\text{moles of photon absorbed (mol s}^{-1})}$$

$$\cong \frac{\Delta C_t}{\frac{\gamma E_{max} A}{U_{365} N_a}} \tag{4.2}$$

where ΔC_t (mol s^{-1}) is the moles of toluene converted per unit of time, U_{365} is the energy of one photon (J) with wavelength of 365 nm and N_a is the Avogadro number and A (cm^2) is the photocatalytic surface area within the reactor.

Table 4.1 experimental operating condition

Test ID	Illumination mode	Period [s]	Duty cycle (β)	$E_{ave.}$ [mW cm^{-2}]
#1	CPI	0.05 0.1 0.2 10	0.5	0.675
	continuous	-	-	0.675
#2	CPI	1	0.2 0.4 0.6 0.8	0.27 0.54 0.8 1.08
	CPI	0.5	0.2 0.4 0.6 0.8	0.27 0.54 0.8 1.08
	continuous	-	-	0.27 0.54 0.8 1.08 1.35

4.3 Results & discussion

4.3.1 Influence of CPI period (frequency)

The photonic efficiencies for different CPI periods at the duty cycle of 0.5 (corresponding to average irradiance of 0.675 mW cm^{-2}) and for equivalent continuous illumination are presented in Figure 4.2. No change in photonic efficiency was found when applying CPI for different periods within the tested range. However, it is possible that the applied periods in this study are

relatively large to observe any influence. In addition, the photonic efficiencies obtained with CPI at different light times are equal to the photonic efficiency from continuous illumination at the equivalent average irradiance.

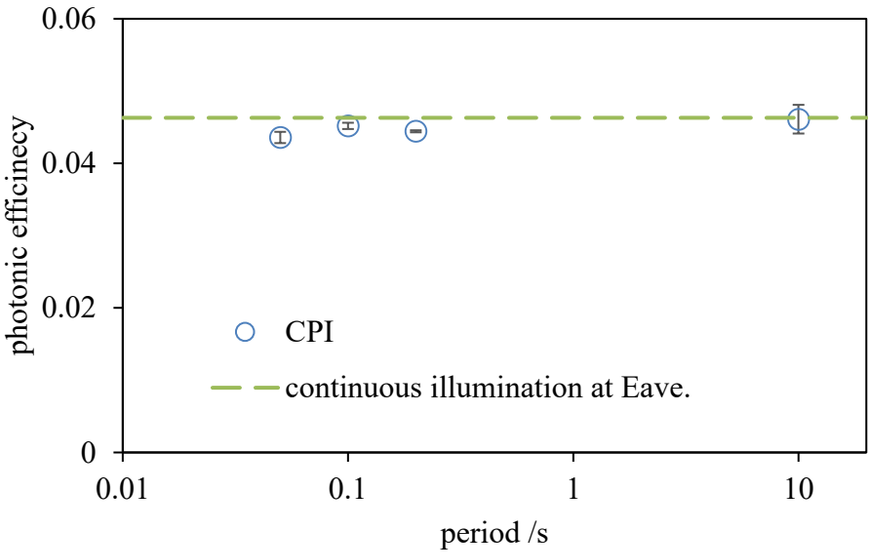

Figure 4.2 Photonic efficiency for toluene photocatalytic degradation under CPI at a duty cycle of 0.5 and under continuous illumination at equivalent average irradiance (E_{ave}) of 0.675 mW cm^{-2}

(Experiment #1) Influence of CPI duty cycle

The effect of CPI duty cycles on the reactor photonic efficiency for two different periods is shown in Figure 4.3. The experimental results show that the photonic efficiency is a function of duty cycle rather than light/dark time, which is in agreement with the previous findings [14] that mass transfer or adsorption/desorption from the catalytic surface of TiO_2 does not limit the reaction. In principle, under a mass-transfer limited regime, the dark periods during CPI provide more time for the reactants to diffuse to the catalytic surface and be adsorbed on the catalytic surface. The measured photonic efficiencies under similar operating conditions, but different volumetric flow rates confirm that there is no significant mass transfer limitation in our reactor (Chapter 3). Therefore, it can be concluded that CPI does not enhance the photonic efficiency if the reactor does not operate under mass transfer limitation but under a kinetically controlled regime.

In addition, it was found that there is no difference in the reactor performance under different illumination conditions as long as the reactor is operated under the same average irradiance, although the recombination of charges is predominant in the reactor (Chapter 3). This result contradicts the initial hypothesis suggested by Sczechowski et al. [5] about impact of CPI on the inhibition of electron-hole recombination. However, both illumination approaches result in higher photonic efficiencies at reduced light intensities. Tokode et al. [14] obtained similar results when comparing the photocatalytic oxidation of methyl orange in the liquid phase using an LED-based photocatalytic reactor under CPI and continuous illumination. They suggested that photonic efficiency enhances since the electron-hole recombination in TiO_2 is not limiting the reaction at lowered light powers.

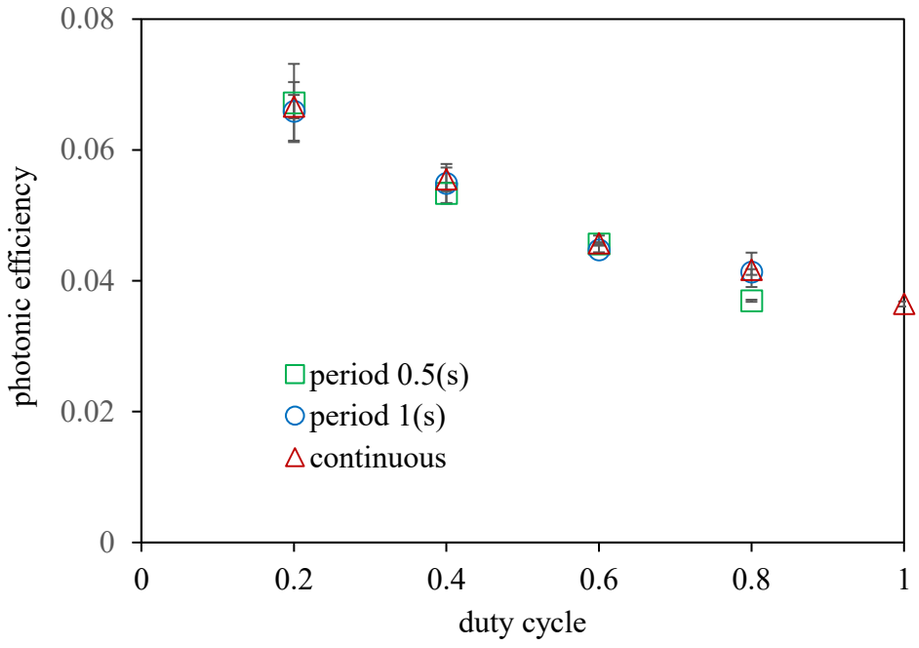

Figure 4.3 Reactor photonic efficiency as a function of duty cycle at constant maximum irradiance and period of 1 s and period of 0.5 s and equivalent average irradiance under continuous illumination. (Experiment #2)

4.4 Conclusion

In this study, the effect of the illumination period of LEDs in the range of 0.05 to 10 s on photonic efficiency of the LED-based photocatalytic reactor was explored at a fixed duty cycle of 0.5, however, no transition in photonic efficiency due to variation in period was observed. In addition, the photonic efficiencies were similar for CPI at different periods and continuous illumination at equivalent average irradiances, which is the maximum possible photonic efficiencies under CPI according to some studies [2, 16, 18]. The photonic efficiency increased with reducing the duty cycle irrespective of the light/dark time, indicating that carrier recombination becomes less dominant at reduced light intensities. Nevertheless, the conversion of toluene under controlled periodic illumination was the same when compared with continuous illumination at equivalent incident irradiance, which can be attributed to the fact that mass transfer or adsorption/desorption on the catalytic surface does not limit the reaction. Although the present study is not in agreement with the original hypothesis suggested by Sczechowski et al. [5] it is in very good agreement with recent findings on the effect of CPI in photocatalytic oxidation of various organic compounds [2, 16, 18]. Future work should aim at exploring the effect of controlled periodic illumination under a diffusion-limited regime. In addition, applying shorter periods for CPI might be of interest for studying the lifetime evaluation of possible reactive intermediates on the catalytic surface in the photocatalytic reaction's kinetics study.

References:

[1] T. Van Gerven, G. Mul, J. Moulijn, A. Stankiewicz, A review of intensification of photocatalytic processes, Chemical Engineering and Processing: Process Intensification 46 (2007) 781-789.

[2] C.J. G. Cornu, A.J. Colussi, M.R. Hoffmann, Quantum Yields of the Photocatalytic Oxidation of Formate in Aqueous TiO_2 Suspensions under Continuous and Periodic Illumination, J. Phys. Chem. B 105 (2001) 1351-1354.

[3] M.A. Grela, A.J. Colussi, Photon Energy and Photon Intermittence Effects on the Quantum Efficiency of Photoinduced Oxidations in Crystalline and Metastable TiO_2 Colloidal Nanoparticles, J. Phys. Chem. B 103 (1999) 2614-2619.
[4] J. G. Sczechowski, C.A. Koval, R.D. Noble, A Taylor vortex reactor for heterogeneous photocatalysis, Chem. Eng. Sci. 50 (1995) 3163-3173.
[5] J.G. Sczechowski, C.A. Koval, R.D. Noble, Evidence of critical illumination and dark recovery times for increasing the photoefficiency of aqueous heterogeneous photocatalysis, J. Photochem. Photobiol. A: Chem. 74 (1993) 273-278.
[6] K.J. Buechler, R.D. Noble, C.A. Koval, W.A. Jacoby, Investigation of the Effects of Controlled Periodic Illumination on the Oxidation of Gaseous Trichloroethylene Using a Thin Film of TiO_2, Ind. Eng. Chem. Res. 38 (1999) 892-896.
[7] G. Stewart, M.A. Fox, The effect of dark recovery time on the photoefficiency of heterogeneous photocatalysis by TiO_2 suspended in non-aqueous media, Res. Chem. Intermed. 21 (1995) 933-938.
[8] S. Upadhya, D.F. Ollis, Simple Photocatalysis Model for Photoefficiency Enhancement via Controlled, Periodic Illumination, J. Phys. Chem. B 101 (1997) 2625-2631.
[9] K.J. Buechler, C.H. Nam, T.M. Zawistowski, R.D. Noble, C.A. Koval, Design and Evaluation of a Novel-Controlled Periodic Illumination Reactor to Study Photocatalysis, Ind. Eng. Chem. Res. 38 (1999) 1258-1263.
[10] K.J. Buechler, T.M. Zawistowski, R.D. Noble, C.A. Koval, Investigation of the Mechanism for the Controlled Periodic Illumination Effect in TiO_2 Photocatalysis, Ind. Eng. Chem. Res. 40 (2001) 1097-1102.
[11] H. W. Chen, Y. Ku, C. Y. Wu, Effect of LED optical characteristics on temporal behaviour ofo-cresol decomposition by UV/TiO_2 process, Journal of Chemical Technology & Biotechnology 82 (2007) 626-635.
[12] W. K. Jo, R.J. Tayade, New Generation Energy-Efficient Light Source for Photocatalysis: LEDs for Environmental Applications, Ind. Eng. Chem. Res. 53 (2014) 2073-2084.
[13] H. W. Chen, Y. Ku, A. Irawan, Photodecomposition of o-cresol by UV-LED/TiO_2 process with controlled periodic illumination, Chemosphere 69 (2007) 184-190.
[14] O.I. Tokode, R. Prabhu, L.A. Lawton, P.K.J. Robertson, Effect of controlled periodic-based illumination on the photonic efficiency of photocatalytic degradation of methyl orange, J. Catal. 290 (2012) 138-142.
[15] W. M. Hou, Y. Ku, Photocatalytic decomposition of gaseous isopropanol in a tubular optical fiber reactor under periodic UV-LED illumination, J. Mol. Catal. A: Chem. 374–375 (2013) 7-11.
[16] E. Korovin, D. Selishchev, A. Besov, D. Kozlov, UV-LED TiO_2 photocatalytic oxidation of acetone vapor: Effect of high frequency controlled periodic illumination, Appl. Catal. B 163 (2015) 143-149.
[17] R. Zhou, M.I. Guzman, CO_2 Reduction under Periodic Illumination of ZnS, J. Phys. Chem. C 118 (2014) 11649-11656.
[18] O. Tokode, R. Prabhu, L.A. Lawton, P.K.J. Robertson, Controlled periodic illumination in semiconductor photocatalysis, J. Photochem. Photobiol. A: Chem. 319-320 (2016) 96-106.

Chapter 5. The Application of Automated Feedback and Feedforward Control to a LED-Based Photocatalytic Reactor

An optimal photon utilization is important for the economic performance of a photocatalytic reactor. However, for the desired reactor performance, it is often difficult to predict the required photon utilization. In this work, automated feedback and feedforward controllers are investigated to maintain the reactor conversion close to a desired value by adjusting the photon irradiance within a LED-based photocatalytic reactor for toluene degradation. The feedback controller was able to control the conversion during a set-point tracking experiment and was able to mitigate the effects of catalyst deactivation in an automated fashion. The feedforward controller was designed based on an empirical steady-state model to mitigate the effect of changing toluene inlet concentration and relative humidity, which were measured input disturbances. The results demonstrated that feedback and feedforward control were complementary and could mitigate the effects of disturbances effectively such that the photocatalytic reactor operated close to desired conditions at all times. The presented work is the first example of how online analytical technologies can be combined with "smart" light sources such as LEDs to implement automated process control loops that optimize photon utilization. Future work may expand on this concept by developing more advanced control strategies and exploring applications in different areas.

Published as: F. Khodadadian, F.G. de la Garza, J.R. van Ommen, A.I. Stankiewicz, R. Lakerveld, The application of automated feedback and feedforward control to a LED-based photocatalytic reactor, Chem. Eng. J. 362 (2019) 375-382.

5.1 Introduction

Photocatalysis is an attractive process to support a broad range of chemical reactions [1-3]. However, despite many successful demonstrations of applications on a lab-scale, large-scale applications are currently limited due to several challenges that need to be resolved. The efficient utilization of light within a photocatalytic reactor is one such challenge, which affects the economic feasibility when using artificial light sources.

Efficient utilization of light depends on several factors including the reactor design, the light source, as well as operating conditions. An efficient reactor design should optimize the interplay between mass transfer and photon transfer [4, 5]. The optimal design of photocatalytic reactors has been studied extensively and different designs have been proposed for various applications involving gas and liquid phases [6-8]. The light source itself also plays an important role in the overall efficiency of a photocatalytic process. Conventional UV lamps such as mercury and xenon lamps have been used for different applications. However, drawbacks related to the toxic disposal, short lifetime, fragility, potential for gas leakage, and low efficiency have triggered the exploration of alternative light sources such as light emitting diodes (LEDs) [9-12]. Compared to conventional UV lamps, LEDs offer several advantages when used within a photocatalytic reactor. In addition to their non-toxicity, potential to reduce costs, robustness, longer lifetime, and higher efficiency, LEDs also provide more degrees of freedom for the design of a photocatalytic reactor due to their small size. Furthermore, the illumination intensity of an LED is proportional to the electrical current, which provides opportunities to smartly control the illumination by, for example, employing periodic illumination [13-16] or by creating an optimal illumination profile within a reactor balancing a desired reaction rate while minimizing operating costs. In the design phase, the combination of a spatial light intensity model and a reactor model can be optimized simultaneously to minimize the total costs for equipment and operation [17]. However, during operation, a LED-based photocatalytic reactor may not operate under optimal conditions due to design uncertainty and the presence of external disturbances acting on the system, which may result in a non-optimal energy consumption of the system.

Automated feedback control is a standard solution for continuous flow reactors to compensate for design uncertainty and to reject disturbances acting on the reactor [18-20]. Usually, rather than directly controlling an economic objective function, a set of controlled variables is chosen such that when kept constant, a minimum loss with respect to the economic optimum is obtained, which is referred to as self-optimizing control [21-26]. A main source of operational costs of a photocatalytic reactor involves the energy required for illumination when artificial light sources are used. Generally, a higher light intensity allows for a faster reaction, but the effect will be limited above a certain conversion. Furthermore, for some applications, only conversion above a certain value may be needed (e.g., in the case of environmental applications). Therefore, maintaining the conversion at a desired value in a feedback control loop with illumination as a manipulated variable could provide self-optimizing control for a photocatalytic reactor. Due to the emergence of ‘smart’ light sources such as LEDs and significant improvements in on-line analytical technologies, such self-optimizing control has now become feasible for LED-based photocatalytic reactors. However, to the best of our

knowledge, no studies on self-optimizing feedback control for LED-based catalytic reactors exist in literature despite its potential to improve the economic performance of photocatalytic reactors.

The objective of this chapter is to demonstrate and characterize automated feedback control for a LED-based photocatalytic reactor. The conversion has been chosen as the controlled variable with the light intensity of the LEDs as a manipulated variable to achieve self-optimizing control in an automated feedback control loop. Furthermore, feedforward control is studied to further improve the performance of the automated control loop. Feedforward control relies on the measurement of a disturbance followed by preventive action to avoid a significant impact on the controlled variable. Since feedforward control has a preventive character and feedback control has a corrective character, a synergistic effect can be achieved through simultaneous application of both control strategies. The photocatalytic oxidation of toluene within an annular LED-based photocatalytic reactor is used as a model system. Toluene is a typical model compound for photocatalytic oxidation studies of volatile organic compounds. Furthermore, toluene is a practically relevant indoor pollutant [27-30]. Finally, in Chapter 3, we have studied the kinetics of toluene oxidation in the same reactor, which provides a reference when mimicking challenging conditions for automated process control (e.g., catalyst deactivation). Real–time monitoring of the reactor outlet by on-line gas chromatography enabled the automation of the control loop. The delay of such online measurement is taken into account in the design of the controller. Finally, for the design of a feedforward controller, relative humidity and toluene inlet concentration are used as typical measured disturbances acting on the system.

5.2 Materials and methods

5.2.1 Equipment and Operating Procedures

The experimental setup and the catalyst preparation procedure have been described in detail in Chapter 3. However, the scheme of experimental set-up including the control units is illustrated in Figure 5.1. In this study, the irradiance emitted by the LEDs is manipulated by controlling the current, as the irradiance of the LEDs is proportional to the applied current, which was achieved by a flexible power supply (Aim TTi model PLH120-P). The reactor inlet is a mixture of nitrogen and oxygen (78 vol% and 22 vol% respectively), toluene in the range of 20 to 90 ppmv, and water in the range of 0 to 80% relative humidity. The volumetric flow rate of the feed is 1020 ml min^{-1} for all experiments, which corresponds to a residence time of 25 s and a laminar flow regime. The reactor operates at 30°C and a back-pressure controller maintains the reactor pressure at 1.1 bar.

For a typical experiment, first, the reactor feed is led to an on-line gas chromatograph through a bypass line to measure the stable feed composition at the start of each experiment, which is assumed to remain constant during operation. Subsequently, the reactor is purged by introducing the feed mixture to the reactor for 2 hours under dark conditions. Finally, the reactor is illuminated to initiate the photocatalytic reactions. The input of irradiance into the reactor is defined as (see Figure 5.1):

$$E_2 = E_1 + \Delta E_{FC} + \Delta E_{FFC} \quad (5.1)$$

where E_2 and E_1 are the future and present irradiance of the LEDs in the reactor, respectively. ΔE_{FC} and ΔE_{FFC} are the contributions of feedback control and feedforward control, respectively, designed to maintain the toluene conversion close to the desired set point (X_{sp}).

A part of the reactor effluent is injected into the on-line Gas Chromatograph (GC) (GC-7890B, Agilent Technologies) at a constant flow rate, measured with a Mass Flow Meter (MFM, F-201CV-1K0-RAD, Bronkhorst, the Netherlands), and the rest of the reactor effluent is directed to a vent. The GC is equipped with a methane convertor, two Flame Ionization Detectors (FID, one for hydrocarbons and another one for CO_2 concentrations lower than 50 ppmv detection) and two Thermal Conductivity Detectors (TCD, one for N_2 and O_2 and another one for CO_2 detection).

In order to facilitate the implementation of automated controllers, a control interface (LabVIEW 2016) was developed to collect all the operating conditions. The feedback and feedforward controllers were implemented via the built-in functions of LabVIEW for real-time control applications. Finally, the control interface allowed for archiving of the process variables for performance characterization.

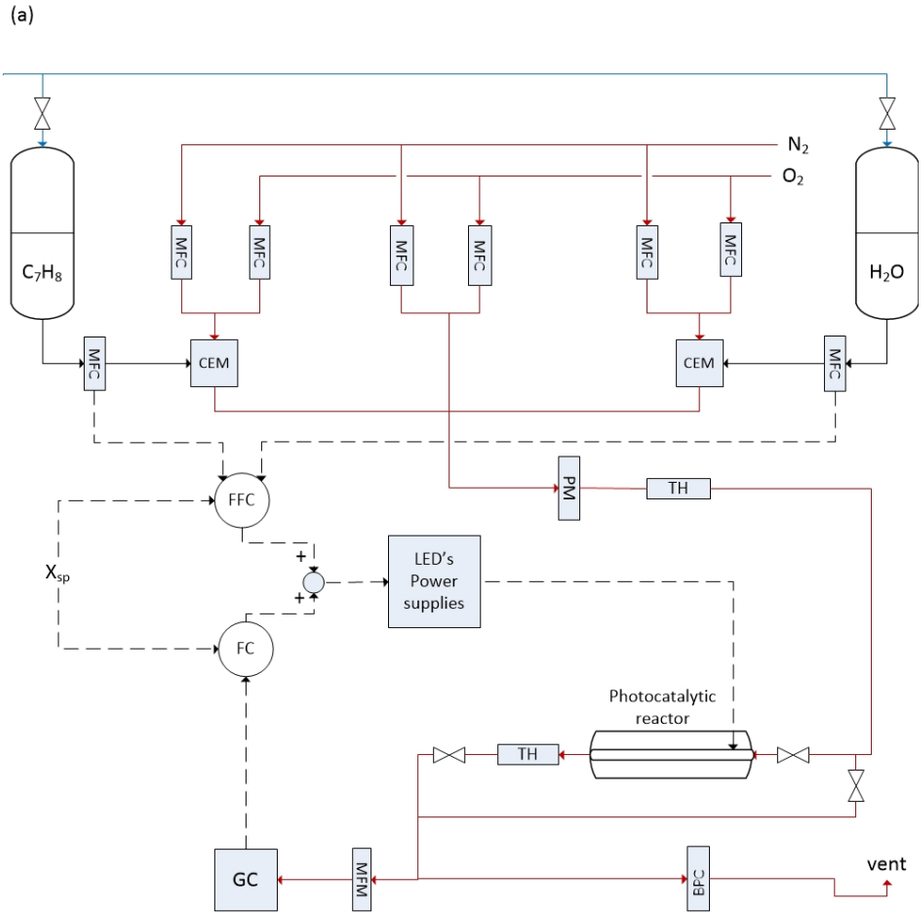

Figure 5.1 Flow diagram of the experimental setup. MFC – Mass Flow Controller; BPC- Back Pressure Controller; CEM – Controlled Evaporator Mixer; TH- Thermo Hygrometer; PM- Pressure meter; FC-Feedback Controller; FFC-Feedforward Controller

To validate the performance of the feedback controller in achieving and maintaining a certain set point, two different sets of experiments were conducted. In the first set of experiments, at constant toluene inlet concentration (C_t) of 40 ppmv and relative humidity (RH) of 60%, the irradiance was manipulated to track different set points.

Our previous study revealed that the ratio of water to toluene inlet concentration plays a significant role in the catalyst deactivation [4]. Water molecules react with the intermediate reaction species, which are accumulated on the catalyst surface, to remove them from that surface in the form of CO_2. Therefore, if the ratio of the water to toluene concentration at the inlet is not sufficiently high, catalyst deactivation becomes significant. Feedback control has the ability to adjust the system automatically to maintain a constant conversion in the presence of catalyst deactivation. Therefore, in the second set of experiments, the feedback controller performance was studied under conditions where catalyst deactivation is expected to be significant. In particular, an experiment at a RH of 40% and a toluene inlet concentration of 40 ppmv was conducted to create such conditions.

Catalyst deactivation is an example of an unmeasured disturbance, which has to be rejected with feedback control. In contrast, measured disturbances can be rejected with feedforward control. The RH and toluene concentration at the inlet of the reactor are examples of measured disturbances in our system. Therefore, in the last part of this study, the ability of a combined feedback and forward control system to reject measured and unmeasured disturbances was investigated. To support the design of the feedforward controllers, the dynamic response of the system was studied when step changes in toluene inlet concentration and relative humidity were present in open-loop mode. First, the toluene conversion was monitored at constant toluene inlet concentration (40 ppmv), relative humidity (40%) and irradiance (6.5 W m^{-2}). Subsequently, a step change in relative humidity from 40% to 60% was implemented. Finally, a step change in toluene inlet concentration from 40 ppmv to 30 ppmv was implemented. The same sequence of step changes was implemented in a separate experiment in closed-loop mode with feedback control only and in closed-loop mode with combined feedback and feedforward control. The operating conditions of all experiments are given in Table 5.1.

Table 5.1. The operating conditions of all experiments

Test ID	RH [%]	C_t [ppmv]	X_{sp} [%]	Irradiance [W m^{-2}]	Controller mode
#1	60	40	40→50→60→30	manipulated variable	closed-loop (feedback)
#2	40	40	40	manipulated variable	closed-loop (feedback)
#3	40 (0-100 min.) 60 (100-200 min.) 60 (200-320 min.)	40 (0-100 min.) 40 (100-200 min.) 30 (200-320 min.)	-	6.6	Open-loop
#4	40 (0-100 min.) 60 (100-200 min.) 60 (200-320 min.)	40 (0-100 min.) 40 (100-200 min.) 30 (200-320 min.)	30	manipulated variable	closed-loop (feedback)
#5	40 (0-100 min.) 60 (100-200 min.) 60 (200-320 min.)	40 (0-100 min.) 40 (100-200 min.) 30 (200-320 min.)	30	manipulated variable	closed-loop (combined feedback and feedforward)

5.3 Controller Design and Tuning

5.3.1 Feedback control

The toluene conversion (X) is the controlled variable and the illumination intensity (E) of the LEDs is the manipulated variable in the automated control loops. The proportional-integral (PI) controller is used as a feedback controller, which has two tuning parameters (i.e., controller gain and time constant). The dynamic input-output behaviour of the system has been characterized experimentally to obtain numerical values for those two tuning parameters. In particular, the process gain, time constant and time delay are estimated by comparing the dynamic response of the system around the expected steady state to a first-order-plus-time-delay process model, which is an approximation of the true dynamics of the system [31].

Figure 5.2 shows the dynamic development of the toluene conversion when the system is perturbed by a series of step changes in irradiance while keeping other process variables constant. The steady-state conversion increases when increasing the irradiance, which is consistent with earlier findings [4]. A time delay of approximately 15 minutes can be seen due to the online measurement. Furthermore, after the delay, a fast increase in conversion can be seen followed by a slow decrease in conversion. The increase is due to the change in manipulated variable (i.e., irradiance), which is to be used in the feedback control loop, whereas latter slow decrease is expected to be the result of catalyst deactivation. The process gain and

process time constant are two characteristic parameters that need to be estimated from the experimental data to design the feedback controller. The process gain (K) is obtained from the ratio of the steady-state conversion before and after the step change in manipulated variable is implemented (see Table 5.2). The average conversion during the last 100 minutes of every step is used to calculate the steady-state conversion. In reality, the reactor has a nonlinear input-output behaviour. Therefore, the calculation of the process gain in principle depends on the operating point at which the step change is implemented. However, it can be seen in Table 5.2 that the process gains calculated from the two different step changes have a similar value. Therefore, a single process gain is used for controller tuning, which is the average of the two process gains.

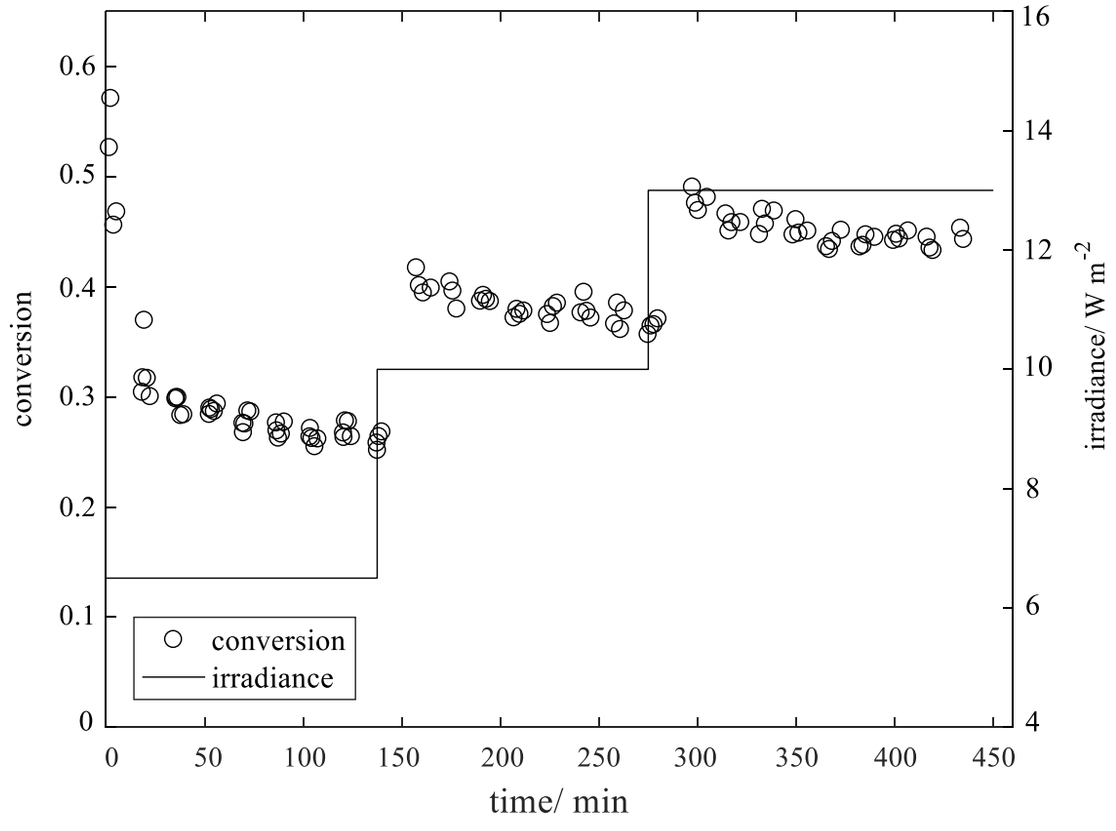

Figure 5.2 Dynamic development of the toluene conversion in response to step changes in irradiance. The RH is 60%, toluene inlet concentration is 40 ppmv, and the volumetric flow rate is 1020 ml min^{-1}.

Table 5.2. Average toluene conversion (X) and process gains corresponding to the step changes of irradiance (*E*)

E_1 [W m^{-2}]	$\bar{X}_1$	E_2 [W m^{-2}]	$\bar{X}_2$	K
6.5	0.25	10	0.36	0.031
10	0.36	13	0.44	0.027

The process time constant (τ) is obtained by determining the time needed to complete 63% of the transition from the old to the new steady-state conversion, which is difficult to obtain since the response is faster than the sampling period. However, the aim is to find a value that is order-of-magnitude correct, as feedback control is a model-free control method based on corrective

actions. In particular, a value of 6 minutes has been used as an approximation of the true time constant of the system. Subsequently, the tuning parameters of the PI feedback controller can be determined using standard methods such as the Internal Model Control (IMC) tuning method [31-33] used in this work. The feedback controller is implemented in so-called velocity form to avoid integral windup:

$$\Delta E_{FC} = K_c[(e_k - e_{k-1}) + \frac{\Delta t}{\tau_I} e_k] \quad (5.2)$$

where K_c is the controller gain and τ_I is the integral time. The desired closed–loop time constant has been chosen to be equal to the process time delay [32]. In addition, Δt is the sampling period and e_k is the measured error at the k_{th} sampling instant. The error is defined as the difference between the set point conversion (X_{sp}) and the measured conversion from the GC. The calculated irradiance is converted to an electrical current in the final control element for LEDs, using a linear relation, which was obtained empirically in previous work [17].

5.3.2 Feedforward control

The feedforward control relies on a process model that can predict the impact of a measured disturbance on a controlled variable such that preventive action can be taken to mitigate the impact of the disturbance. Since feedforward control is normally used simultaneously with the feedback control, a simple model often suffices, as feedback control can still drive the controlled variable to the desired set point. Therefore, in this work, an empirical steady-state model is used to design the feedforward controller. Typical disturbances for environmental oxidation reactions in the gas phase that have an impact on conversion and that can be measured include the inlet concentration of the organic compound and the relative humidity of the simulated air stream. Both disturbances are used to design the feedforward controller, which will be implemented by adding the outputs of the feedforward and feedback controllers together to calculate the value of the manipulated variable.

In our earlier work [4], the steady-state toluene conversion was experimentally measured as a function of toluene inlet concentration, relative humidity, volumetric flow rate as well as irradiance at typical operating conditions. For a toluene concentration (C_t) in the range of 20 to 90 ppmv and a relative humidity up to 70%, a volumetric flow rate (Q) of 0.8 to 1.3 l min^{-1} and an irradiance of 3 to 13.5 W m^{-2}, the relation between conversion (X_{FFC}) as a function of inlet concentration, and relative humidity is empirically modelled as follow:

$$X_{FFC} = -0.02 Q C_t (RH)^{1.3} + 0.2 E^{0.5} + 0.2 \quad (5.3)$$

A parity plot (see Figure 5.3) shows that the model is reasonably well capable of describing the conversion at steady state for the tested operating conditions despite its simplicity and lack of first principles.

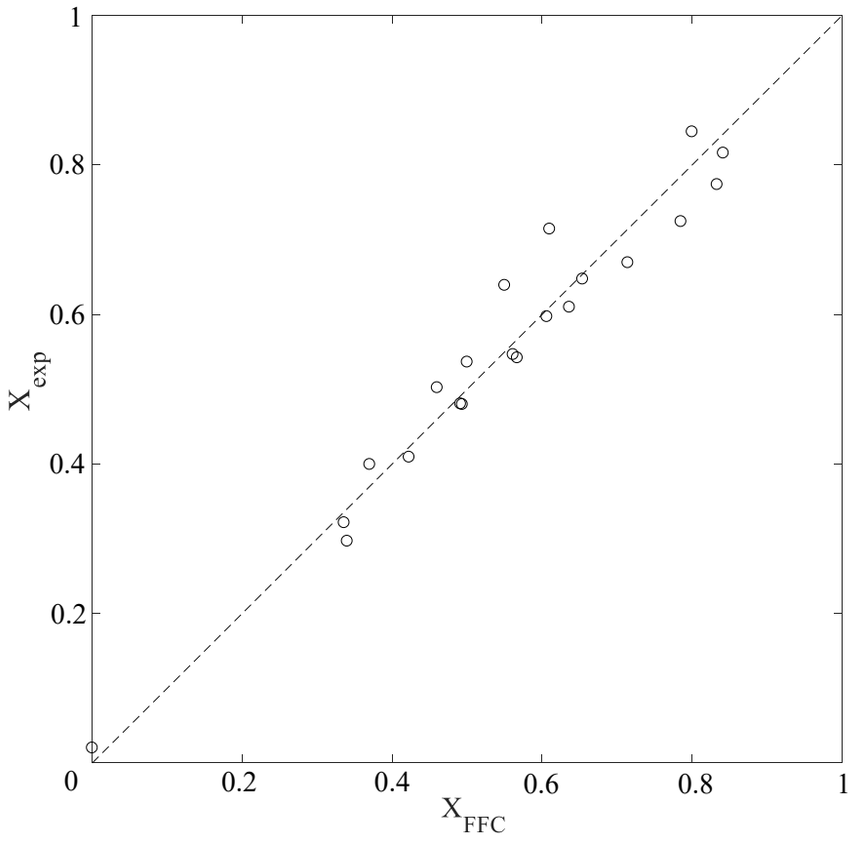

Figure 5.3 Experimental conversion (X_{exp}) vs. conversion predicted via equation (5.3) (X_{FFC})

From equation (5.3), the anticipated difference in steady-state conversion ($X_{m,\ FFC}$) due to measured changes in inlet concentration and relative humidity can be calculated when assuming negligible changes in volumetric flow rate. Furthermore, the irradiance to compensate the effect of the disturbance error on the steady-state conversion can also be calculated as below:

$$E_{2,\mathrm{FFC}} = [E_1^{0.5} + 0.1Q(C_{\mathrm{t},2}(\mathrm{RH}_2)^{1.3} - C_{\mathrm{t},1}(\mathrm{RH}_1)^{1.3})]^2 \tag{5.4}$$

where $E_{2,\ FFC}$ is the irradiance output of the feedforward controller, i.e., the sum of present irradiance (E_1) and the contribution of feedforward control (ΔE_{FFC}).

5.4 Results & discussion

5.4.1 Performance characterization of PI feedback control

The conversion and irradiance as a function of time during a set-point tracking experiment with feedback control are illustrated in Figure 5.4 (Experiment #1). The data demonstrate that the PI controller is well capable to track set points for conversion within the tested range by using the irradiance as the manipulated variable in an automated fashion. In general, the conversion reaches the set point rapidly without large overshoots or unstable behaviour despite the significant measurement delay from the GC.

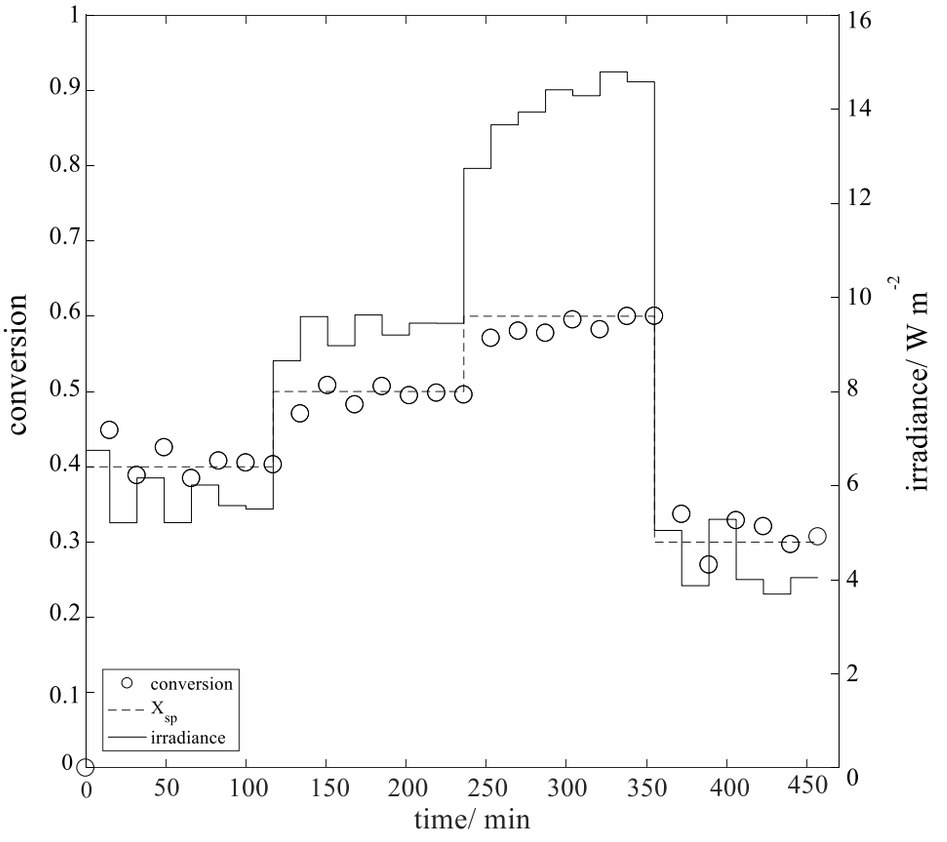

Figure 5.4 Dynamic development of the toluene conversion (controlled variable) and irradiance (manipulated variable) during a set-point tracking experiment in closed-loop mode with feedback control (Experiment#1).

Figure 5.5 shows the dynamic development of conversion and irradiance during a disturbance-rejection experiment with feedback control (Experiment #2). The data show that the PI controller is well capable to reject the effect of the catalyst deactivation on the conversion at a constant set point. The irradiance increases steadily over time to maintain the conversion close to the desired set point. Therefore, the PI controller can optimize the light utilization within the reactor automatically in case substantial catalyst deactivation occurs.

The feedback controllers were designed with commonly used tuning methods, which already yielded satisfactory performance. However, it is expected that further optimization of the controller design would allow for improved closed-loop performance. An investigation into the influence of operational variables such as residence time on the controller design and performance is of interest for future research. The closed-loop time constant is determined by the measurement delay, which is an order of magnitude larger than the space time and several times larger than the estimated process time constant. However, the controller gain should be changed for different operating conditions to account for the nonlinear process behaviour, which is also of interest for future research.

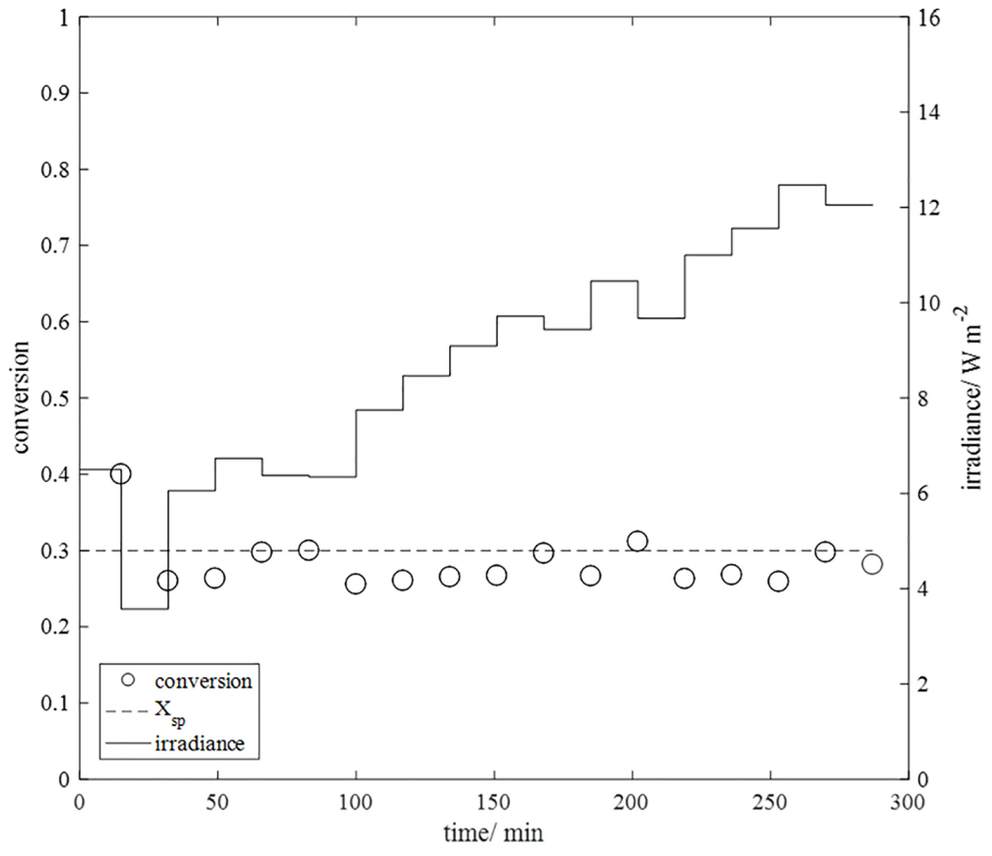

Figure 5.5 Dynamic development of the toluene conversion (controlled variable) and irradiance (manipulated variable) during a disturbance-rejection experiment in closed-loop mode with feedback control (Experiment#2).

5.4.2 Performance characterization of feedback and feedforward control

Figure 5.6 demonstrates the dynamic development of the conversion during an open-loop experiment in which the irradiance was kept constant at 6.5 W m^{-2} and the RH of the feed stream was increased after 100 minutes, and toluene inlet concentration was decreased after 200 minutes (Experiment #3). The conversion decreased gradually during the first 100 minutes due to the catalyst deactivation, while after the increase in RH from 40 to 60% at 102 minutes, a sharp drop in the conversion from 25% to 18% was observed. Subsequently, the conversion increased gradually over time due to the catalyst regeneration facilitated by the high RH [4]. In the last phase of the experiments, the system was disturbed at 200 minutes by a decrease in toluene concentration from 40 to 30 ppmv and consequently, the conversion showed a further increase over time due to increased catalyst regeneration rate at the higher ratio of water to toluene inlet concentration in the last phase of the experiment. The data of the open-loop experiment demonstrate that the toluene conversion does not remain constant when the inlet water to toluene ratio changes over time. The conversion can be stabilized with feedback control. In addition, since both concentrations are measured, a feedforward controller can be designed to supplement feedback control, as illustrated next.

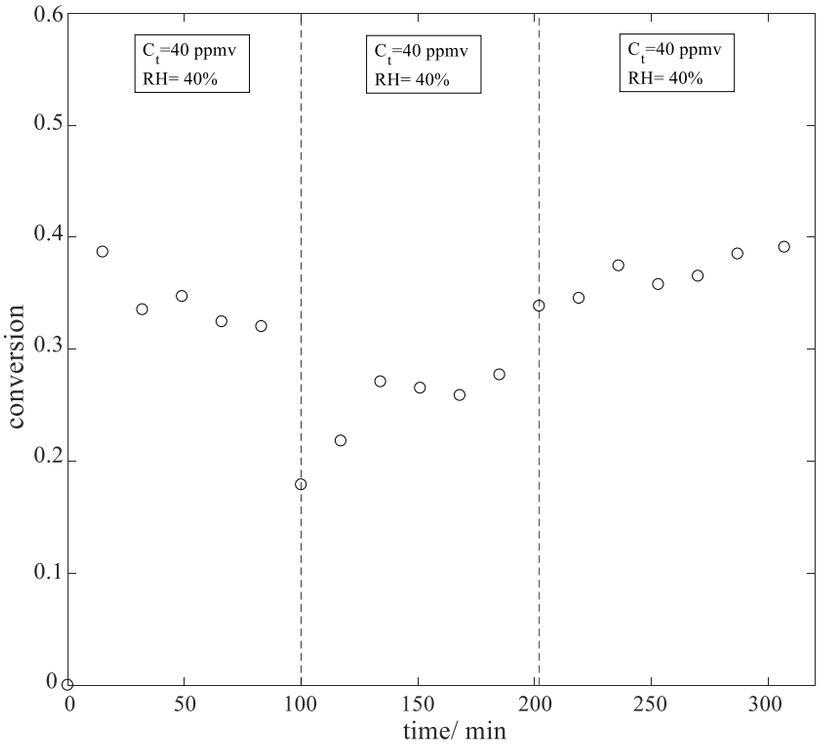

Figure 5.6 Toluene conversion during three different operating conditions at a constant irradiance of 6.5 W m^{-2} and flow rate of 1020 ml min^{-1} in open-loop mode (Experiment #3).

Figures 5.7 and 5.8 show the variation of toluene conversion and irradiance when the same changes in toluene inlet concentration and RH are implemented, respectively with feedback control only and with feedback control in combination with feedforward control (Experiment #4 and #5). The irradiance was used in both cases as the manipulated variable in closed-loop mode. In the first 100 minutes, for both cases the controllers were well capable to maintain the conversion close to the desired set point. However, when the first disturbance was introduced after 100 minutes, a distinct difference can be seen. In case of feedback control only (Figure 5.7), the conversion dropped below the set point and it took some time before the irradiance had been sufficiently increased to reject the disturbance. In contrast, when feedback control was used in combination with feedforward control, irradiance was increased much more rapidly due to the contribution of feedforward action. Consequently, the toluene conversion stayed close to the desired set point and the mitigation of the inlet disturbance was much more effective. Subsequently, the irradiance was gradually reduced due to the regeneration of the catalyst at higher RH, which was driven by feedback control, as this trend could be seen for both cases and was not used to design the feedforward controller. A similar behaviour could be observed when the second disturbance was introduced after 200 minutes of operation. In this situation, a higher conversion was measured shortly after the disturbance was introduced when only feedback control was used, as it took time to lower the irradiance. In contrast, feedforward control predicted the required lowering of the irradiance, which resulted in much better controller performance. In summary, both control schemes were eventually capable to reject input disturbances. However, the addition of feedforward control resulted in a more effective mitigation of the disturbances due to the combination of impact prediction of the measured

disturbances (i.e., feedforward control) and the corrective action of unmeasured disturbances and model uncertainty (i.e., feedback control).

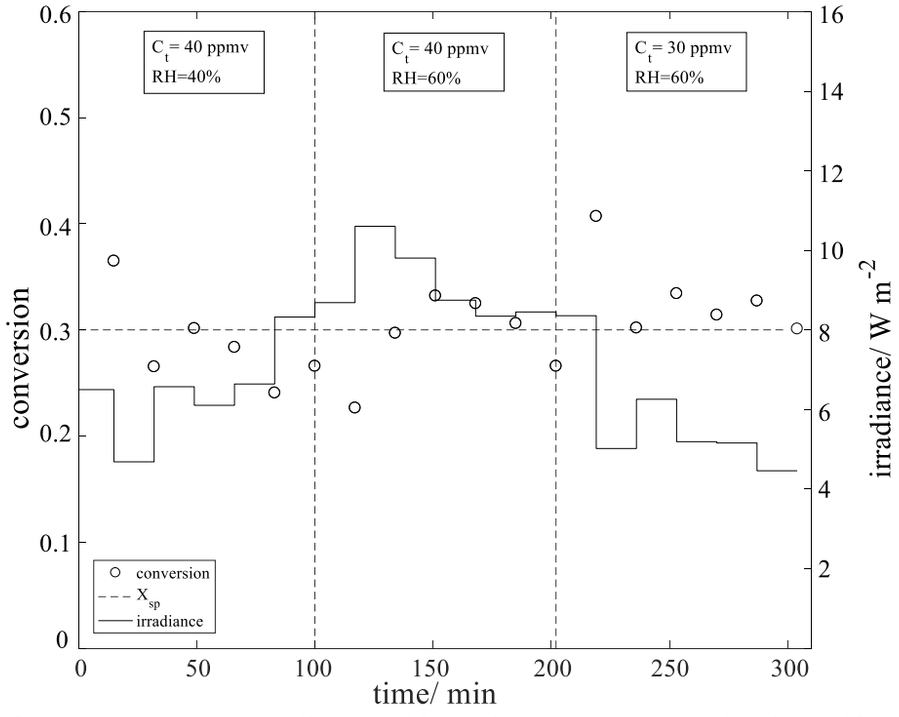

Figure 5.7 Toluene conversion (controlled variable) and irradiance (manipulated variable) in closed-loop mode in case of, a) PI feedback controller only (Experiment#4).

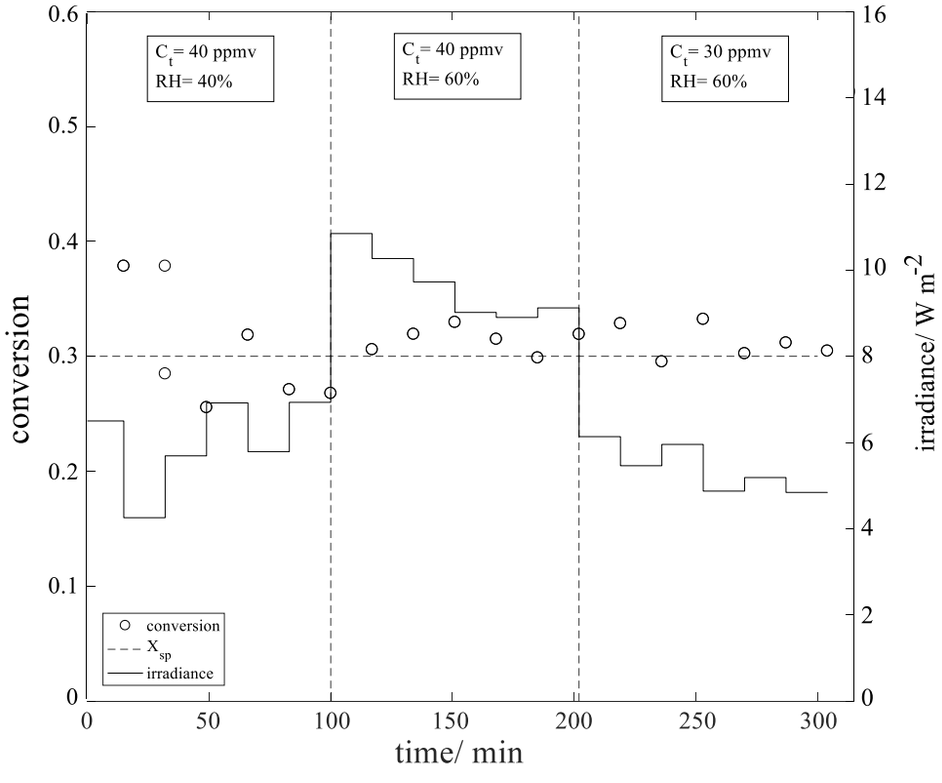

Figure 5.8 Toluene conversion (controlled variable) and irradiance (manipulated variable) in closed-lo op mode in case of PI feedback controller and feedforward controller (Experiment #5).

5.5 Conclusion

Online process analytical technologies can be combined with LEDs in automated control loops to maintain the conversion of toluene in a gas-phase photocatalytic reactor close to a desired value in the presence of disturbances. In particular, the experimental results demonstrated that a proportional-integral feedback controller could manipulate the irradiance within the reactor to achieve desired conversions effectively in the presence of disturbances. In case of measured disturbances, such as toluene or water inlet concentrations, the control scheme could be augmented with a feedforward controller based on an empirical steady-state model. A comparison of experiments without any control and with feedback control only demonstrated that feedback control effectively mitigated catalyst deactivation. However, the combined feedback and feedforward control scheme demonstrated superior behaviour in case measured disturbances were added to the same set of experiments.

This work demonstrates for the first time how fast online analytical technologies can be combined with "smart" light sources in automated control loops to maintain the conversion close to a desired value for optimal process operation. Future work may focus on developing more advanced control strategies (e.g., model-predictive control) or exploring other applications.

References:

[1] C. McCullagh, N. Skillen, M. Adams, P.K.J. Robertson, Photocatalytic reactors for environmental remediation: a review, J. Chem. Technol. Biotechnol. 86 (2011) 1002-1017.

[2] A. Fujishima, K. Honda, Electrochemical Photolysis of Water at a Semiconductor Electrode, Nature 238 (1972) 37-38.

[3] A.F. Tooru Inoue, Satoshi Konishi, Kenichi Honda, photoelectrocatalytic reduction of carbon dioxide in aqueus suspension of semiconductor powders, Nature 277 (1979) 2.

[4] F. Khodadadian, M.W. de Boer, A. Poursaeidesfahani, J.R. van Ommen, A.I. Stankiewicz, R. Lakerveld, Design, characterization and model validation of a LED-based photocatalytic reactor for gas phase applications, Chem. Eng. J. 333 (2018) 456-466.

[5] M. Motegh, J.J. Cen, P.W. Appel, J.R. van Ommen, M.T. Kreutzer, Photocatalytic-reactor efficiencies and simplified expressions to assess their relevance in kinetic experiments, Chem. Eng. J. 207 (2012) 607-615.

[6] F. Khodadadian, M. Nasalevich, F. Kapteijn, A.I. Stankiewicz, R. Lakerveld, J. Gascon, CHAPTER 8 Photocatalysis: Past Achievements and Future Trends, Alternative Energy Sources for Green Chemistry, The Royal Society of Chemistry 2016, pp. 227-269.

[7] T. Van Gerven, G. Mul, J. Moulijn, A. Stankiewicz, A review of intensification of photocatalytic processes, Chem. Eng. Process. 46 (2007) 781-789.

[8] R.J. Braham, A.T. Harris, Review of Major Design and Scale-up Considerations for Solar Photocatalytic Reactors, Ind. Eng. Chem. Res. 48 (2009) 8890-8905.

[9] W.-K. Jo, R.J. Tayade, New Generation Energy-Efficient Light Source for Photocatalysis: LEDs for Environmental Applications, Ind. Eng. Chem. Res. 53 (2014) 2073-2084.

[10] M.R. Eskandarian, H. Choi, M. Fazli, M.H. Rasoulifard, Effect of UV-LED wavelengths on direct photolytic and TiO2 photocatalytic degradation of emerging contaminants in water, Chem. Eng. J. 300 (2016) 414-422.

[11] T.S. Natarajan, M. Thomas, K. Natarajan, H.C. Bajaj, R.J. Tayade, Study on UV-LED/TiO_2 process for degradation of Rhodamine B dye, Chem. Eng. J. 169 (2011) 126-134.

[12] K. Song, F. Taghipour, M. Mohseni, Microorganisms inactivation by continuous and pulsed irradiation of ultraviolet light-emitting diodes (UV-LEDs), Chem. Eng. J. 343 (2018) 362-370.

[13] E. Korovin, D. Selishchev, A. Besov, D. Kozlov, UV-LED TiO_2 photocatalytic oxidation of acetone vapor: Effect of high frequency controlled periodic illumination, Appl. Catal. B 163 (2015) 143-149.

[14] O. Tokode, R. Prabhu, L.A. Lawton, P.K.J. Robertson, Controlled periodic illumination in semiconductor photocatalysis, J. Photochem. Photobiol. A: Chem. (2015).

[15] Y. Ku, S.-J. Shiu, H.-C. Wu, Decomposition of dimethyl phthalate in aqueous solution by UV–LED/TiO_2 process under periodic illumination, J. Photochem. Photobiol. A: Chem. 332 (2017) 299-305.

[16] O. Tokode, R. Prabhu, L.A. Lawton, P.K.J. Robertson, The effect of pH on the photonic efficiency of the destruction of methyl orange under controlled periodic illumination with UV-LED sources, Chem. Eng. J. 246 (2014) 337-342.

[17] F. Khodadadian, A. Poursaeidesfahani, Z. Li, J.R. van Ommen, A.I. Stankiewicz, R. Lakerveld, Model-Based Optimization of a Photocatalytic Reactor with Light-Emitting Diodes, Chem. Eng. Technol. 39 (2016) 1946-1954.

[18] M. Barkhordari Yazdi, M.R. Jahed-Motlagh, Stabilization of a CSTR with two arbitrarily switching modes using modal state feedback linearization, Chem. Eng. J. 155 (2009) 838-843.

[19] M.I. Neria-González, R. Martínez-Guerra, R. Aguilar-López, Feedback regulation of an industrial aerobic wastewater plant, Chem. Eng. J. 139 (2008) 475-481.

[20] R. Caetano, M.A. Lemos, F. Lemos, F. Freire, Modeling and control of an exothermal reaction, Chem. Eng. J. 238 (2014) 93-99.

[21] D.C. Fabry, E. Sugiono, M. Rueping, Self-Optimizing Reactor Systems: Algorithms, On-line Analytics, Setups, and Strategies for Accelerating Continuous Flow Process Optimization, Isr. J. Chem. 54 (2014) 341-350.

[22] C. Houben, A.A. Lapkin, Automatic discovery and optimization of chemical processes, Curr. Opin. Chem. Eng. 9 (2015) 1-7.

[23] A.J. Parrott, R.A. Bourne, G.R. Akien, D.J. Irvine, M. Poliakoff, Self-optimizing continuous reactions in supercritical carbon dioxide, Angew. Chem. Int. Ed. 50 (2011) 3788-3792.

[24] V. Sans, L. Porwol, V. Dragone, L. Cronin, A self-optimizing synthetic organic reactor system using real-time in-line NMR spectroscopy, Chemical Science 6 (2015) 1258-1264.

[25] D.C. Fabry, E. Sugiono, M. Rueping, Online monitoring and analysis for autonomous continuous flow self-optimizing reactor systems, React. Chem. Eng. 1 (2016) 129-133.

[26] S. Skogestad, Plantwide control: the search for the self-optimizing control structure, J. Process Control 10 (2000) 487-507.

[27] G. Marcì, M. Addamo, V. Augugliaro, S. Coluccia, E. García-López, V. Loddo, G. Martra, L. Palmisano, M. Schiavello, Photocatalytic oxidation of toluene on irradiated TiO_2: comparison of degradation performance in humidified air, in water and in water containing a zwitterionic surfactant, J. Photochem. Photobiol. A: Chem. 160 (2003) 105-114.

[28] Z. Pengyi, L. Fuyan, Y. Gang, C. Qing, Z. Wanpeng, A comparative study on decomposition of gaseous toluene by O_3/UV, TiO_2/UV and O_3/TiO_2/UV, J. Photochem. Photobiol. A: Chem. 156 (2003) 189-194.

[29] Y.-p. Zhang, R. Yang, Q.-j. Xu, J.-h. Mo, Characteristics of Photocatalytic Oxidation of Toluene, Benzene, and Their Mixture, J. Air Waste Manage. Assoc. 57 (2007) 94-101.

[30] P.C. Yao, S.T. Hang, C.W. Lin, D.H. Hai, Photocatalytic destruction of gaseous toluene by porphyrin-sensitized TiO_2 thin films, J. Taiwan Inst. Chem. Eng. 42 (2011) 470-479.

[31] D.E. Rivera, M. Morari, S. Skogestad, Internal model control: PID controller design, Ind. Eng. Chem. Process Des. Dev. 25 (1986) 252-265.

[32] S. Skogestad, Simple analytic rules for model reduction and PID controller tuning, J. Process Control 13 (2003) 291-309.

[33] C.E. Garcia, M. Morari, Internal model control. A unifying review and some new results, Ind. Eng. Chem. Process Des. Dev. 21 (1982) 308-323.

Chapter 6. Conclusion & Outlook

6.1 The main outcome of this thesis

One of the main challenges for industrialization of photocatalytic reactors is to increase the low overall efficiency of the process. Pairing the reactor with more efficient light sources will enhance the overall reactor efficiency if the light is utilized efficiently. The focus of this thesis is to demonstrate several approaches for optimum photon utilization within LED-based photocatalytic reactors. An optimal photon utilization can be realized in two different phases: design phase and operating phase of the reactor.

In response to the key question on how to select the optimal combination of design variables related to both light sources and reactor design simultaneously, in Chapter 2, this thesis demonstrates for the first time a rigorous mathematical optimization of an integrated process model involving material, momentum, and radiation balances. Specifically, the reactor model is developed for toluene degradation in the gas phase in an annular wall photocatalytic reactor. Because the viability of any process depends on its economic feasibility, an objective function, representing a trade-off between capital investments and operating costs, was defined. The reactor and the light source design variables such as the reactor dimensions and the number of LEDs were calculated such that the economical objective function is minimized. In another optimization study, the capability of the LED-based photocatalytic reactor in controlling the local reaction rate is demonstrated. In particular, the optimal positioning of LEDs is obtained to achieve a desire concentration profile along the full length of the reactor. Although the concentration profile in this study is chosen arbitrarily, this capability may become useful when a local reaction rate control is of interest for different purposes such as controlling the reactor's selectivity. In general, Chapter 2 has demonstrated the importance of model-based optimization for LED-based photocatalytic reactors and has proven to be a crucial tool to handle systematically the inherent trade-offs that exist in design and operation.

A validated process model is crucial for effective optimization studies. Furthermore, characterization of process trends is needed when developing operational strategies such as automated control approaches. Therefore, Chapter 3 focuses on the validation of the model of the reactor presented in Chapter 2, which requires a representative experimental set-up for conducting experiments at different operating conditions. To this end, a mini-pilot experimental set-up including a 60 cm long annular LED-based photocatalytic reactor was designed and developed. The LED assembly including 246 LEDs was in the center of the reactor, providing a near uniform photon distribution on the catalyst. The reactor model is validated experimentally, and the kinetic parameters of the model are fitted to the experimental data accordingly.

The precise role of water in the photocatalytic oxidation of volatile organic compounds has been a major topic of debate in recent literature. Chapter 3 has provided some important new insights into the role of water. In particular, under the operating conditions tested in this study, it is found that the catalyst deactivation depends strongly on the water to toluene molar ratio. By increasing the water content in the feed, the rate of catalyst deactivation decreased. On the other hand, there is a competition between water and toluene for adsorption on the catalyst

active sites and, therefore, in the absence of water, the highest toluene conversion rate was obtained. Therefore, an optimal water to toluene molar ratio can be found balancing the need to preserve the catalyst activity as well as to obtain the desired degradation rate. Electron-hole recombination is believed to be the most important factor causing the low efficiency of a photocatalytic process. It has been suggested that continuous introduction of photons stimulates charge recombination process and hence, results in inefficient usage of photons. On the other hand, the experimental result presented in Chapter 3 of this thesis suggests that electron-hole recombination is predominant in the reactor system for all tested irradiance levels. Therefore, the impact of periodical illumination of LEDs on the performance of the reactor is studied in Chapter 4. In particular, the impacts of period and duty cycle were studied on the reactor photonic efficiency for toluene photocatalytic degradation in the gas phase. It is concluded that the photonic efficiencies under CPI and continuous illumination at equivalent average irradiances are comparable for all tested periods and duty cycles since mass transfer does not limit the reactor, despite electron-hole recombination prevalence in the system.

The developed computational approaches and validated models can be used to identify optimal equipment dimensions and nominal operating conditions for efficient utilization of light within the photocatalytic reactor. However, an optimal light utilization may still not be achieved in practice due to design uncertainties and external disturbances acting on the system. LEDs are often referred to as “smart” light sources due to their flexibility in providing varying light intensity instantaneously. Furthermore, analytical techniques have made great progress in recent decades. Therefore, it has become possible now to combine the flexibility of LEDs and rapid analytic techniques such as GC in automated control loops. Chapter 5 provides the first experimental demonstration of such automated control loops. In particular, the combination of an on-line analytical system (GC), a control algorithm and LEDs as controllable light sources has been demonstrated for achieving a self-optimizing LED-based photocatalytic reactor. The excellent capability of the feedback PI controller in tracking different conversion set points was shown in the presence of unmeasured and measured disturbances to maintain a desired conversion of toluene. Furthermore, the performance could be further improved when adding the predictive capability of a model-based feedforward controller to the existing feedback controller. Environmental applications often require a maximum threshold for the concentration of pollutants. Since excessive conversion of pollutants (beyond the maximum threshold) would lead to high and unnecessary operating costs, an effective self-optimizing LED-based photocatalytic system was developed to adjust the conversion rate by monitoring the pollutant concentration of the inlet, without manual intervention.

6.2 Suggestions for future studies

6.2.1 Optimization

In minimizing the reactor cost and achieving a certain conversion, the light source and reactor design parameters described in Chapter 2 resulted in a non-uniform photon distribution pattern on the catalytic surface, which arguably violates the conventional wisdom of providing uniform lighting to the catalytic surface. It would be of interest for future research to validate such results by focusing on the effect of non-uniform irradiation patterns. Some studies with direct comparison of LEDs and conventional UV-lamps under similar irradiance level have attributed the lower efficiency of the LED-based reactors compared to conventional UV lamps-based

reactors to the non-uniform radiation pattern from the LED assembly. However, the current state-of-art does not consider the costs associated with obtaining a uniform light pattern, which may bring only marginal improvements to the conversion of the pollutant at the expense of significantly increased costs. Future work should, therefore, adopt a broader perspective and aim to optimize the economic performance of the complete system, which would provide experimental validation of some of the specific results that came out of the optimization studies presented in this thesis. Finally, a comprehensive economic comparison of a LED-based photocatalytic reactor to a system with a conventional UV-lamp would be of interest, as the conventional system has limited flexibility in creating a non-uniform photon distribution.

One of the advantages of LEDs is their narrow wavelength spectrum compared to conventional UV-lamps. In recent years, the number of studies on different photocatalyst action spectra i.e. photonic efficiency as a function of excitation wavelength, for degradation of different photocatalytic reactions has increased [1-4]. In many cases, the action spectra is proportional to the fraction of radiated photons absorbed by the photocatalyst [1]. For instance, the action spectra of P25 for several model compounds decrease as the photon wavelength increases [3,4]. On the other hand, the efficiency of converting electrical power to photons decreases when decreasing the photon wavelength [4]. Therefore, there is a trade-off between the reactor cost and the reactor photonic efficiency. In the optimization formulation presented in Chapter 2, the wavelength was considered as a fixed parameter, however, consider it as one of the degrees of freedom for the design of the LED illumination system to find the optimum action spectrum is an interesting subject for follow-up studies.

6.2.2 Other reactor configurations

In this thesis, a basic and simple reactor geometry is chosen for illustrative purposes, and different approaches for optimum photon utilization have been applied to it successfully. However, more sophisticated reactor designs have been proposed in the literature to improve mass and photon transfer. Hence, applying the proposed methodologies for optimum photon utilization, presented in this thesis for other reactor configurations, integrated with LEDs, could be a useful follow-up of the current study. The reactor can be modelled based on the first principles and validated experimentally as shown in Chapter 3, although the details of mass, momentum and photon transfer might be different for different configurations. However, the validated model can be used in the mathematical optimization approach suggested in Chapter 2, to obtain the optimal design parameters. For instance, many studies in photocatalysis are conducted in slurry reactors, especially in the liquid phase, where overcoming the mass transfer limitations and obtaining the radiation transfer equation due to photon scattering and absorption are challenging. However, optimization of LED-based slurry photocatalytic reactor has rarely been reported. In addition, the application of the PI control scheme presented in Chapter 5, can be studied directly for different LED-based reactors.

6.2.3 Reactor control

Although basic automated control approaches were successfully applied for the LED-based photolytic reactor in this study, more advanced control schemes could be developed to improve performance. For example, the empirical model used to design the feedforward controller could

be based on first principles and could include dynamics, which would offer a broader range of applicability. Future work may aim for more advanced control approaches such as model-predictive control (MPC), which relies on a validated dynamic model. The optimization strategies from Chapter 2 could provide a useful starting point for the numerical challenges regarding optimization, whereas the process model described in Chapter 3 could provide the starting point for model development. Finally, the actuators and process analytical technologies from Chapter 5 can be the basis for the physical implementation of the closed-loop structures of MPC.

In this study, a uni-variant controlling approach was used where irradiance was the only manipulated variable. However, other operating parameters such as temperature, relative humidity, etc. could be considered as the manipulated variables. Furthermore, the reactor could be optimized for other criteria than photon utilization such as minimizing an undesired product or maximizing the ratio of two products. Therefore, future studies could focus on conducting multivariate and multi-objective control algorithms when designing self-optimizing photocatalytic processes.

6.2.4 Reactor model improvements

The effectiveness of an optimization, control or scale-up methodology relies on the process model, which translates the system behavior to an abstract mathematical model. The photocatalytic reaction kinetic model is one of the main building blocks in such process model and, in recent decades, several studies have been conducted to understand the mechanism of the photocatalytic reactions. However, there is yet a lack of knowledge on intrinsic reaction kinetics, describing the reactions taking place in the reactor for many applications such as toluene degradation, which is due to the complex nature of the reactions. Although most of the reaction kinetics proposed in the literature for photocatalytic degradation of toluene were investigated in the model parameter estimation study in this thesis, none of them could explain the reaction behavior accurately at a broad range of conditions including at no or very low water concentrations. Since water is an inevitable part of so many practical applications of photocatalysis, such inaccuracies in the reaction kinetics may impose uncertainties in the model and consequently optimization or control results. An alternative to applying traditional methods for kinetic studies, such as the ones using differential reactors with a recycling system, is applying a hybrid modeling approach, which combines mechanistic and data-driven modeling within a single overall model. Especially when fundamental models are not able to describe the system behavior for a certain range of operating conditions, a hybrid model could result in a better description of the system. Therefore, such a technique is of interest as a basis for a model of a complicated photocatalytic process aiming to describe the system response also when the mechanism behind the system behavior is not fully understood.

In addition, the reactor system in our study was not mass transfer limited for the tested range of operating conditions, however, variations in design or operating conditions could impose mass transfer limitation in the reactor. Furthermore, at higher volumetric flow rates where the assumption of fully laminar flow is violated, the reactor model should account for different mass transfer mechanisms and flow regimes.

Furthermore, applying catalysts with higher specific surface areas such as nanotube-structured catalysts can improve the reactor performance. However, internal photon and mass transfer diffusion could play a role in these cases. Therefore, future studies are needed to focus on the integrated reactor models for different mass and photon transfer regimes.

Finally, catalyst deactivation is observed for some organic compounds due to the strong adsorption of reaction intermediates to the catalytic surface, as it was observed for toluene degradation in this study. However, the catalyst deactivation was not incorporated into the reaction model, which could be considered in the future studies as well.

6.2.5 Equipping a photocatalytic reactor with local sensors

In Chapter 2, the capability of the LED-based reactor to control the local reaction rate was shown in theory. Often, the initial photocatalytic reaction rate is used to model the reactor; however, photocatalysis often involves a chain of reactions where several intermediates and side products are generated on the catalytic surface. Therefore, future work may aim to design LED-based reactors equipped with a sensor system, which provides in-situ local concentration measurement. Such a system would provide opportunities for studying the reactor selectivity when kinetic details are known as well as investigating novel control approaches for the reactor focusing on selectivity in addition to conversion. In addition, such a system could facilitate studying the local photocatalytic reactions and revealing the unknown kinetics data.

6.2.6 Scale-up studies

A scaled-up photocatalytic reactor should satisfy a high mass transfer as well as optimal photon utilization in the reactor. However, the interplay between those phenomena is scale dependent, which could result in expensive reactors due to a deficient photon utilization or mass transfer limitations. However, mathematical models for LED-based reactors as suggested in this thesis can act as a powerful tool for mass and photon transfer predictions at larger scales. Furthermore, control structures are known to scale-up well, i.e., a control structure that works well on small scale often works well on large scale as well, which provides opportunities to simplify scale-up by transferring the developed automated control loops to larger scales.

6.2.7 Nanostructured photocatalysts

Different nanostructured TiO_2 catalysts such as nanotubes, nanofibers, nanospheres, and nanowires have been successfully applied for different photocatalytic applications. However, the comparison between these structures under similar conditions to find the optimum structure has rarely been reported, which can be interesting for future studies. In this regard, we have taken an initial step to study different TiO_2 nanostructures in a newly developed LED-based photocatalytic reactor. The results of this initial study to compare the photocatalytic activity of some nano-structured TiO_2 are reported in Appendix I. Some suggestions for further studies in this area have been provided based on our results as well.

6.2.8 New generation of UV-LEDs

Although UV-LEDs are more energy efficient and long lasting in comparison to conventional UV-lamps, the efficiency of UV-LEDs is significantly lower than visible LEDs. In addition to

the complicated process of production, they require expensive materials for fabrication and a bulky heat sink for heat dissipation [5]. Therefore, there have been many investigations and continuous improvements on the performance of UV-LEDs based on developing novel materials as the emitters or changes in their structure to overcome the mentioned drawbacks in the recent years. Organic light emitting diodes (OLEDs) in the UV range have been developed [6] while incorporation of ultra-small colloidal nanocrystal quantum dots (NQD) based on metal chalcogenides is another promising approach to develop more efficient UV-LEDs (QLEDs) [5]. Coupling photocatalytic reactors with such new generation of UV-LEDs is another interesting subject of research for developing more economically feasible photocatalytic processes.

References:

[1] S. K. Lee, A. Mills, C. O'Rourke, Action spectra in semiconductor photocatalysis, Chem. Soc. Rev. 46 (2017) 4877-4894.

[2] S. Sarina, E. Jaatinen, Q. Xiao, Y.M. Huang, P. Christopher, J.C. Zhao, H.Y. Zhu, Photon Energy Threshold in Direct Photocatalysis with Metal Nanoparticles: Key Evidence from the Action Spectrum of the Reaction, The Journal of Physical Chemistry Letters 8 (2017) 2526-2534.

[3] R. Quesada-Cabrera, A. Mills, C. O'Rourke, Action spectra of P25 TiO2 and a visible light absorbing, carbon-modified titania in the photocatalytic degradation of stearic acid, Applied Catalysis B: Environmental 150-151 (2014) 338-344.

[4] M. Martín-Sómer, B. Vega, C. Pablos, R. van Grieken, J. Marugán, Wavelength dependence of the efficiency of photocatalytic processes for water treatment, Applied Catalysis B: Environmental 221 (2018) 258-265.

[5] J. Kwak, J. Lim, M. Park, S. Lee, K. Char, C. Lee, High-Power Genuine Ultraviolet Light-Emitting Diodes Based On Colloidal Nanocrystal Quantum Dots, Nano Lett. 15 (2015) 3793-3799.

[6] Q. Zhang, X. Zhang, B. Wei, Highly efficient ultraviolet organic light-emitting diodes and interface study using impedance spectroscopy, Optik 126 (2015) 1595-1597.

Appendix I. Comparison of Different TiO_2 Nanostructures in a LED-based Photocatalytic Reactor

I.1 Introduction

Heterogeneous photocatalysis is attracting much attention due to its large number of applications [1, 2]. Nevertheless, its commercialization has been hindered by the low overall efficiency of the process [3]. The reactor, light source and photocatalyst are the three main elements in a photocatalytic process. The main challenges include efficient reactor design with optimal photon and mass transfer and developing more efficient photocatalysts. To overcome the poor photon utilization within a photocatalytic reactor, selecting a more efficient light source is important. Conventional UV-lamps such as low-pressure mercury lamps, restrict the reactor design due to their large size and rigid design. Moreover, fragility, toxicity, gas leakage and disposal issues are other disadvantages of mercury lamps [4]. Alternatively, Light Emitting Diodes (LEDs) are promising light sources for photocatalysis applications [5]. LEDs are robust, energy-efficient, non-toxic and long-lasting light sources. In addition, LEDs can be placed flexibly within each reactor configuration due to their small size and ability to deliver a range of intensities and different radiation patterns. The focus of this thesis is on optimal design and operation of LED-based photocatalytic reactors. However, the efficiency of the photocatalyst also has a major impact on the design and operation of such reactors. Extensive research has been done on developing more efficient photocatalysts, and yet TiO_2 is the most frequently applied photocatalyst. The reason is due to its high catalytic activity, chemical- and photo-stability, low cost, nontoxicity and favorable band gap energy [1]. For practical applications, immobilization of the photocatalyst makes operation easier, since no separation of the particles from the stream (e.g., by filtering) is required. On the other hand, dense films of immobilized photocatalysts may have mass transfer limitations and a lower catalytic surface area as drawbacks. Applying open structure nanosized TiO_2 catalysts which can provide extended surface area and ease of reactants access to the catalytic sites can be an attractive alternative. Different nanostructure TiO_2 catalysts such as nanotubes, nanofibers, nanospheres, and nanowires have been successfully applied for different photocatalytic applications [6, 7]. However, the comparison between these structures under similar conditions to find the optimum structure has been rarely reported.

The objective of the initial study reported in this appendix was to compare the performance of several well-known nano-structures of TiO_2 such as nanoparticles and nanotubes, which were prepared by hydrothermal methods and applied to gas-phase photocatalytic reactions. A disk LED-based photocatalytic reactor was designed and built for testing of these different photocatalysts. The reactor's design allowed for finding the optimal illumination pattern on the catalyst's surface easily by changing the variables of the light sources such as the distance to the catalyst surface and LED-to-LED distance. The model reaction was the photocatalytic degradation of toluene. The reactor effluent was analyzed with gas chromatography. The reactor was operated in the continuous mode and at the room temperature and atmospheric pressure.

I.2 Materials & methods

I.2.1 Catalysts preparation

TiO_2 nanoparticles and nanotubes were used in this study. The TiO_2 NPs were synthesized according to a protocol reported elsewhere [8]. Briefly, 2 ml of titanium isopropoxide (97%)

was mixed with 30 ml ethanol (analytical grade) and the solution was stirred at 400 rpm. Subsequently, 3 ml of acetic acid glacial was added to the solution while the solution was stirred. After 5 minutes, 5 ml of ultra-pure water was added. The final solution was baked in an oven for 15 minutes at 120 °C. The final product was washed with ethanol and centrifuged at 900 rpm for 3 times.

The synthesis procedure for the TiO_2 nanotubes was adopted from Ma et al. [9]. In summary, 33.25 g of solid NaOH was dissolved in 80 ml of water and later, 4 g of solid TiO_2 (anatase powder) was dispersed in the aqueous solution of NaOH. The solution was stirred for one hour and then, the solution was charged into two Teflon-lined autoclaves. The autoclaves were put into an oven for 48 hours at a temperature of 150 ºC. After the hydrothermal treatment, the solution was separated from the precipitates via filtration. Subsequently, the precipitates were added to 500 ml of 0.1 M HCl and stirred overnight. The solution was divided into six centrifugation tubes. The samples were re-dispersed and sonicated in water for one week. After reaching a pH in the range of 7 to 7.5, the product was dried in an oven at 60 ºC for 12 hours and calcined at 500 ºC in air for 2 hours.

Commercial TiO_2, (P25 from Evonik), which is the most applied catalysts for various photocatalytic applications, was used as the reference catalyst in this study. Two batches of each sample were prepared for testing the repeatability of the synthesis procedure.

I.2.2 Catalyst carrier and coating method

The catalyst carriers were 316 stainless steel discs of 6 cm in diameter, with a height of 0.5 cm and the approximate surface roughness (Ra) of 0.8 µm. The discs were coated with the catalysts using different methods such as dip coating, spin coating and spraying. However, the catalyst loading on the discs were non-uniform and mostly low in weight for conducting the photocatalytic reactions with measurable output. Therefore, the carriers were treated by different pre-treatment methods including surface oxidation, polishing with sandpapers and sand blasting with two different sand bead sizes (50 and 100 µm), to improve the adhesion of the catalyst to the carrier surface as well as to increase the catalyst weight loading.

Among the tested methods, using a sandblaster (GoldSmith, ZK8045, air pressure of 1 bar, sandblasting angle of 90° and the distance of 150 mm) with the larger sand beads (100 µm) in combination with spraying the catalyst solution on the disc resulted in more uniform, cracked-free and a higher catalyst loading on the discs. Before coating, the discs were ultrasonically cleaned with acetone and later with ethanol and finally dried in an oven at 120 ºC for 15 minutes.

The suspensions for spraying were prepaid by dissolving 200 mg of each sample in 20 ml of absolute ethanol followed by stirring the suspension on a magnetic stirrer for 2 hours. For coating the samples on the discs, an air spray gun with a nozzle of 0.8 mm diameter and air pressure of 2 bar was used. The samples were sprayed on the carriers manually, while the distance of the gun nozzle to the discs was kept constant at 50 mm. After the spray coating, discs were dried in an oven at 120 ºC for more than 3 hours. The catalyst weight on each disc was measured by weighing the discs before and after the coating.

I.2.3 Catalyst characterization techniques

The crystalline state of the samples was studied by X-ray diffraction (XRD) analysis using a Bruker D8 advance and CuKα radiation. Transmission electron microscopy (TEM) was used to investigate the morphology and size of the samples (FEI Tecnai F30, 300 kV). For TEM analysis, an extremely small amount of each sample was dissolved in ethanol and a droplet from the solution was dispersed on a 200-mesh carbon coated copper grid (Electron Microscopy Science). The copper grid was dried at room temperature before the analysis. Scanning electron microscopy (SEM) images were obtained (FEI instrument, Inspect F50) to investigate the surface structural quality of the deposited catalytic films on the disc carriers.

I.2.4 Equipment and Operating Procedures

The reactor was made of anodized aluminum and consisted of a reaction and an illumination module. The reaction module was a disc with internal diameter of 7 cm and cavity of 6 cm diameter and had 0.5 cm depth in the middle for placing the catalytic disc. The reaction module had a jacket in which water could flow at a controlled temperature from a thermostatic bath to keep the reactor at a desired temperature. The reactor inlet was designed to distribute the flow over the catalytic disc uniformly. The topside of the reactor had a quartz window for illumination. The reaction module was covered by the illumination module, which consisted of 72 UV-LEDs (NSSU100CT, Nichia, Japan) mounted on a printed circuit board (PCB). The distance of the LEDs to the topside of the reactor was tuneable. The PCB was connected to an aluminum bar, which exhibited several fins to increase the heat dissipation from the LEDs to the environment and to keep the LEDs at room temperature. The temperature of the LEDs was monitored with temperature sensors mounted at different points on the PCB. The design schematics as well as a photo of the reactor are shown in Figure I.1 (a) and (b).

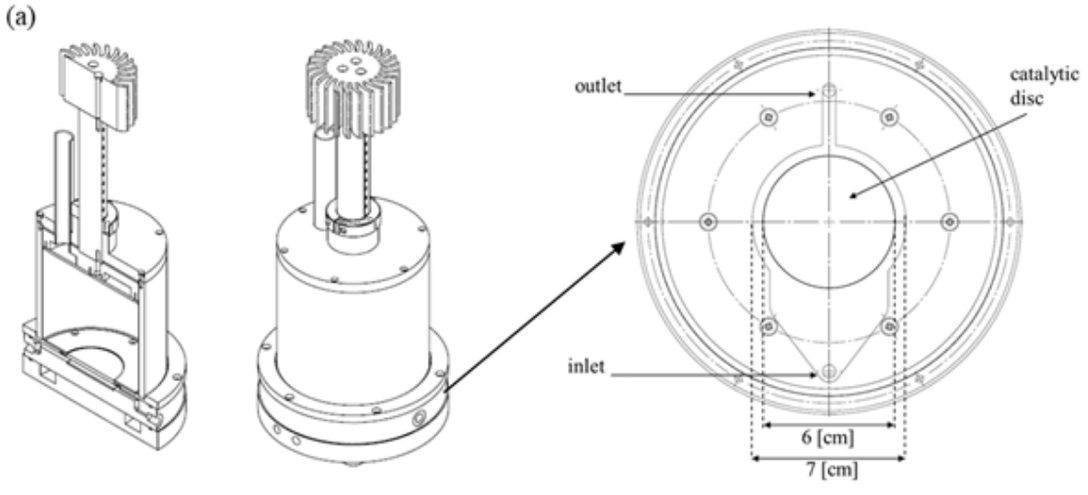

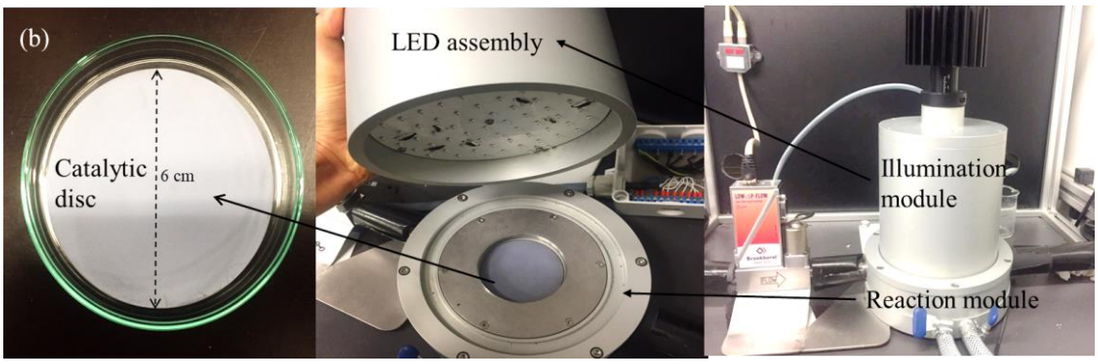

Figure I.1. Disc LED-based photocatalytic reactor (a) schematic drawing; (b) prototype in the laboratory.

The disc LED-based photocatalytic reactor was a part of an experimental set-up, which has been described in detail in Chapter 3 and was connected to the feeding system via a three-way valve (see Figure I.2). The carrier gas was a mixture representing air consisting of N_2 (78%) and O_2 (22%). The reactor feed was generated by mixing three gas streams as has been described in Chapter 3, while the reactor inlet flow rate was controlled with a mass flow controller. The operating conditions are listed in Table I.1.

Table I.1. Operating conditions of photocatalytic reactions

Toluene inlet concentration	60	ppmv
Relative humidity	60	%
Volumetric flow rate	20	ml min^{-1}
Reactor volume	14.13	ml
Residence time	43	s
Average irradiance	14	W m^{-2}

Before initiating the photocatalytic reaction, the reactor was purged for one hour with feed without illumination to reach an equilibrium state. Subsequently, the illumination was started and the concentrations of the various chemical fractions in the reactor's effluent were measured with GC at 20 minutes after initiating the reactor illumination. All the experiments with each catalytic disc were repeated at least three times. Toluene conversion was calculated my measuring the toluene at the reactor inlet and outlet according to equation (3.6) in chapter 3.

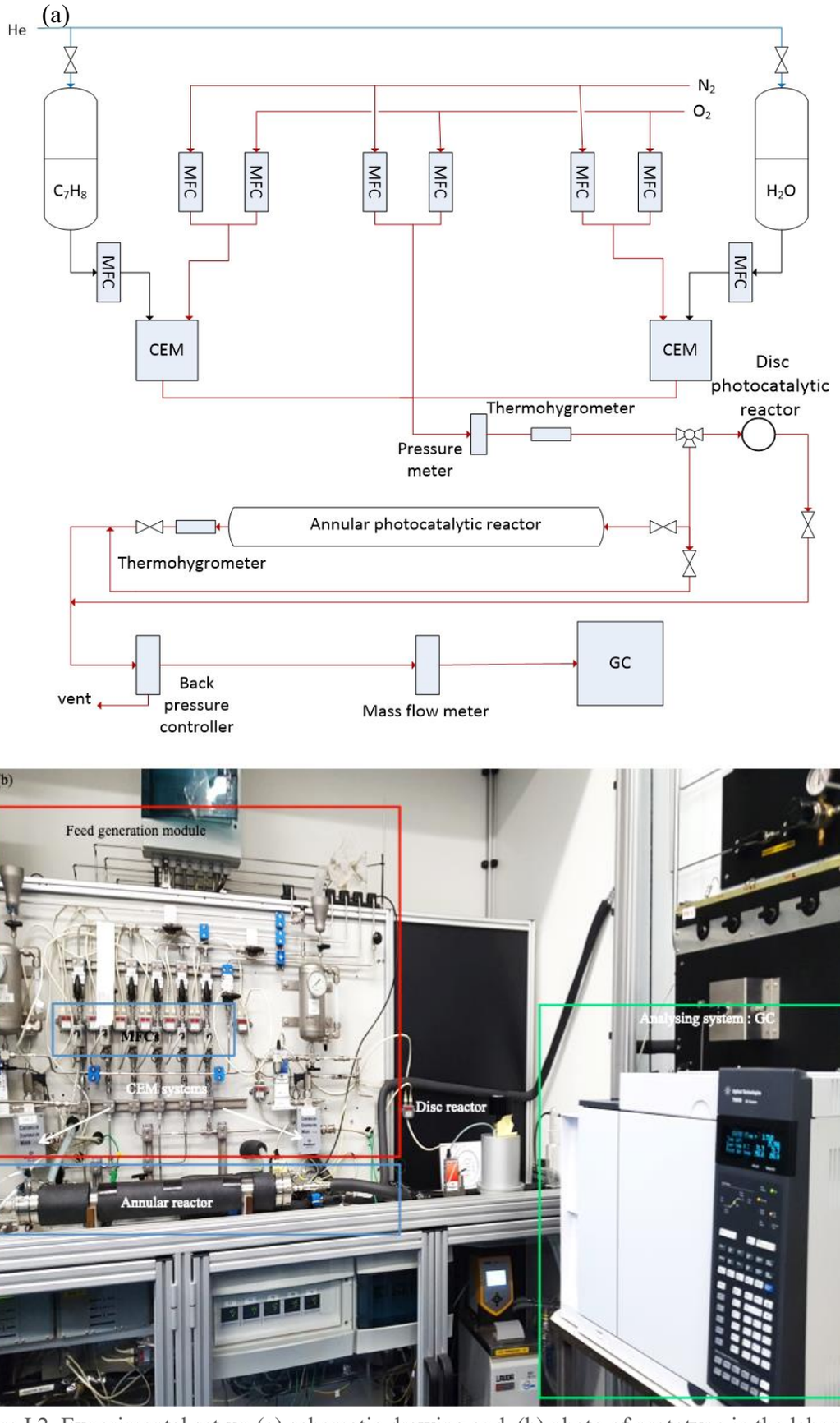

Figure I.2. Experimental set-up (a) schematic drawing and, (b) photo of prototype in the laboratory

I.3 Experimental Results

I.3.1 Catalyst characterization

The XRD pattern (not shown here) of NP samples showed mainly existence of anatase phase in the sample structure while no extra signals corresponding to other crystalline phases such as rutile or brookite were detected. However, the diffraction peaks obtained from NT samples analysis are broader than normal crystal structures, meaning the sample is mostly amorphous to microcrystalline (see Figure I.3). No crystalline phases and specifically rutile and anatase were identified in the NT samples structure. In addition, the combination of 805 anatase and 20% rutile crystalline phase was confirmed from XRD analysis of P25 samples (Data not shown).

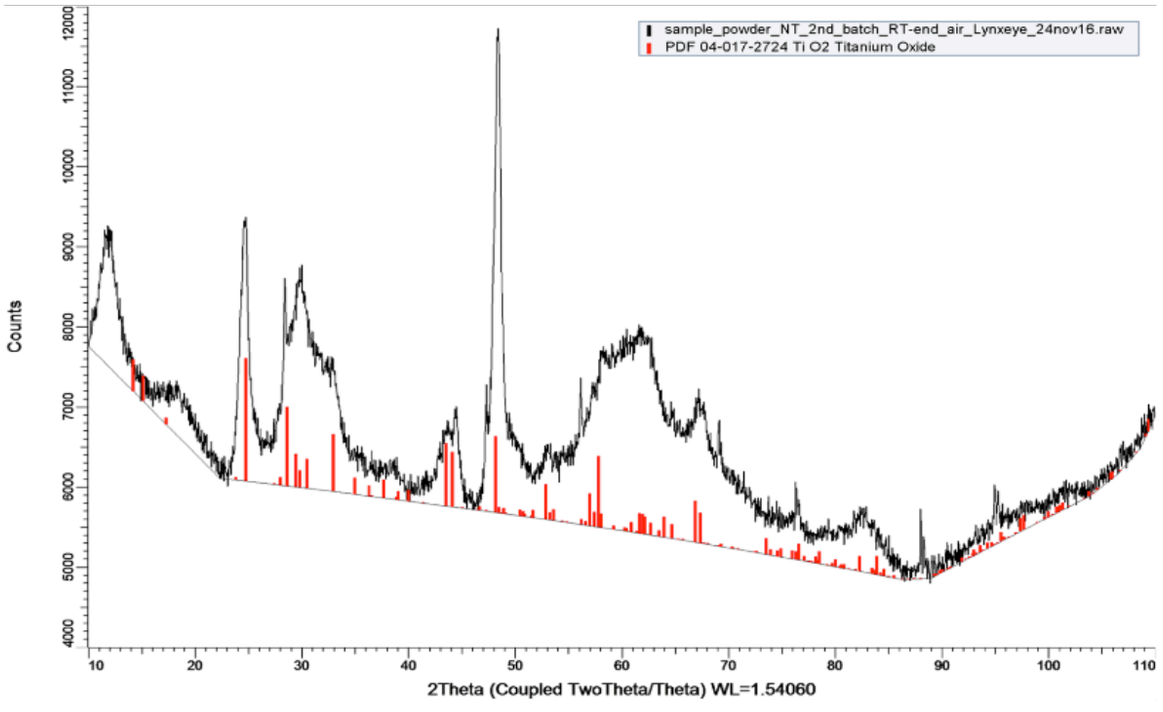

Figure I.3. XRD pattern of synthesized NT (in black) and possible peak positions and their intensities (in red)

The morphology and the particle size of the synthesized TiO_2 NPs and NT are compared with P25 samples in Figure I.4 (a), (b) and (c). NP consists of cubical particles with approximate size of 5 -10 nm. In Figure I.4, the tubular structure of NTs with low variation in their diameters (≈ 5 nm for inner diameter and≈ 10 nm for outer diameter), whose lengths can extend to few hundreds of nanometres can be observed. P25 particles are mainly spherical with particle sizes of 20-30 nm.

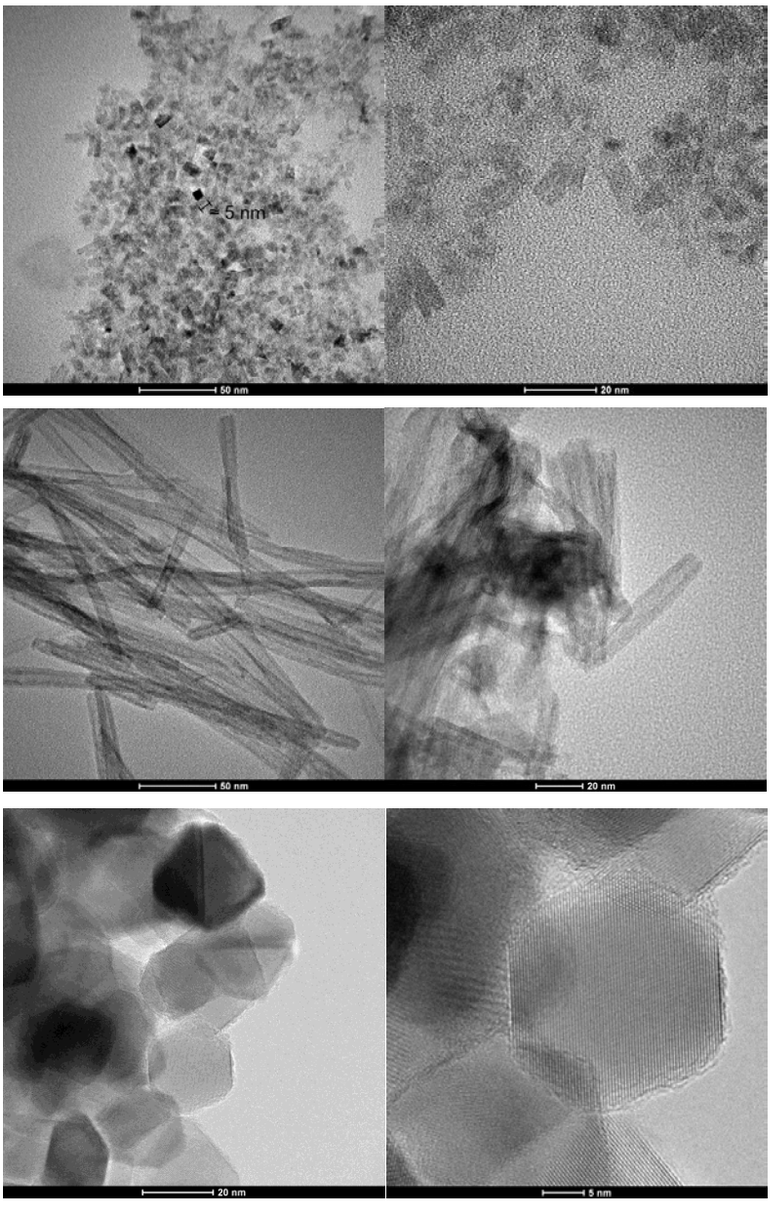

Figure I.4. TEM images of (a) synthesized NP, (b) synthesized NT and (c) P25.

Figure I.5 (a) and (b) show the stainless steel disc surface before and after sandblasting. It is observed that a relatively polished surface of the disc has changed to a more rough and matt state by sandblasting. The SEM analysis of the disc surface shows clearly the random deformation of the disc surface and creation of irregular squeezes due to the contact with the abrasive sand beads (see Figure I.6). The approximate roughness (Ra) of 2.5 µm was obtained by analyzing the disc surface after sandblasting via a profilometer (Dektak 8).

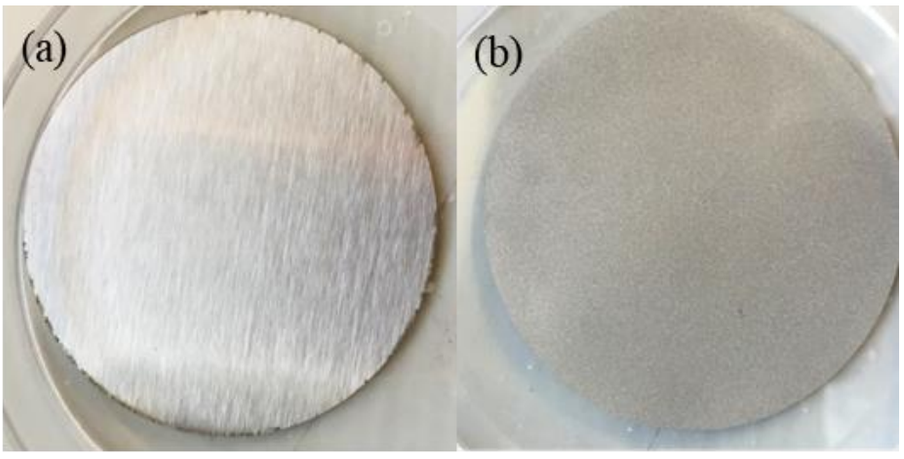

Figure I.5. The stainless steel disc (a) before and (b) after sandblasting (sand beads of 100 μm)

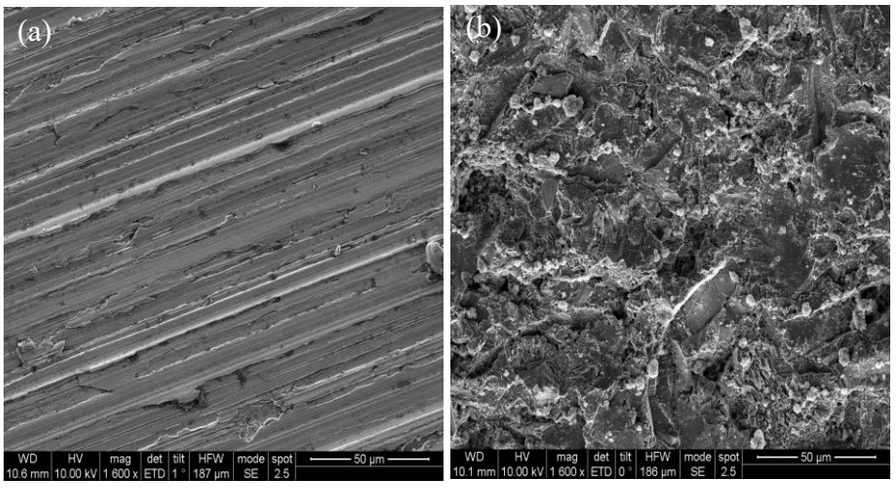

Figure I.6. SEM images of the stainless steel disc surface (a) before and (b) after sandblasting (sand beads of 100 μm)

It is observed that all coated catalytic films present a similar uniformity on the discs at low magnification (Figure I.7). However, comparing the SEM images (see Figure I.8) for the surface morphology of the catalytic films, the NP film presents more uniformity on the disc, while the other two samples and specifically NT show more particles agglomerations with diameter of few microns in the surface structure. The creation of the catalytic film by stacking of the agglomerates has resulted in creation of some pores for these samples.

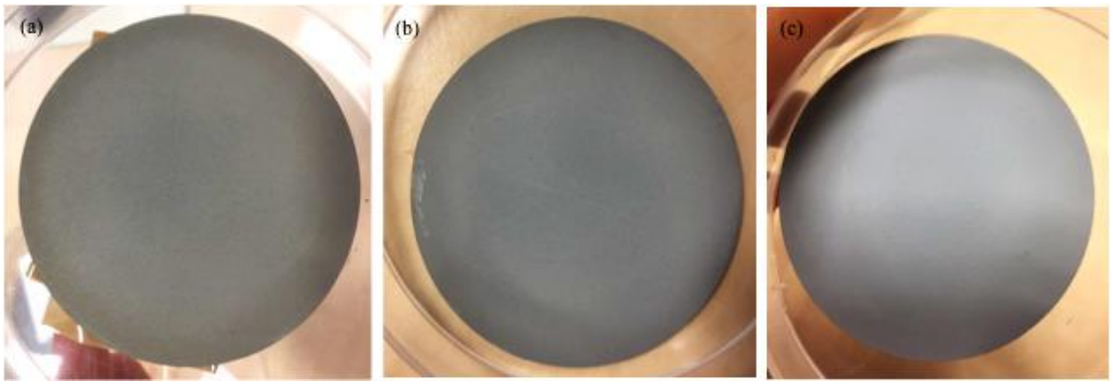

Figure I.7 Coated disc via (a) synthesized NP, (b) synthesized NT and (c) P25

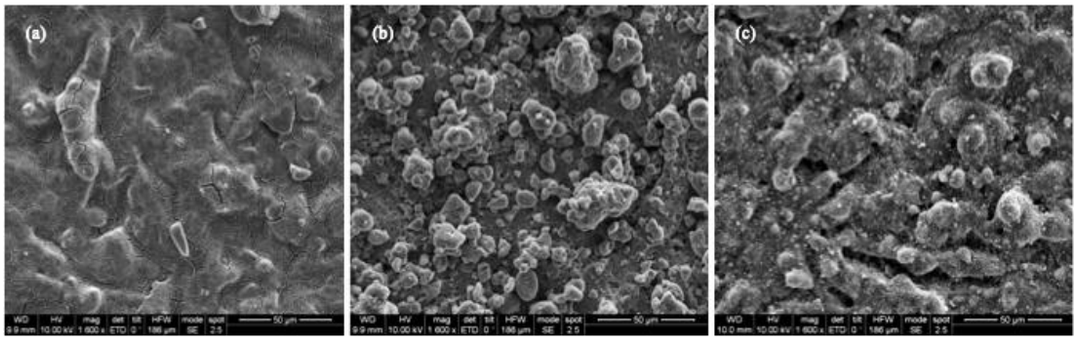

Figure I.8 SEM images of the (a) synthesized NP, (b) synthesized NT, and (c) P25 coated film surface on the discs.

Controlling the catalyst weight on each disc via spraying was found to be challenging. Therefore, several discs from each catalyst batch were prepared and the discs with an approximately similar catalytic weight were tested. The list of catalytic samples and their weights are listed in Table I.2.

I.4 Photocatalytic experimental results

Toluene conversions for different catalytic samples are listed in Table I.2. The reactor performance for discs with P25 catalyst from the same batch but with different catalytic weights showed a near linear relation between toluene conversion and the catalyst weight within the tested range. By increasing the catalyst weight, the catalyst surface increases, which leads to more photon absorbance and consequently, more active sites for the catalytic reaction.

Table I.2. Toluene photocatalytic conversion for different TiO_2 photocatalysts

Samples	Weight [mg]	Conversion	± error
P25#1	4.4	0.29	0.01
P25#1	8.4	0.36	0.02
P25#1	15.1	0.47	0.02
P25#2	14.6	0.45	0.01
NP#1	15.9	0.56	0.02
NP#2	14.5	0.53	0.01
NT#1	14.8	0	0
NT#2	18	0	0

The NP samples showed a higher toluene conversion compared to conventional P25 catalyst at a similar catalyst weight. The higher photocatalytic activity of the NP samples could be attributed to their smaller particles sizes compared to P25, which results in a higher catalytic surface area. In addition, the crystalline structure of NP samples is mainly anatase, while P25 is a mixture of 80 % anatase and 20 % rutile. It is well known that the anatase phase has higher photocatalytic activity compare to rutile [10] and therefore, this can be another reason why NPs showed higher photocatalytic activity compare to P25.

On the other hand, none of the NT samples showed photocatalytic activity, which might be attributed to the absence of TiO_2 in the form of rutile or anatase, which was proven by the XRD analysis.

I.4.1 Discussion and recommendations

The goal of this brief study was to take an initial step to compare different types of catalysts and compare them in a photocatalytic reactor. The results showed that is the structure has a meaningful impact on the catalyst activity. However, a significant portion of the results produced in this study are not reported here, due to lack of consistency and reproducibility, which calls for refined and possibly extended experimental protocols, especially for coating the carriers with catalysts.

The lack of photocatalytic activity of the hydrothermally synthesized NT was surprising. It was suggested that the lack of activity might be due to the lack of anatase and rutile TiO_2 in their structure. However, the protocol used for the synthesis of these catalyst particles led to anatase phase in other studies [9,11]. Therefore, it is recommended to test other synthesis protocols for TiO_2 nanotubes and to compare the nanotube catalysts produced with those protocols (containing anatase and/or rutile structures) with the other nano-structured catalysts.

The mesoporous natures of nanofibers are of interest for conditions in which mass transfer is limiting, which suggests for a systematic comparison between the performance of TiO_2 nanofibers, nanoparticles and nanotubes in the reactor.

The reactor, designed and build in this study could be applied effectively for comparison of different catalysts. Also, this reactor allows finding the optimal illumination pattern on the catalysts surface by changing design variables related to the light sources such as distance to the catalysts surface and LED-to-LED distance. Therefore, using this reactor (design) the next step could be to find the optimal light distribution for each specific catalyst structure.

References

[1] J.M. Herrmann, Heterogeneous photocatalysis: state of the art and present applications In honor of Pr. R.L. Burwell Jr. (1912–2003), Former Head of Ipatieff Laboratories, Northwestern University, Evanston (Ill), Top. Catal. 34 (2005) 49-65.

[2] M.R. Hoffmann, S.T. Martin, W. Choi, D.W. Bahnemann, Environmental Applications of Semiconductor Photocatalysis, Chem. Rev. 95 (1995) 69-96.

[3] T. Van Gerven, G. Mul, J. Moulijn, A. Stankiewicz, A review of intensification of photocatalytic processes, Chem. Eng. Process. 46 (2007) 781-789.

[4] W.-K. Jo, R.J. Tayade, New Generation Energy-Efficient Light Source for Photocatalysis: LEDs for Environmental Applications, Ind. Eng. Chem. Res.53 (2014) 2073-2084.

[5] D.H. Chen, X. Ye, K. Li, Oxidation of PCE with a UV LED Photocatalytic Reactor, Chem. Eng. Technol. 28 (2005) 95-97.
[6] K. Nakata, A. Fujishima, TiO_2 photocatalysis: Design and applications, J. Photochem. Photobiol. C: Rev. 13 (2012) 169-189.
[7] F. Memarian, M.A. Tehran, M. Latifi, TiO_2 nanofiber yarns: A prospective candidate as a photocatalyst, J. Ind. Eng. Chem. 23 (2015) 182-187.
[8] V. Gomez, A. Clemente, S. Irusta, F. Balas, J. Santamaria, Identification of TiO_2 nanoparticles using La and Ce as labels: application to the evaluation of surface contamination during the handling of nanosized matter, Environ. Sci.: Nano 1 (2014) 496-503.
[9] R. Ma, Y. Bando, T. Sasaki, Nanotubes of lepidocrocite titanates, Chem. Phys. Lett. 380 (2003) 577-582.
[10] T. Luttrell, S. Halpegamage, J. Tao, A. Kramer, E. Sutter, M. Batzill, Why is anatase a better photocatalyst than rutile?--Model studies on epitaxial TiO2 films, Sci Rep 4 (2014) 4043.
[11] D. Aphairaj, T. Wirunmongkol, S. Niyomwas, S. Pavasupree, P. Limsuwan, Synthesis of anatase TiO2 nanotubes derived from a natural leucoxene mineral by the hydrothermal method, Ceram. Int. 40 (2014) 9241-9247.

List of publications

F. Khodadadian, M. Nasalevich, F. Kapteijn, A.I. Stankiewicz, R. Lakerveld, J. Gascon, CHAPTER 8 Photocatalysis: Past Achievements and Future Trends, Alternative Energy Sources for Green Chemistry, The Royal Society of Chemistry 2016, pp. 227-269.

F. Khodadadian, A. Poursaeidesfahani, Z. Li, J.R. van Ommen, A.I. Stankiewicz, R. Lakerveld, Model-Based Optimization of a Photocatalytic Reactor with Light-Emitting Diodes, Chem. Eng. Technol. 39 (2016) 1946-1954. https://doi.org/10.1002/ceat.201600010

F. Khodadadian, M.W. de Boer, A. Poursaeidesfahani, J.R. van Ommen, A.I. Stankiewicz, R. Lakerveld, Design, characterization and model validation of a LED-based photocatalytic reactor for gas phase applications, Chem. Eng. J. 333 (2018) 456-466. https://doi.org/10.1016/j.cej.2017.09.108

F. Khodadadian, F.G. de la Garza, J.R. van Ommen, A.I. Stankiewicz, R. Lakerveld, The application of automated feedback and feedforward control to a LED-based photocatalytic reactor, Chem. Eng. J. 362 (2019) 375-382. https://doi.org/10.1016/j.cej.2018.12.134

A. Poursaeidesfahani, M.F. de Lange, F. Khodadadian, D. Dubbeldam, M. Rigutto, N. Nair, T.J.H. Vlugt, Product shape selectivity of MFI-type, MEL-type, and BEA-type zeolites in the catalytic hydroconversion of heptane, J. Catal. 353 (2017) 54-62. https://doi.org/10.1016/j.jcat.2017.07.005

About the author

Maryam was born on 16 January 1985 in Tehran, Iran. She obtained her B.Sc. degree in Chemical engineering with honors in 2007. Following her bachelor study, she studied for a master's degree in chemical engineering Faculty of Tarbiat Modares University in Tehran, Iran. Her Master Thesis was about the effect of cerium and phosphorous loadings on HZSM-5 zeolite performance in hydrocracking of Naphtha. She received her M.Sc. degree with honors in 2011. After her graduation, she worked as Health and safety engineer (HSE) at Nargan consulting engineers Co. in Tehran, Iran. In September 2012, she joined the intensified reaction and separation system (IRS) group in the Process and Energy Department of TU Delft to peruse a Ph.D. program. Under superviosn of prof. Andrzej Stakiewicz, prof. Richard Lakerveld and prof. J. Ruud van Ommen, she conducted her PhD studies with the focus on developing approaches and methods for optimum utilization of photons in LED-based photocatalytic reactors. Since May 2017, Maryam has been working at ASML, Veldohven, the Netherlands.

Acknowledgment

"Life is not what one lived, but what one remembers and how one remembers it in order to recount it."

Gabriel García Márquez

Finally, my prolonged Ph.D. journey comes to its end, after working for 4 years and 6 months at TU Delft and later, 2 years of struggling with finishing writing the thesis and a full-time job simultaneously. Looking back at the last 7 years evokes contradictory feelings and memories: failing and achieving, bitter and sweet. The journey was fun and joyful, full of many great experiences of learning and self-development but also filled with many obstacles, which most of them I could have never overcome if it was not for many people whose technical or mental supports made the completion of this work possible. Although impossible to name everyone, I seize the opportunity to express my sincere gratitude to the best that I can.

First of all, I would like to express my profound gratitude to my promoter and supervisors, Prof. Andrzej Stankiewicz, prof. Richard Lakerveld and prof. J. Ruud van Ommen. Thank you, Andrzej, for giving me the opportunity of doing my Ph.D. in the IRS group. Thank you for your all valuable inputs and guidance's during our technical discussions and your incredible support and understanding along the way. In addition, I would like to thank you for creating such a nice environment for research, for wonderful discussions on a variety of subjects during IRS meetings, and for our memorable times in group outings and conference excursions. Richard, as your first Ph.D. student at TU Delft, I am sincerely grateful for all the lessons that I have learned from you. You taught me how to conduct research and analyse the results. Providing me with valuable inputs, you allowed me to research freely and steered me in the right direction whenever I needed it. For about two years, I had the privilege of dropping by your office if I had any questions or ideas. It was not easy for me when you decided to leave TU Delft to develop your own group at Hong Kong University of Science and Technology, but you managed to supervise me while being a continent far away for the next 5 years. You made always yourself available whenever I asked for a Skype meeting. Your justified criticism on my research and your extensive and constructive corrections and remarks on my scientific reports improved the quality of my work significantly. During the last two years, you kept me motivated to finish writing my thesis and supported me whenever I asked. Thank you Ruud, for accepting to supervise me in mid-way of my Ph.D, for providing me guidance and valuable discussions and for making yourself available for our bi-weekly discussions despite your super busy agenda. Anytime, that I asked for an extra discussion session, you made just yourself available. I appreciate all the valuable feedback on my work and paper drafts and also for keeping me motivated to finish writing my thesis in the past year. I also, would like to thank my committee members, prof. Javier Marugán, prof. Guido Mul, prof. Timothy Noël and prof. Atsushi Urakawa, for taking the time to read the draft of the thesis.

Further, I would like to thank all the staff of Process & Energy department of TU Delft, especially our amazing secretaries Leslie and Helma for being so helpful and nice, Rob for his

understanding and support during my PhD and also arranging all the finance works of my project, Michel for his assistance and support for working with GC and safety matters in the P&E lab and finally Jaap for his support regarding to the lab issues.

The development and running of the experimental set-ups in this work were not possible without the help and support of the experts from DEMO lab: thanks to Danny de Gans, for all the help with the design of the PCBs and LEDs mountings, to Martijn for making all the electrical connections of the set-ups, to Bas and Daniel for assembling and piping of the set-up and to Lennart for the lab-view programming.

My sincere thanks also goes to Dr. Rene Poelma from department of microelectronics of TU Delft for sharing some of his knowledge about LEDs with me in the first year of my work, to Ruben Abellon from the Optoelectronic Materials group in the Chemical Engineering Department at TU Delft for assisting me by profilometer and integrating-sphere measurements, to Ruud Hendrix for conducting XRD measurements of my catalytic samples, to Prof. Henk Nugetren from Chemical Engineering Department at TU Delft for arranging some experiments on catalyst preparation for me in his lab, to Mojgan Talebi for those moments that I was desperately searching in the labs for some piping connections to continue my experiments and she provided me with what was available in her lab to help, to Eugene Straver for being my mentor for about two months while working in Kavli Nanolab of TU Delft, and finally to Jaap Verborg who helped me in the construction of mini LED-based reactor.

I should thank the M.Sc. students who did contribute greatly to my work by doing their final graduation project with me and giving me the opportunity of supervision: Zonghan, Merijn and Francisco.

I do extend my appreciation to prof. Jesús Santamaría Ramiro for hosting me for about two months in Nanoporous Films and Particles Research Group (NFP) at the University of Zaragoza. That was a great learning experience for me becoming familiar with some catalysts synthesis methods and different characterization techniques. My special thank goes to Dr. Jose Luis and Dr. Carlose Bueno for their daily supervision, to Dr. Alberto Clemente for assisting me with the catalyst coating, and to Heidy, Nacho, Peppe, Catarina and Juan Jose for their friendship and making my stay more fun and joyful in Zaragoza.

My time at Delft was made enjoyable in large part due to the many friends and groups that became a part of my life:

First, I would like to thank Fluid Mechanics and Hydrodynamic group and prof. Jerry Westerweel for hosting us in their section for the first two years of my time at TU Delft before moving to the new P&E building. Although being separated from our own group, they made us feel so comfortable in their department. There, I enjoyed the discussion over daily 10 am-coffee breaks and lunchtime with the group members especially with Sedat, Manu, Danielle, and Pedro.

A very special thanks to my very first officemate Iza, who not only made the office a pleasant place to work but to become my most compassionate friend in the first two years of my Ph.D.

A big thank goes to Guido, who supported me technically with his great knowledge as fast as possible whenever I was in need for his help and for our nice long chats that we had times to times in the department. Also, thanks to Lalit, who joined our office a few months later after me, and was always very patient and kind nevertheless all the disturbances caused by me in the office. Thanks to Marloes, the “holy mother”! for all the fun nights when we did rehearse a screenplay and she was our director and for all other joyful moments which we shared during our time at P&E. Thanks to Wei Wei for being such a pleasant colleague and friend to share a discussion from science to society and politics. I also would like to thank my dear colleagues and friends in the P&E for all the good times that we shared together: Alex, Anamaria, Christian, Samir, George, Daniel, Javier, Rohit, Mirhossein, Ahmadreza, Jiulia, Manuela, Nikolaos, and Noura.

With a special mention to the members of “Shabhaye Del-Shekasteh” group: thank you Farnaz Maman Aqdas & Meysam & Radin, our little new member, Hassan & Elaheh, Mojdeh & Hamed, Tayebeh & Framarz for all the gathering nights of dining, singing, Mafia game, pantomime, jokes and laughs, which energized me for a week of facing with the Ph.D. challenges!

Thank you, Shiva for all those very early morning! swim sessions, lured by a free breakfast for the first-time attendants, which I could only bear for just few sessions. Anyway, we have continued our friendship outside the pools! thanks for all the mental supports and compassionate talks, accompanied by many laughter’s, Farzad Reqabtjoo! for all those swimming competitions on Wednesday nights and Sunday mornings, Pooria for all those scientific and non-scientific discussions during coffee times, for motivating us to do boot-camping! I always admire your positive attitude for almost everything in life, Shima and Arash for the great hospitality whenever I have been at your place, Amin Karam, for being such a nice neighbor to me for two years, Bud, for all the support whenever I asked for and the nice talks during our tea times in Aula, and, Dara, Anahid, Yasin, Mohammad for all the nice and fun moments that we have made together.

Fatima, you are my very first and so the oldest friend in the Netherlands. Later, you joined the IRS group in P&E, where we were office neighbours for more than two years. The two years that became indeed more pleasant for me because of our regular coffee breaks and nice relieving talks. Thanks to Erfan, witnessing you falling in love and being truly loved was one of the greatest moments of those two years. During the past 7 years, you have always shown me that I can count on your support anytime.

I also appreciate all the mental support that I have received from my colleagues at ASML during the past two years, specifically from Edwin Lenderink, Stephane Ronchi and people in Pellicle Defectivity group: I could have not asked for better colleagues than you!

Ali, the time that you stepped into our office for the first time in September 2014, I was spending the most difficult days during my Ph.D. Having you as the officemate was the sunshine in those gloomy days as not only you became a very close friend to me but also you showed a lot of interest in my work, which encouraged me to move forward and finally resulted in our

collaboration in the first and second papers of this thesis. I am always grateful for all the unsparing support and care during the last 5 years and I treasure our friendship forever.

My dear Mostafa, words cannot express my gratitude for all the continued and unfailing love and support received from you during my Ph.D. and specially writing the thesis, which made the completion of this thesis possible. You were always around at times that I thought that it is impossible to continue, you helped me to keep things in perspective. You are not only my teammate for life but of keen intellect, you are the friend to lend an ear and give the best advises. Immensely logical and unsentimental! you are the most bighearted, compassionate and supportive person that I know when it comes to family. I have learned so many life lessons from you and I am still learning. I cherish truly every moment of your companionship and support in my life.

Finally, my foremost gratitude goes to my parents, Khosro and Afsar, and my sister, Reyhan, not only for the last 7 years but for a lifetime of unconditional love and support: Baba, thanks for raising me with the love for science and poem, for encouraging me to believe in myself, for being so open-minded and fully trusting on me and supporting me in every decision that I made. I am forever indebted to you for all I have achieved in life. Maman, you are my hero, the one who has never stopped chasing her dreams beside a demanding full-time job and taking very good care of her family. You have always shown me how to move forward and overcome the obstacles to realize my goals. I am eternally grateful for all the sacrifices you have made for me. Reyhan, you are my biggest fan! Although being apart in distance, I have never felt lonely in the Netherlands as you showed me that the distance does mean nothing when there is true love. You are my sister by blood and the best friend by choice. My brother (in-law), Meysam, thanks for taking good care of Reyhan and Nikan and being always a true brother for me and a son for my parents. My late grandmother, Mamani Joonam, you were more than just a grandma, it was magic in your touch and sunshine in your smile, you were my peace. Losing you was one of the most difficult things that I had to cope with during my Ph.D. I always carry your words of encouragement, and your voice, calling my name is always in my ears. Miss you forever and rest in peace.

Maryam

Veldhoven, May 2019

ای بیخبران شکلِ مُجَسَّم هیچ است،

وین طارَمِ نُه سپهر اَرقَم هیچ است!

خوش باش که در نشیمن کَون و فَساد،

وابسته یک دمیم و آن هم هیچ است!

خیام (427-510 هجری شمسی)

Alas! That this Invested Four (human body) is naught!

This Piebald Asp (day & night) of Nine-Fold Lore (nine spheres of sky) is naught!

Beware! Amidst the Heave of Life and Death

A gasp is ours, and that once more is naught!

Khayyam (1408-1131 AC)

Translation by: R. Parchizadeh